

Advances and challenges in two-dimensional materials for oxygen evolution

Tianmi Tang¹, Saisai Li², Jianrui Sun², Zhenlu Wang¹, and Jingqi Guan¹ (✉)

¹ Institute of Physical Chemistry, College of Chemistry, Jilin University, Changchun 130021, China

² School of Chemistry and Life Science, Changchun University of Technology, Changchun 130012, China

© Tsinghua University Press 2022

Received: 15 April 2022 / Revised: 21 May 2022 / Accepted: 24 May 2022

ABSTRACT

Oxygen evolution reaction (OER) plays an important role in many energy conversions and storage technologies, such as water splitting, rechargeable metal air batteries, renewable fuel cells, and electrocatalytic carbon dioxide reduction and nitrogen reduction, but its slow kinetics and high overpotential seriously affect the energy efficiency. Fabrication of high-performance and well-stocked OER catalysts is the key to the large-scale implementation of these energy-related technologies. Two-dimensional (2D) materials get a lot of attention as OER catalysts due to their large specific surface area, abundant active sites, and adjustable structures and compositions. Here, an overview is presented for the latest achievements in design and synthesis of 2D materials (including layered double hydroxides, metal-organic frameworks and their derivatives, covalent-organic frameworks, graphene, and black phosphorus) for the OER, emphasizing novel strategies (including metal/nonmetal doping, defect engineering, interface engineering, lattice strain, and fabrication of heterojunction) for achieving high electrocatalytic activity. Peculiarly, the structure–function relationship is analyzed in detail to gain deeper insight into the reaction mechanism, which is crucial to rational design of more high-performance 2D materials for the OER. Finally, the remaining challenges to improve the OER performance of 2D electrocatalysts are put forward to indicate possible future development of 2D materials.

KEYWORDS

two-dimensional material, oxygen evolution reaction, layered double hydroxide, metal-organic framework, covalent-organic framework

1 Introduction

The increasing energy demand and the imminent energy crisis promote the extensive research of renewable energy production and storage technologies [1–4]. The development of rich, efficient, and stable catalysts for oxygen reduction reaction (ORR), hydrogen evolution reaction (HER), and oxygen evolution reaction (OER) is the core of renewable energy technologies such as fuel cells and water splitting [5–14]. Among them, electrocatalytic water splitting has become an important sustainable hydrogen production technology. In water splitting, OER, as the anode reaction, involves a complex proton–electron coupling process involving four electrons, resulting in slow dynamics and low energy efficiency [15–21]. Therefore, the catalytic efficiency of water splitting mainly depends on the OER process. To reduce the energy loss in energy conversion equipment as much as possible, it is urgent to develop efficient OER catalysts to promote OER process, reduce the anode overpotential, and improve the overall catalytic efficiency [22–24].

Although precious metal oxides (IrO₂ and RuO₂) and two-dimensional (2D) Rh-based nanosheets can effectively catalyze OER and reduce energy loss, they cannot meet the requirements of large-scale commercial application due to their low reserves and high cost [25–29]. Therefore, it is necessary to develop cheap and abundant OER catalysts. Due to abundance, cheapness, and feasibility of large-scale synthesis, transition metal-based 2D

materials show enormous potential in water splitting application. Since Novoselov et al. peeled graphene from graphite in 2004 [30], a large amount of research has focused on 2D materials. Large layered 2D materials have weak van der Waals forces between the layers, and thin nanostructured materials can be obtained by stripping technology [31]. With the development of research, there are many 2D nanomaterials with layered structures, such as graphene nitride, hexagonal boron nitride (h-BN), graphitic carbon nitride (g-C₃N₄), black phosphorus (BP), covalent-organic frameworks (COFs), layered double hydroxides (LDHs), layered metal oxides, transition metal dichalcogenides (TMDs), metal-organic frameworks (MOFs), carbides, nitrides, and carbonitrides (MXenes) [32–44].

Due to unique geometric configuration and electronic structure of 2D nanomaterials, they are widely used in many fields, such as sensors [45–51], catalysis [52–57], energy conversion and storage [58–62], biomedicine [63–68], electronics, and optoelectronics [69–74]. Although the electrocatalytic performance of original 2D materials is poor due to lack of enough surface active sites, they can show good catalytic activity after adjusting their geometric and electronic structures. By reducing the thickness of the layered 2D material, the surface area of the catalyst is increased, exposing more active sites and enhancing electrical conductivity. By doping metal/nonmetal atoms on 2D materials, constructing defect sites, and forming heterojunctions, the local electronic structure can be

Address correspondence to guanjq@jlu.edu.cn

optimized, the interfacial charge transfer and mass transfer rate are improved, and the reaction energy barrier is reduced [75–78]. In addition, density functional theory (DFT) was used to calculate and construct 2D material model to further understand the relationship between catalyst structure and catalytic performance.

In recent years, the development of synthesis and characterization of 2D catalysts has provided support for the design of suitable and efficient OER catalysts. In this review, the synthesis, characterization, and OER mechanism of 2D materials (including LDHs, COFs, MOFs, and hybrids) are introduced, and the catalytic OER performance of 2D materials modified with different strategies is discussed. Meanwhile, the relationship between the structure and electrocatalytic performance of 2D materials is analyzed by theoretical calculations. Finally, the challenges and future opportunities of 2D materials for the OER are presented.

2 Synthesis methods

2D OER electrocatalysts can be prepared by a variety of methods, including top-down and bottom-up processes [79]. The top-down exfoliation technique is more favorable for the synthesis of monolayer nanosheets, while the bottom-up technique is more suitable for the preparation of multilayer nanosheets [80]. For LDH materials, bulk LDH materials dispersed in polar solvents will lead to infinite expansion of the main lattice, resulting in monolayer LDH nanosheets [81]. In the process of exfoliation, monolayer LDH nanosheets can also be obtained by intercalation technology. In addition, LDH nanosheets can also be prepared by liquid exfoliation, and the main lattice is formed in an appropriate solvent for ultrasonic exfoliation [82]. 2D COF materials can usually be prepared by mechanical stripping, solvothermal treatment, ionic heat treatment, and microwave treatment [83]. The covalent network would be influenced by thermodynamic equilibrium, reaction media, and conditions such as temperature, pressure, and

templates. The reaction media mainly include mixed solvents and molten metal salt, which can provide suitable reaction conditions for solvent and ionic heat. COFs can be quickly synthesized by microwave reaction under solvothermal conditions. MOFs based on carboxylate are generally synthesized by water/solvothermal method, microwave heating, and electrochemical deposition, while MOF derivatives with different structures are usually synthesized by calcination method [84]. Hybrids are usually synthesized by atomic layer deposition, self-assembly, water/solvothermal, and electrochemical intercalation [85]. In the following sections, we will introduce the synthesis methods of 2D LDHs, COFs, MOFs, and various hybrid materials, including hydrothermal/solvothermal, exfoliation, coprecipitation, electrochemical deposition, wet chemistry, and other synthesis methods.

2.1 Hydrothermal/solvothermal method

Hydrothermal/solvothermal method is the most common method to prepare 2D materials. Usually, water or common organic solvents are used as dispersants to synthesize 2D materials under high temperature and high pressure [86, 87]. The prepared materials generally possess uniform size, and the reaction conditions are safe, simple, and economical [88, 89]. Li et al. obtained FeOOH/LDH nanocomposites by hydrothermal synthesis, in which the size of FeOOH nanoparticles (NPs) was 2.0–18.0 nm (Fig. 1(a)). The strong interfacial interaction of FeOOH NPs can regulate the local electronic structure of Ni-Fe LDH, and the synergistic effect of FeOOH/LDH composite on electrocatalytic OER became stronger with the decrease of the average size of FeOOH NPs. When the average size of FeOOH NPs is 2.0 nm, the overpotential (η_{10}) of FeOOH/LDH in alkaline solution is 174 mV at 10 mA·cm⁻² [90]. Xu et al. synthesized Co/CoO nanoparticles (Co/CoO@COF) on imide COF by solvothermal method (Fig. 1(b)). In this catalyst, the conjugation effect between Co/CoO and COF increases the electron cloud

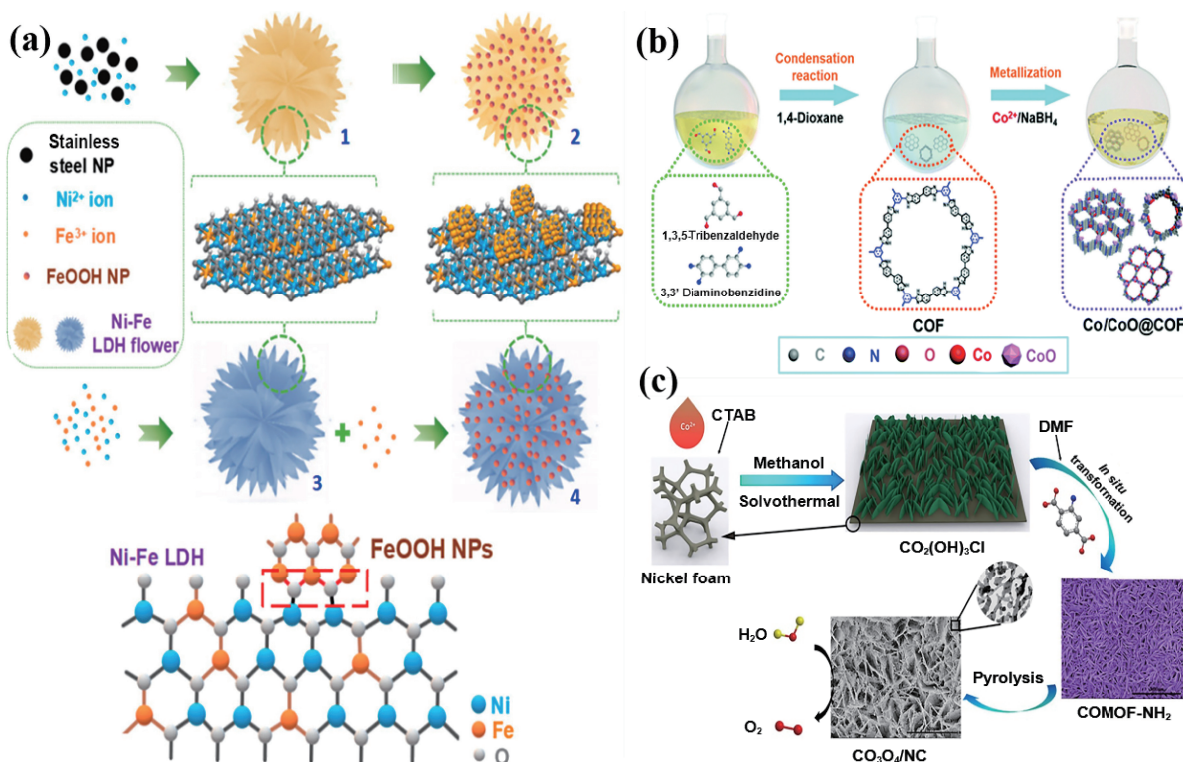


Figure 1 (a) Diagram of FeOOH/LDH synthesis. Reproduced with permission from Ref. [90], © American Chemical Society 2018. (b) Schematic for the preparation of Co/CoO@COF. Reproduced with permission from Ref. [91], © The Royal Society of Chemistry 2021. (c) The synthesis process of Co₃O₄/NC. Reproduced with permission from Ref. [92]. © Elsevier B.V. 2020.

density of the delocalized large π bond, thus improving the conductivity of Co/CoO@COF. In addition, the combination of Co/CoO@COF enhanced the stability and increased catalytic active sites. Under alkaline condition, Co/CoO@COF catalyzed OER with an overpotential (η_{10}) of 278 mV [91]. Yang et al. synthesized $\text{Co}_3\text{O}_4/\text{NC}$ with nitrogen doped carbon structure interconnection by two-step solvothermal and heat treatment (Fig. 1(c)). The rich pore structure of the $\text{Co}_3\text{O}_4/\text{NC}$ facilitated mass and electron transport, which showed excellent catalytic activity for OER ($\eta_{10} = 235$ mV and $\eta_{100} = 264$ mV). The low Tafel slope of $\text{Co}_3\text{O}_4/\text{NC}$ (80 mV $\cdot\text{dec}^{-1}$) indicated that the catalyst has fast electron transfer kinetics [92].

2.2 Exfoliation techniques

Exfoliation techniques are commonly used to synthesize single or several layers of 2D nanomaterials, which can be divided into mechanical exfoliation, liquid phase exfoliation, plasma-assisted exfoliation, and chemical lithium imbedding assisted exfoliation [93–95]. Ultrasound assisted liquid exfoliation is an effective way to peel materials with van der Waals layer structure. This method has advantages, such as convenience, economy, and high yield, but the thickness range of the stripped materials is wide. The stripping efficiency can be improved by the embedded lithium chemical auxiliary exfoliation technology [96]. The van der Waals interaction between layers can be weakened by embedding ions between layers of layered materials to increase the distance. In addition, solution pH, reaction temperature, surfactant, and solution type will affect the morphology and properties of the peeled materials [97–99].

Liquid phase exfoliation is a typical stripping strategy for the synthesis of 2D materials [100]. Hu et al. dispersed anionic

intercalated NiFe LDH into purified formamide and stirred it under the protection of inert gas to obtain monolayer LDH [101]. The exfoliated LDH nanosheets showed good electrochemical OER activity, and the η_{10} was reduced by 40–54 mV compared with the original one. However, liquid exfoliation strategies are often time-consuming, inefficient, and incomplete. Zhao et al. assembled monolayer NiFe LDH nanosheets (NiFe-LDH-NS) and graphene oxide nanosheets (GO-NS) into 2D materials by inserting solid phase exfoliation and breaking interlayer forces. Then, the two kinds of nanosheets with opposite charges are self-assembled by electrostatic force to form NiFe-LDH/GO nanohybrid, showing an η_{10} of 273 mV for the OER (Fig. 2(a)) [102]. Zhou et al. obtained layered MOF nanosheets from original layered MOF crystals by intercalation chemical exfoliation method (Fig. 2(b)). In addition to liquid phase exfoliation, plasma-assisted exfoliation can avoid the harm of solvent. Wang et al. synthesized ultra-thin CoFe LDH with a large number of O, Co, and Fe vacancies by Ar plasma etching dry stripping technique [103]. The formation of abundant vacancies makes the base plane have low coordination number and a large number of dangling bonds, which greatly enhanced the catalytic OER activity of CoFe LDH ($\eta_{10} = 266$ mV).

2.3 Coprecipitation method

Coprecipitation is a simple preparation method. After the precipitant is added to the solution, the ions are precipitated out by chemical reaction, which is affected by many factors, such as the solvent, pH value, and temperature [104, 105]. However, the materials synthesized by coprecipitation are often irregular and have poor morphology. Geng et al. designed a controllable co-reduction and co-oxidation strategy for the synthesis of Ni-Fe

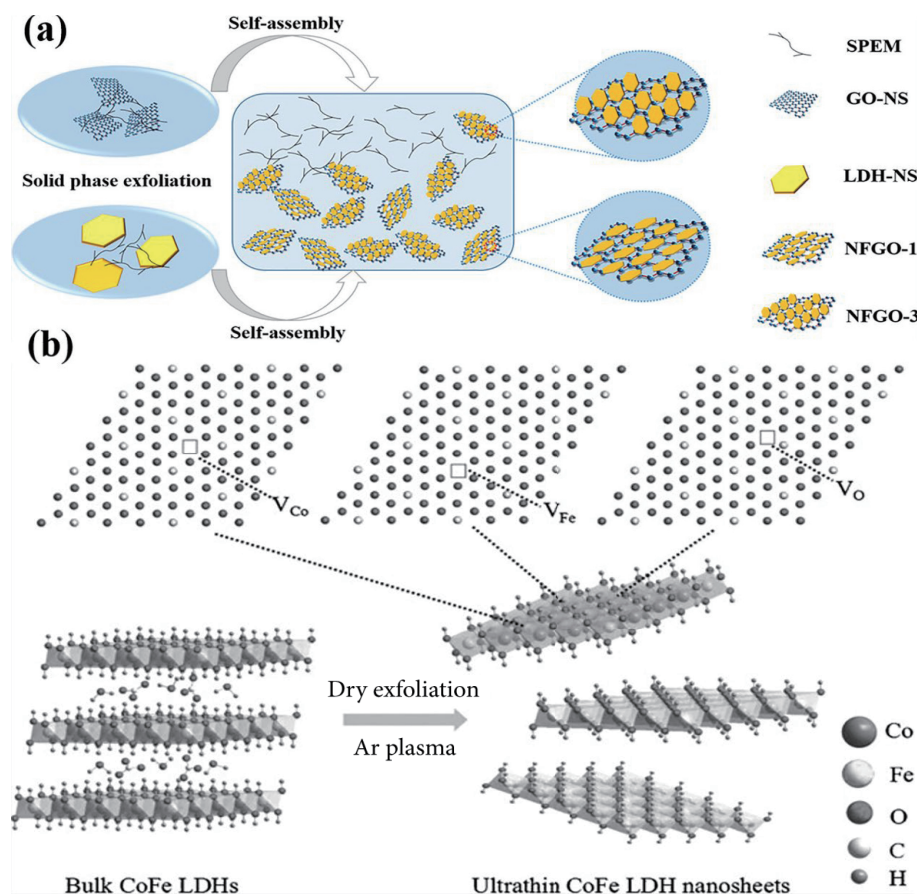


Figure 2 (a) Preparation of NiFe-LDH/GO nanohybrids based on the solid-phase exfoliation-liquid-phase assembly strategy. Reproduced with permission from Ref. [102], © American Chemical Society 2019. (b) CoFe LDH nanosheets by Ar plasma exfoliation. Reproduced with permission from Ref. [103], © Wiley-VCH Verlag GmbH & Co. KGaA, Weinheim 2017.

LDH nanosheets under mild conditions. During the synthesis process, the ion concentration in solution is controlled by changing the ratio of raw materials and the optimal morphology can be obtained. Compared with common coprecipitation in alkaline solution, in this synthesis method, ions are firstly reduced to bimetallic nanoparticles by strong reducing agent and then oxidized to form LDHs nanosheets with good morphology [106]. Yan et al. synthesized 2D LDHs with monocelled thickness and abundant surface defects using a simple and rapid precipitation technique. The ultra-thin LDH had abundant active sites and a large double-layer capacitance (C_{dl}) value, resulting in high catalytic OER activity ($\eta_{10} = 280$ mV). Theoretical calculations showed that the introduction of Co and Fe can tune the electronic structure of LDH and improve the conductivity in the OER process [107]. Gao et al. prepared ultra-thin Ni-Fe-LDH with inherent oxygen vacancy using co-precipitation strategy, which showed excellent catalytic OER activity under alkaline conditions ($\eta_{10} = 230$ mV). Theoretical calculations showed that the deprotonation promoted surface reestablishment and the formation of p–n interface. In this process, the vacancy can adjust the electron density at the metal site, thus reducing the OER energy barrier. In addition, the electrocatalytic activity is related to the surface and bulk of the catalyst [108]. Yan et al. synthesized CoMn-LDH@g-C₃N₄ composite by *in situ* coprecipitation at room temperature and found that the interlayer electron interaction between CoMn-LDH and g-C₃N₄ improved the conductivity [109].

2.4 Electrochemical deposition

Electrochemical deposition is a kind of electrochemical technology, by which catalysts can be directly deposited on the electrode and the morphology of the deposited materials can be modulated by adjusting electrodeposition time, electrolyte molar

ratio, and electrochemical sweep rate. The principle of electrochemical deposition is to reduce or oxidize metal ions in the solution onto the electrode by applying potential. Xu et al. synthesized free-standing NiFe layered dihydroxide/nitrogen doped graphite foam (NiFe LDH/NGF) by electrochemical deposition [110]. The catalyst exhibited high electrocatalytic OER activity with an overpotential of 239 mV in alkaline solution. The high catalytic activity was attributed to the uniform dispersion of NiFe LDH on NGF, which provided channels for electron transport and abundant active sites. Cao et al. reported a step-by-step electrodeposition strategy for the synthesis of ultra-thin NiFe-hydroxide films, in which nickel-based films were deposited at the cathode, followed by Fe species integration under the action of cyclic voltammetry (CV) at the anode (Figs. 3(a) and 3(b)). The interconnected reticular membrane structure obtained by gradual deposition is beneficial to mass and charge transfer and improve the OER activity ($\eta_{10} = 329$ mV) [111]. Fischer et al. prepared NiFe-BDC (BDC = 1,4-phthalic acid) surface mounted metal-organic framework (SURMOF) by layer-by-layer deposition, which was subsequently converted to NiFe-BDC(X)SURMOFD in an alkaline electrolyte (Figs. 3(c)–3(f)). The highest OER activity can be obtained when the Ni/Fe feed ratio was 6:1 and the η_{200} was only about 210 mV [112].

2.5 Wet chemical method

Wet chemical reaction is the reaction in solution, including leaching, chemical reduction, and photochemical reaction. Wet chemical method is relatively simple to operate, and the reaction conditions are relatively mild, by which a gram scale catalyst can be synthesized. At the same time, the surface energy of 2D nanomaterials can be reduced by using end sealers in the synthesis process, which is conducive to the growth of metal nanocrystals along a certain crystal orientation. Kundu et al. synthesized

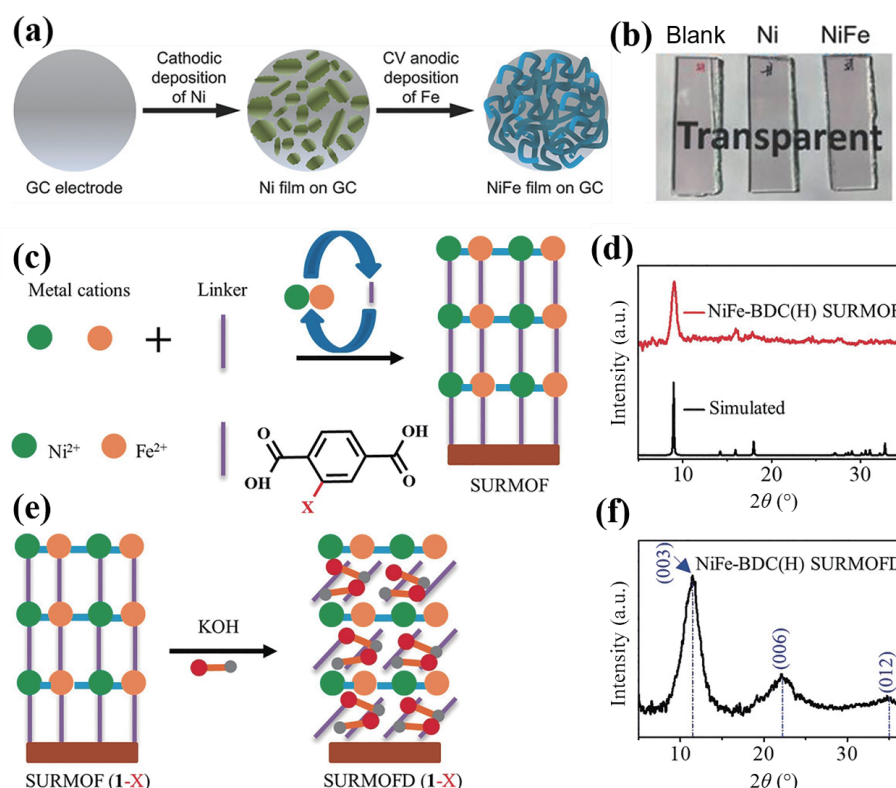


Figure 3 (a) Illustration of the synthesis of NiFe-SW film by stepwise electrodeposition strategy. (b) Corresponding optical images of the films on indium tin oxide (ITO). (c) Preparation of NiFe-BDC(X)SURMOFs by layer-by-layer deposition. (d) Grazing incidence XRD (GIXRD) of NiFe-BDC(H)SURMOF. (e) Transformation of NiFe-BDC(X)SURMOFs to NiFe-BDC(X)SURMOFDs. (f) GIXRD of NiFe-BDC(H)SURMOFD. (a) and (b) Reproduced with permission from Ref. [111], © WILEY-VCH Verlag GmbH & Co. KGaA, Weinheim 2017. (c)–(f) Reproduced with permission from Ref. [112], © Li, W. J. et al. 2020.

trimetallic NiCoV-LDH by wet chemical method. The catalyst showed good OER performance with an overpotential of 280 mV (η_{10}), and the introduction of trivalent vanadium promoted electron transfer [113]. Chen et al. synthesized 2D NiFe₂O₄/NiFe LDH composite by wet chemical method at low temperature. The synergistic effect of NiFe LDH and NiFe₂O₄ improved the catalytic OER activity, and the minimum overpotential was 190 mV (η_{100}) [114]. Kundu et al. prepared three different MOF fiber networks using wet chemistry and then synthesized the corresponding nanofibers (zeolitic imidazolate framework (ZIF-67) NFs, Fe-ZIF NFs, and Fe-incorporated ZIF-67 NFs) using electrostatic spinning technique. In the bimetal ZIF, the synergistic effect of Co and Fe promoted the rapid diffusion of intermediates and reduced the OER energy barrier. When FeOOH was formed in the reaction process, the reaction rate was improved. Fe-incorporated ZIF-67 NFs showed a small η_{10} of 278 mV during OER [115]. The advantages and disadvantages of the five synthesis methods are listed in Table 1.

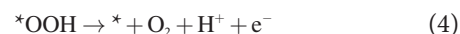
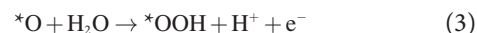
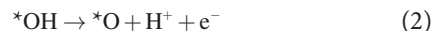
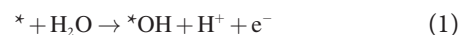
2.6 Other methods

Besides the above methods, chemical vapor deposition (CVD) and pyrolysis method are also used to synthesized 2D materials. CVD is a process in which gaseous materials react at gas or gas–solid interface at a certain temperature to form solid products with few structural defects [127]. Pyrolysis technology is usually used for the synthesis of 2D COF and MOF derivatives. The precursors are synthesized by hydrothermal synthesis or other technologies and their derivatives are obtained by pyrolysis. Han et al. synthesized S-doped NiFe-LDH nanosheets (NiFe-LDH-S) on porous carbon cloth using CVD technology. The catalyst showed excellent electrocatalytic activity ($\eta_{100} = 296$ mV) and stability in seawater [128]. Cao et al. synthesized ultra-thin (~ 1.3 nm) and mesoporous Co-LDH by CVD method, which showed high catalytic OER activity ($\eta_{10} = 265$ mV) [129]. Guan et al. synthesized NiO microflake@NiFe LDH nanosheets on nickel foam by two-step hydrothermal synthesis and calcination [130]. Peter et al. synthesized tetrazine-based COF (TZA-COF) on redox graphene (TZA-COF-RGO) and subsequently obtained Co-encapsulated nitrogen-doped graphite carbon (Co@NGC-600) by leaching and annealing. Among them, Co around C–N bond is the key active site to improve the activity, where Co atoms can adjust the electronic characteristics of N-doped carbon matrix, resulting in high activity and high selectivity [131]. By calcination of ZIF-67/COF composite, Wang et al. obtained highly dispersed Co₃O₄ nanoparticles (Co₃O₄/NPC) on N-doped porous carbon with uniform particle size and high surface area. DFT calculations showed that the catalytic OER performance of Co₃O₄/NPC was due to the geometric and electronic effects on the activation and adsorption/desorption [132].

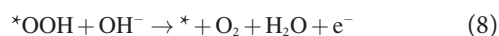
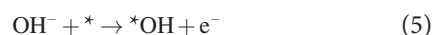
3 OER mechanism

Due to four-electron coupled with proton transfer, the sluggish

dynamics of OER usually requires a high thermodynamic potential [133]. With the help of theoretical model, four-step OER route in acidic or alkaline media is proposed as follows
OER in acidic media:



OER in alkaline media:



where * represents the adsorption site in OER. In acidic media, H₂O is adsorbed on the catalyst surface, and OH* is produced, which in turn breaks down into O*, and then combines with H₂O to form the intermediate *OOH. Finally, oxygen is released. However, in alkaline media, the OER mechanism is different. First, the HO⁻ in the solution is adsorbed to form OH*, which is then decomposed into O* and H₂O. The resulting O* continues to combine with OH⁻ to form *OOH, which combines with HO⁻ to release O₂ and H₂O. In the OER process, the reaction rate is determined by the highest kinetic energy barrier step, that is, the rate control step, which determines the performance of the catalyst [134].

OER is more likely to occur under alkaline conditions, which is attributed to the fact that under alkaline conditions, the presence of a large amount of OH⁻ is conducive to the formation of reaction intermediates *O and *OOH, thus facilitating the release of oxygen. In acidic solution, OH⁻ comes from the decomposition of H₂O, and the concentration is far lower than that in alkaline solution. In addition, for LDH catalysts, they usually display good catalytic ability and tolerance in alkaline solution, but they are inevitably dissolved in acidic solution. OER evolution mechanism can be divided into two kinds, namely, adsorbent evolution mechanism (AEM) and lattice oxygen oxidation mechanism (LOM) (Fig. 4) [135]. However, most of the current reports are based on AEM, that is, the continuous adsorption and desorption of the reaction intermediates take place at active sites. There are few reports on LOM, and most are based on LDH catalysts with cobalt participation.

DFT calculations can be used to study the electrochemical reaction process at the micro level [136]. At present, the relationship among catalyst structure and active center needs to be

Table 1 Comparison of the advantages and disadvantages of the synthesis methods

Synthesis method	Advantage	Disadvantage	References
Exfoliation techniques	Mild conditions, simple process, and easy to synthesize single or few layers of 2D materials	Uncontrollable size, low production rate, and high energy consumption	[116–118]
Hydrothermal/solvothermal method	Suitable for large-scale synthesis	Needing specialized equipment and hard to precisely control nanosheet layers	[119, 120]
Coprecipitation method	Easy to operate, low cost, and low temperature synthesis	Easy agglomeration and hard to obtain high-quality 2D materials	[109, 121]
Electrochemical deposition	Controllable thickness and size and low consumption	Uncontrollable microstructure and formation of byproduct	[122–124]
Wet chemical method	Convenient operation and suitable for large-scale synthesis	Uncontrollable microstructure	[125, 126]

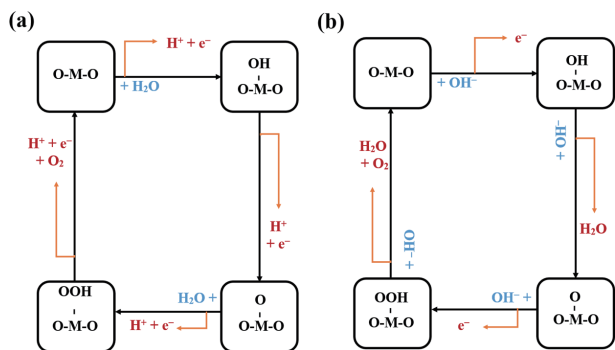


Figure 4 OER mechanisms under (a) acid and (b) alkaline conditions.

discussed in detail. The relationship between structure, reaction and mechanism should be established by combining theory and experiment. At the same time, the combination is conducive to studying the mechanism of surface atom interaction and understanding the electrocatalytic OER process from the perspective of atoms [137]. Gibbs free energy diagram in DFT calculations includes thermodynamic state and kinetic state, which can intuitively judge the reactive site and rate determining step (RDS) [138, 139]. In this section, we will discuss some important results of DFT calculations for electrocatalytic OER, including Gibbs free energy diagram, state density, band structure, and charge analysis.

3.1 Gibbs free energy diagram

Gibbs free energy diagram is one of the most commonly used activity evaluation criteria for electrocatalysis. In the diagram, the relative energy of basic steps in the reaction process can be given. The reaction thermodynamics determines the activation energy barrier between each step, and they determine the OER overpotential. Gibbs free energy diagram has been widely used to compare the intrinsic activity of different catalysts. Figure 5 shows the 4e⁻ mechanism and the four-step Gibbs free energy diagram of OER on CoFe-LDHs and Ru/CoFe-LDHs [140]. Ru/CoFe-LDHs

were obtained by loading the ruthenium hydroxyl complex on the (001) crystal plane of CoFe-LDHs, in which Ru atoms are coordinated with five oxygen atoms. The formation of the *OOH species from the *O species (step III) in the OER is the RDS. The Gibbs free energy of RDS at the Ru site on the surface of CoFe-LDHs is 1.52 eV, which is lower than that of Fe site at the edge of CoFe-LDHs (1.94 eV) and the overpotential on Ru active site in Ru/CoFe-LDHs (0.29 eV) is lower than the overpotential on Fe site in CoFe-LDHs (0.71 eV). These results indicated that Ru atom is the key active site for the OER. The adsorption of reaction intermediates is closely related to their structure and composition. The introduction of dopants can change the chemical environment around the active site and change the activity, thus producing different energy diagrams. Theoretical calculations showed that the catalytic OER performance of bimetallic electrocatalysts is often better than single metallic electrocatalysts. When Ni was introduced into Co-C system, the interaction reduced OER energy barrier, which was consistent with the experimental results [141].

3.2 Density of states (DOS) and band structure

DOS can be used to measure the conductivity of catalysts, especially those containing similar structures and components. The smaller the band gap between valence band (VB) and conduction band (CB), the higher the DOS around the Fermi level, indicating that the higher the concentration of charge carriers, the higher the electronic conductivity. Figure 6 shows that electrons transfer from Ni-MOF to LDH, and the charge density of Ni atom is reduced. In addition, according to the signal intensity near Fermi level, VB (1.09 eV) moves to the negative vacuum level (VB_{max/LDH} = 1.18 eV) after the formation of Ni-MOF and LDH heterostructure, which indicates that DOS and conductivity near Fermi level increase in the Ni-MOF/LDH. In addition, the d-band center of Ni in the heterogeneous structure moves upward (-1.33 eV), indicating that Ni-MOF/LDH has stronger adsorption for intermediates. Compared with LDH and

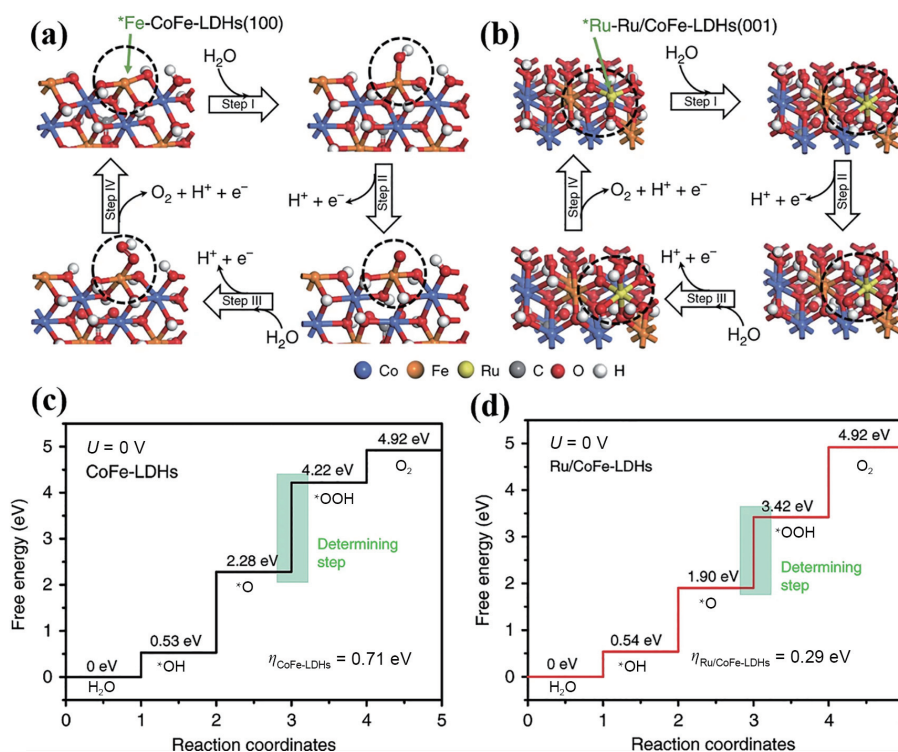


Figure 5 Proposed 4e⁻ mechanism of OER on (a) CoFe-LDHs and (b) Ru/CoFe-LDHs Gibbs free-energy diagram for the OER on (c) CoFe-LDHs and (d) Ru/CoFe-LDHs. Reproduced with permission from Ref. [140], © Li, P. S. et al. 2019.

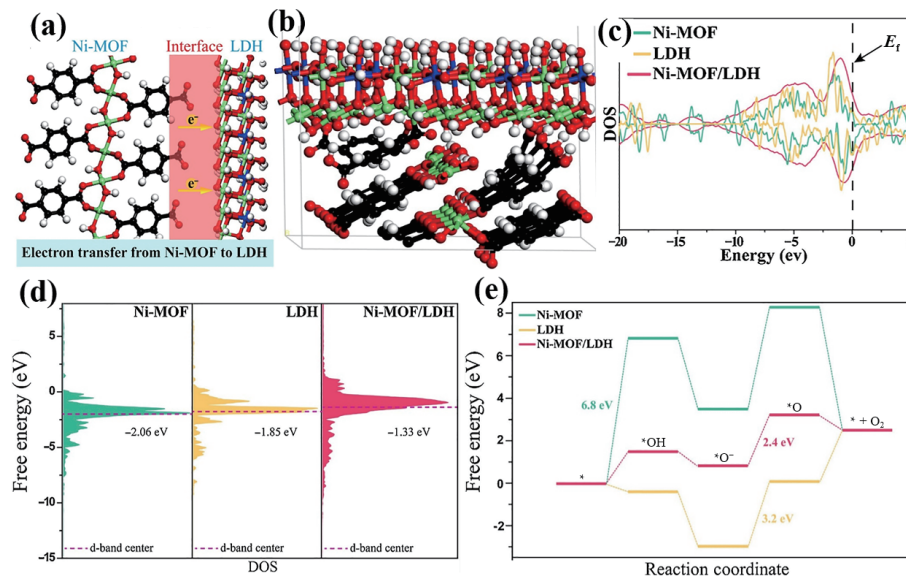


Figure 6 (a) Schematic of the partial electron transfer at the interface. (b) The optimized heterostructure of Ni-MOF/LDH. (c) DOS of Ni-MOF, LDH, and Ni-MOF/LDH. (d) DOS of Ni 3d orbitals of Ni-MOF, LDH, and Ni-MOF/LDH. (e) Gibbs free energy diagram on the surface of catalysts. Reproduced with permission from Ref. [142], © Elsevier B.V. 2021.

Ni-MOF, the energy barrier of RDS on Ni-MOF/LDH is lower ($\Delta G = 2.4$ eV) [142].

By tuning the structure of catalysts, the internal band structure can be adjusted. Luo et al. doped nitrogen into NiFe-MOF to synthesize N-NiFe-MOF. Under alkaline conditions, H was removed from the terminal ligand to obtain irreversible structure. The d-band density (d-DOS) of Fe atoms in NiFe(NO)-MOF is farther from the Fermi level than that in NiFe(OOH)-MOF, while the p-DOS of *O adsorbed on NiFe(NO)-MOF moved upward, indicating that the adsorption capacity of oxygen decreased and the energy barrier of the rate-control step decreased, which is beneficial to the OER [143]. Luo et al. calculated the d-DOS of Co over $Co(OH)_2$, Co-MOF, and $Co(OH)_2/Co-MOF$ (Co1 and Co2) and found that the d-band of *Co1 on $Co(OH)_2/Co-MOF$ is farther from the Fermi level than the d-band of *Co on $Co(OH)_2$, indicating that the adsorption of oxygen intermediates on $Co(OH)_2/Co-MOF$ is weak. After OH adsorption, the oxygen density of $Co(OH)_2/Co-MOF$ is between the other two catalysts, which indicates that the oxygen intermediate on $Co(OH)_2/Co-MOF$ catalyst has the best adsorption free energy [144].

3.3 Charge distribution analysis

The spatial distribution of electron density in catalysts is usually described by charge density. The charge density of active site affects the adsorption and desorption of reaction intermediates during electrochemical reactions. The formation of heterojunction, interface, or new bond can cause charge rearrangement, and the difference is called charge density difference. Xuan et al. synthesized $FeS_2/CoNiSe_2$ heterostructure, and the different charge densities of the heterostructure indicated that charge transfer occurred on the heterogeneous interface, and the electrons showed a transfer trend from $CoNiSe_2$ to FeS_2 . The charge density of Ni atoms at the interface decreased, and the chemical state of Ni increased, which was more conducive to the OER [145].

In addition to the formation of heterostructures, the introduction of dopants is a common method to adjust the charge density, which can significantly improve the activity of catalysts in OER. Zhang et al. supported monatomic gold on NiFe LDH ($^*Au/NiFe$ LDH), and the OER activity increased by 6 times when modified by 0.4 wt.% Au ($\eta_{10} = 0.21$ V) [146]. The introduction of gold resulted in a charge difference of 0.32 e on the catalyst. The

charge was redistributed from Au to LDH, and electrons were induced to transfer to the surrounding O, Fe, and Ni atoms. The optimized charge density promoted the adsorption of OH^- and reduced the adsorption energy of the O^* and OOH^* intermediates (Fig. 7(a)). Chen et al. synthesized FEF-MOF array by solution-recrystallization method. Figures 7(b) and 7(c) show that when partial nickel was replaced by iron, charge was redistributed and electrons in the overlapping region of Ni 3d and Fe 3d were transferred to the surrounding O atoms, which is beneficial to the adsorption and desorption of reaction intermediates in the OER [147].

4 Characterization of 2D materials

2D materials have ordered layered structure, strong chemical bonds between planes, good electrical conductivity, large specific surface area, and easy to be modified. In theory, the relationship between structural properties and catalytic properties can be understood through computational models, but in experiments, there are still some problems in the in-depth study of reaction mechanism, which hinders the design and development of high-performance electrocatalysts. Therefore, it is necessary to clarify the reaction mechanism of electrocatalysts to obtain efficient 2D electrocatalysts. At present, various characterization techniques have been developed to detect the morphology, geometric configuration, catalytic active site, surface oxidation state, and local electronic structure of catalysts. In this section, the structural characterization of 2D electrocatalysts is briefly introduced.

4.1 Structural characterizations

The morphology of 2D materials can be observed by scanning electron microscopy (SEM) and transmission electron microscopy (TEM). The spatial resolution and energy resolution of advanced TEM can reach 0.05 nm and 7 meV, respectively [148–150]. X-ray photoelectron spectroscopy (XPS) can provide information about chemical bonding on the surface of 2D materials [151–153]. The crystal structure of catalysts can be determined by X-ray diffraction (XRD) [154]. The morphology and lattice can be detected by high angle annular dark field scanning transmission electron microscopy (HAADF-STEM). From Figs. 8(a)–8(d), the lattice fringes of single nanoparticles and core nanocrystals can be clearly seen [155]. Atomic force microscopy (AFM) can accurately

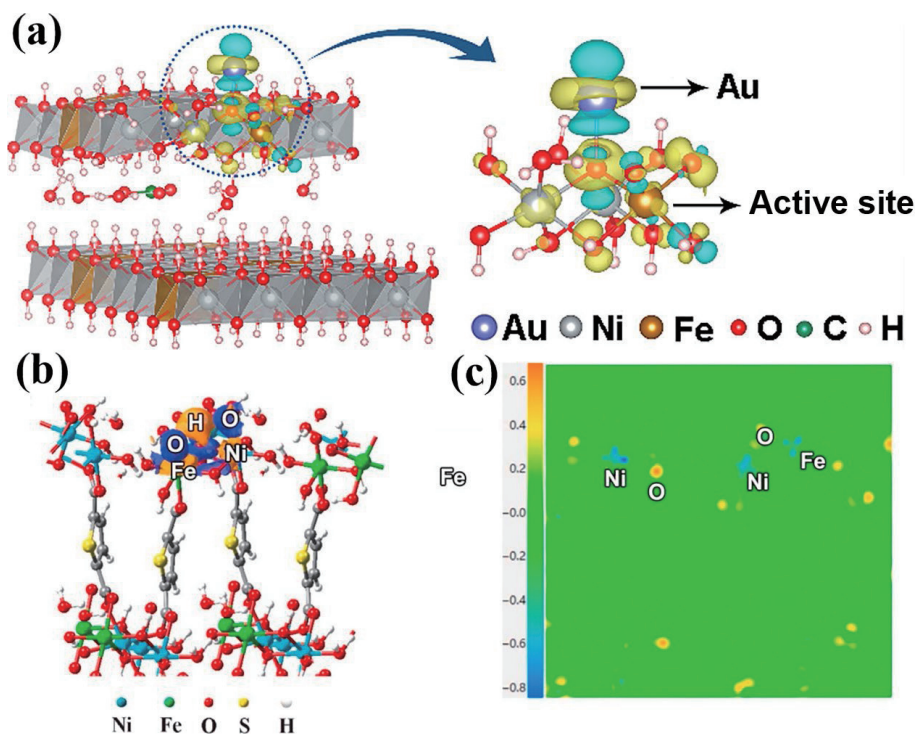


Figure 7 (a) Differential charge densities of NiFe LDH with and without Au atom. (b) Schematic 3D image of charge density difference of NiFe-MOF. (c) Schematic 2D slice of charge density difference of NiFe-MOF. (a) Reproduced with permission from Ref. [146], © American Chemical Society 2018. (b) and (c) Reproduced with permission from Ref. [147], © Elsevier B.V. 2021.

reflect the surface structure and properties of catalysts at atomic scale [156]. In Fig. 8(e), according to the size of the nanosheet, it can be judged that ultrafine nanoparticles were embedded into the MOF lattice to form heterogeneous nanosheets [157]. X-ray absorption fine structure (XAS) can be used to detect the local structure and electronic configuration of 2D materials. X-ray absorption near edge structure (XANES) and extended X-ray absorption fine structure (EXAFS) spectra can provide the coordination number, atomic spacing, and structural disorder [146, 158–160]. Compared with the standard NiO, the shift and rise of the peaks confirmed the positive charge state of Ni in Ni-COF, and the coordination of Ni atom with two N atoms and two O atoms in Ni-COF can be obtained from the position and strength of various characteristic peaks (Figs. 8(f)–8(j)) [161].

4.2 Operando spectroscopic studies

Monitoring the changes of atomic and electronic structures at active sites during electrocatalytic OER is of great help in designing catalysts with high catalytic performance. *In situ* characterization technology can be used to study the change of oxidation state and local electronic structure of catalyst surface under actual working conditions, which can provide information of the effective active site of the electrocatalyst in OER, catalyst structure evolution, and reaction mechanism, so as to further study the relationship between catalyst structure and catalytic activity. Raman spectroscopy is not easily disturbed by aqueous solution and is specific to oxides, which shows extremely high sensitivity at low frequencies. It can be used to measure and monitor the gradual oxidation, structure evolution, and reaction intermediates of catalysts under electrochemical conditions [162]. Figure 9(a) shows a schematic diagram of the electrochemical/Raman spectroscopic system [163]. Using *in situ* Raman spectroscopy, Luo et al. demonstrated that the structure of MOF in alkaline media is a self-reconstruction of the removal of H in the ligand, followed by oxidation at the metal center or on the ligand [143].

In situ XAS is a key technique for studying the electronic

structure and local geometric configuration of metal atoms on catalyst surface under electrochemical working conditions. XANES can be used to determine the valence state of adsorbed atoms. In addition, the front edge energy has a linear relationship with the oxidation state of bulk oxides. EXAFS can reflect the local geometric structure of adsorbed atoms by scattering photoelectrons by the number, distance, and arrangement of adjacent atoms. Figure 9(b) shows a schematic diagram of the *in situ* XAS characterization device [164]. Zhou et al. studied the catalytic mechanism of NiFe(OH)_x by using XANES spectroscopy. By monitoring the unoccupied state of metal 3d orbital in the OER process, the nickel changed from bivalent to trivalent and up to +3.6, and the iron increased from trivalent to tetravalent, showing a highly covalent Fe⁴⁺–O bond. The transfer of electrons between Ni and Fe led to the high catalytic activity of NiFe(OH)_x [165]. Bell et al. used XAS to obtain the local electronic environment of Ni and Fe cations in Fe-doped NiO_x catalyst during OER process, and monitored the oxidation and M–O bond length change with the increase of applied potential. As the applied potential increased, iron was oxidized to +3, and Ni was oxidized to +3. It was revealed that Fe³⁺ occupied the octahedral position in Ni_{1-x}Fe_xOOH, and the Fe–O bond spacing was very short, because it shared the edge with the surrounding [NiO₆] octahedron [166].

5 OER application

2D materials have good catalytic performance in electrochemical field due to their surface physicochemical properties and crystal structure. 2D materials have ordered layered structure, strong chemical bonding between planes, and good electrical conductivity. In addition, 2D materials are easy to be modified and regulated, and the surface of 2D materials has a high exposure rate of atoms, while atoms on the surface are prone to escape and form vacancy defects, providing more active sites for electrocatalytic reactions. In 2D materials, the electrocatalytic properties can be improved by optimizing the electronic structure.

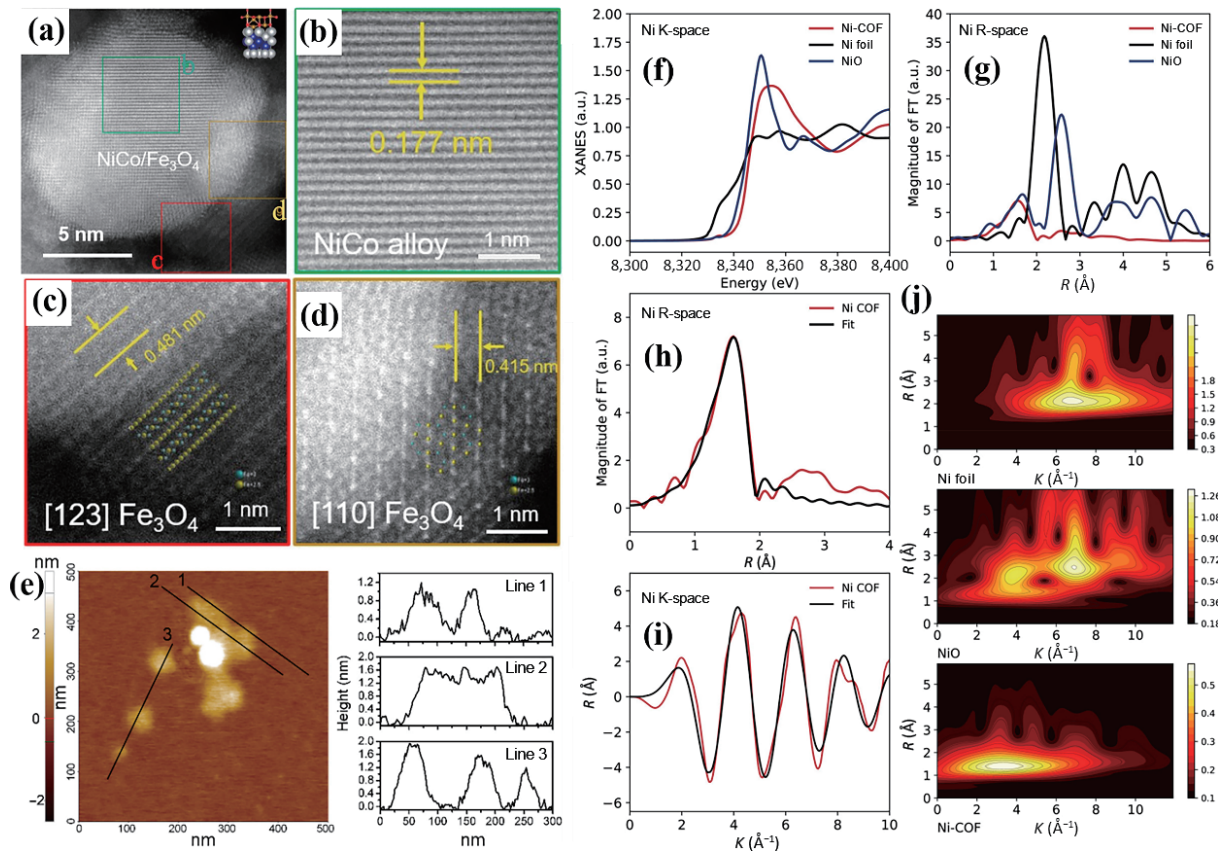


Figure 8 (a) HAADF-STEM image of NiCo/Fe₃O₄ nanoparticle and (b)–(d) enlarged high-resolution HAADF images. (e) AFM image of M-PCBN and the corresponding height profiles. (f) XANES spectra of Ni-COF. (g) Fourier transforms of the EXAFS spectra for Ni-COF, Ni foil, and NiO. (h) and (i) EXAFS fitting curves of Ni-COF at R-space and K-space. (j) Wavelet transform (WT) of Ni foil, NiO, and Ni-COF. (a)–(d) Reproduced with permission from Ref. [155], © American Chemical Society 2018. (e) Reproduced with permission from Ref. [157], © American Chemical Society 2020. (f)–(j) Reproduced with permission from Ref. [161], © American Chemical Society 2021.

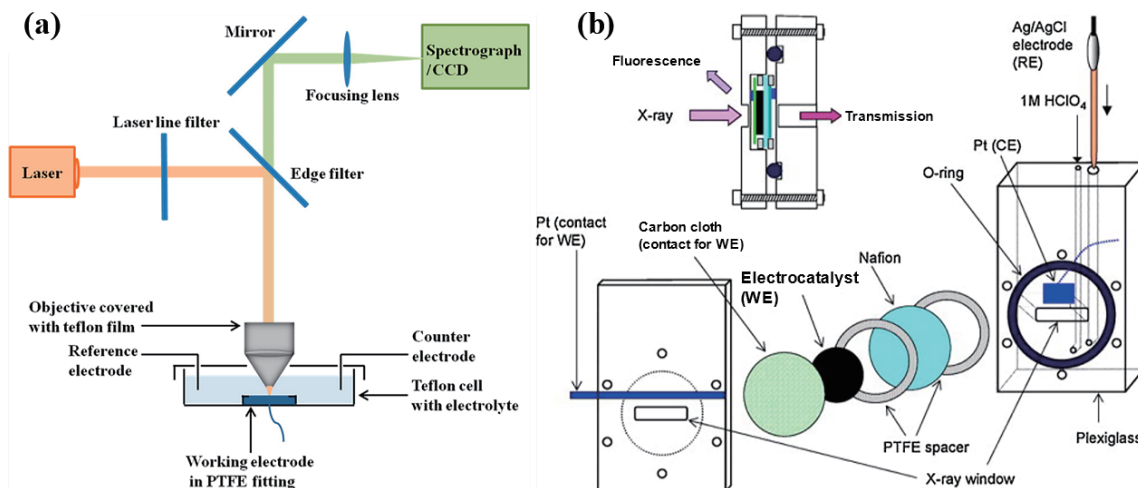


Figure 9 (a) Schematic diagram of an electrochemical/Raman spectroscopy setup. (b) Schematic diagram of *in situ* electrochemical cell used for XAS. (a) Reproduced with permission from Ref. [163], © American Chemical Society 2017. (b) Reproduced with permission from Ref. [164], © Elsevier Ltd. 2010.

The homogeneity of 2D materials and the small density of electronic states between the layers provide opportunities for modification, surface function, and heterostructure construction, thus providing directional control of the electronic structure and geometric configuration to improve the catalytic activity of OER. In this section, we mainly introduce the regulation of the catalytic activity of four kinds of 2D materials (LDHs, COFs, MOFs, and hybrids) for OER.

5.1 LDH electrocatalysts

LDHs are a kind of ionic solids with 2D layered structure. They

are composed of three parts, namely the upper and lower layers and the interlayer, which are positively charged brucite-like main layer, negatively charged anion, and neutral solvent particle in the interlayer region, respectively. Positively charged metal cations, usually with a +2 or +3 valence, occupy a center surrounded by six hydroxide ions, forming MO₆, which repeats the unit to form a two-dimensional sheet. The monolayer composed of octahedral MO₆ is positively charged and therefore requires a negatively charged anion to lie between the two layers to keep the whole LDH electrically neutral [167–170]. Metal cations and anions give LDHs unique redox properties, big interlamellar areas, and

adjustable lamellar material properties, which make the OER catalytic activity greater than bulk transition metal oxides/hydroxides [171]. In addition, there are two layers of hydroxides between the cation layers of LDH, which can exchange ions or introduce macroanions or water molecules, allowing electrolyte ions to move freely between layers.

Amongst non-noble metal LDHs, NiFe-LDHs, due to their affordable price, rich contents, and unique 2D structure, show great prospects in catalyzing OER in basic electrolytes [94, 172]. Through the functionalization of NiFe-LDHs, including doping element, manufacturing defect, and hybridization with other materials, and changing their surface structure and composition, the OER catalytic activity of NiFe-LDHs can be greatly improved [173–175]. In addition, by regulating the electronic structure of NiFe-LDHs, the optimal active site for the adsorption/desorption of OER intermediates can be formed, and the energy barrier can be reduced, which is conducive to the release of oxygen [176].

By regulating Ni/Fe ratio in NiFe-LDH, the formation efficiency and specie of OER intermediates can be affected, and the catalytic capacity of NiFe-LDH can be improved. Wang et al. synthesized NiFe-LDHs nanosheets by hydrothermal method, in which the iron content was adjusted from 0% to 36% [177]. When the Fe content was 25%, the OER overpotential was the lowest ($\eta_{10} = 140$ mV), and the evolution of NiFe(OH)₂ to NiFeOOH occurred during the reaction. Zhou et al. prepared a series of Fe-Ni hydroxide nanosheets with different Ni/Fe ratios, in which the η_{10} was 261 mV at 60% Fe content [178]. The excellent OER performance can be attributed to the enhancement of electrochemical area of the nanosheet network structure, the appropriate metal proportion adjusting the electronic structure, and increased transfer of electrons.

In situ growth is an excellent synthesis method for preparing 2D materials. Ultra-thin Ni-Fe LDH was prepared by Xie et al., which showed a current density of 284.4 mA·cm⁻² at overpotential of 500 mV [179]. Zhou and coworkers studied the influence of interlayer ions on electrochemical OER activity [180]. A variety of characterizations revealed that interlayer ions changed the electronic structure of metal atoms exposed on the surface. As we all know, anions have a strong reduction ability and tend to provide more electrons to NiFe layer, which makes the metal active sites in the outer layer tend to high valence stable state. This method is a very important strategy to improve OER activity. Different interlayer ions have different effects on OER activity.

5.1.1 Metal modified NiFe-LDHs

DFT calculations showed that 3d metal oxides can be regulated by non-3d high-valence metal tungsten to provide optimal adsorption energy for OER intermediates. Using this property, Jin et al. synthesized a trimetal NiFeCr layered hydroxide electrocatalyst. The three metals have a variety of valence states, which provided the possibility to produce robust electron interactions inside the catalyst. Moreover, the synergistic interaction between Ni, Fe, and Cr improved the catalytic activity of OER. Feng et al. synthesized hybrid Co-NiFe layered dihydroxide by hydrothermal method [181]. The introduction of cobalt changed the electronic structure of NiFe-LDH, and the rapid transfer of electrons and reaction intermediates promoted the release of O₂, thus achieving the purpose of improving the catalytic performance of OER ($\eta_{10} = 278$ mV). Wang et al. synthesized FeV-doped nickel hydroxide and successfully introduced them into the lattice, which well-adjusted the local coordination environment and electronic structure [182]. DFT calculations showed that vanadium site in the catalyst was the best site for OER, and the overpotentials ($\eta_{10} = 200$ mV and $\eta_{100} = 264$ mV) were lower than those of undoped sample.

The doping of the third element could transform LDHs into trimetallic layered hydroxides. Wang et al. prepared ternary layered LDH by spontaneous ion exchange [183]. Dinh et al. reported the application of ternary layered hydroxide NiFeV in OER, obtaining the optimal molar ratio of the metal NiFeV [184]. The introduction of the third species can effectively change the local electronic structure and promote the OER process [185]. The Pt-NiFe LDH OER electrocatalyst reported by Anantharaj et al. can reach the current density of 10 mA·cm⁻² at an overpotential of 230 mV [169].

5.1.2 Defect modified NiFe-LDHs

Defects are easy to be introduced in 2D NiFe-LDHs. Changes in composition and structure of metal hydroxide in the synthesis process will produce various defects, and due to low coordination environment, unsaturated defects are often conducive to structural reforming [186, 187]. However, in Fe-Ni based hydroxides, the configuration of vacancy defects is relatively simple, usually Fe³⁺ or Ni²⁺ vacancy, which can not only act as active sites but also activate the surrounding metal sites, thus improving the OER activity [188]. Kim et al. synthesized NiFe-LDHs with oxygen deficiency by direct growth method, and the karst morphology and oxygen deficiency enabled the catalyst to have rich number of active sites and accelerated mass transfer [189]. Sun et al. used flame etching to introduce a large number of oxygen vacancies and nanohexagonal defects in NiFe-LDH [190]. Abundant oxygen vacancies, electron-rich structures at metal sites, and low coordination numbers reduced the initial OER potential. Theoretical calculations showed that the introduction of defects reduced the reaction energy barrier. In the NiFe-LDH catalyst with oxygen vacancy, ΔG of only 0.84 eV was needed to initiate OER, which was lower than that (0.92 eV) without defects.

The rearrangement of electrons and the change of metal valence state caused by defects play an important role in the OER catalysis, and the unsaturated coordination and metal sites have an important effect on the formation and transformation kinetics of reaction intermediates. Sun et al. synthesized NiFe LDH with unsaturated coordination sites by using fluoride precovering strategy [191]. The unsaturated metal sites could be controlled on the surface of NiFe LDH, showing a low overpotential ($\eta_{10} = 243$ mV). The catalytic activity for OER was significantly better than that of the original NiFe LDH catalyst. Zhang et al. prepared layered NiFe LDH microtubules rich in oxygen vacancies (*v*-NiFe LDH) with the help of template assisted strategy [192]. The catalyst has abundant active sites and good structure stability. The existence of defects improved the conductivity. The defects significantly improved the OER activity of the *v*-NiFe LDH, showing an overpotential (η_{10}) as low as 195 mV and almost no degradation of the catalytic activity after 20 h. DFT calculations revealed that the iron site was the main active site of OER, and the oxygen vacancy mainly affected the band gap to improve the conductivity and improve the reaction kinetics.

The construction of NiFe LDHs with micro-nano structures rich in defects can provide abundant electrochemical active sites for the OER. Yan et al. synthesized layered dihydroxide nanosheets with a thickness of about 1.3 nm by rapid coprecipitation method, in which the Faraday efficiency of NiFe-LDH NSs was close to 100% [107]. There are a large number of defect sites and distorted lattice structure in the catalyst. Theoretical calculations showed that there is an extremely low band gap and spin polarization in the NiFe-LDH catalyst, which can improve the electron migration rate in the OER.

Most of the current reports on NiFe-LDHs focused on the OER activity, and few studies focused on their stability, which determines whether they can be used on a large scale in industry.

Liu et al. revealed that the catalytic OER activity of massive NiFe LDH decreased gradually [193]. They reported the inactivation mechanism, that is, the OER activity and proton transfer could be enhanced in the interlaminar basal plane, while the OER activity was continuously decreased due to the continuous dissolution of NiFe LDH in the interlayer. Stripping NiFe LDH into atomic thin layer can effectively improve the stability of OER. Waterhouse et al. revealed that the instability of the NiFe-LDH catalyst in alkaline solution is caused by partial inactivation of the active sites and the formation of independent NiOOH and FeOOH [175]. They proposed that cation vacancy constructed on the NiFe-LDH substrate can effectively improve its OER stability since the introduction of cationic vacancy greatly slows down the dissolution of metal cations. Metal cations in NiFe-LDH form octahedral coordination with oxygen atoms, and the introduction of divalent metal cations reduces vacancy, while trivalent metal cations increase vacancy, suggesting that the valence state of nickel can be adjusted by introducing metal cations with different

valence states. In the hybridization of Fe 3d-O 2p, increasing vacancies can enhance the binding energy of iron and oxygen and reduce the dissolution of ferric ions (Figs. 10(a) and 10(b)). The metal at the edge site is more soluble than the metal at the base plane site. However, when the cation vacancy is introduced, the dissolution of metal atoms at the edge site is significantly increased, and the dissolution ability of edge and base plane is basically equal. The dissolution energy of iron ion is higher than that of nickel ion no matter where it is located (Figs. 10(c) and 10(d)). Fe plays an important role in controlling the stability of NiFe-LDH catalyst. The vacancy around the iron provides space for the twisted FeO₆ octahedron, making the iron in the lattice insoluble (Figs. 10(e) and 10(f)). To sum up, the principle of introducing vacancy to inhibit metal dissolution is to enhance the binding energy between metal and oxygen and release lattice distortion. From Figs. 10(g)–10(l), both voltage and vacancy will affect the OER intermediates. Compared with original NiFe LDH catalyst, the introduction of trivalent metal ion vacancy makes the

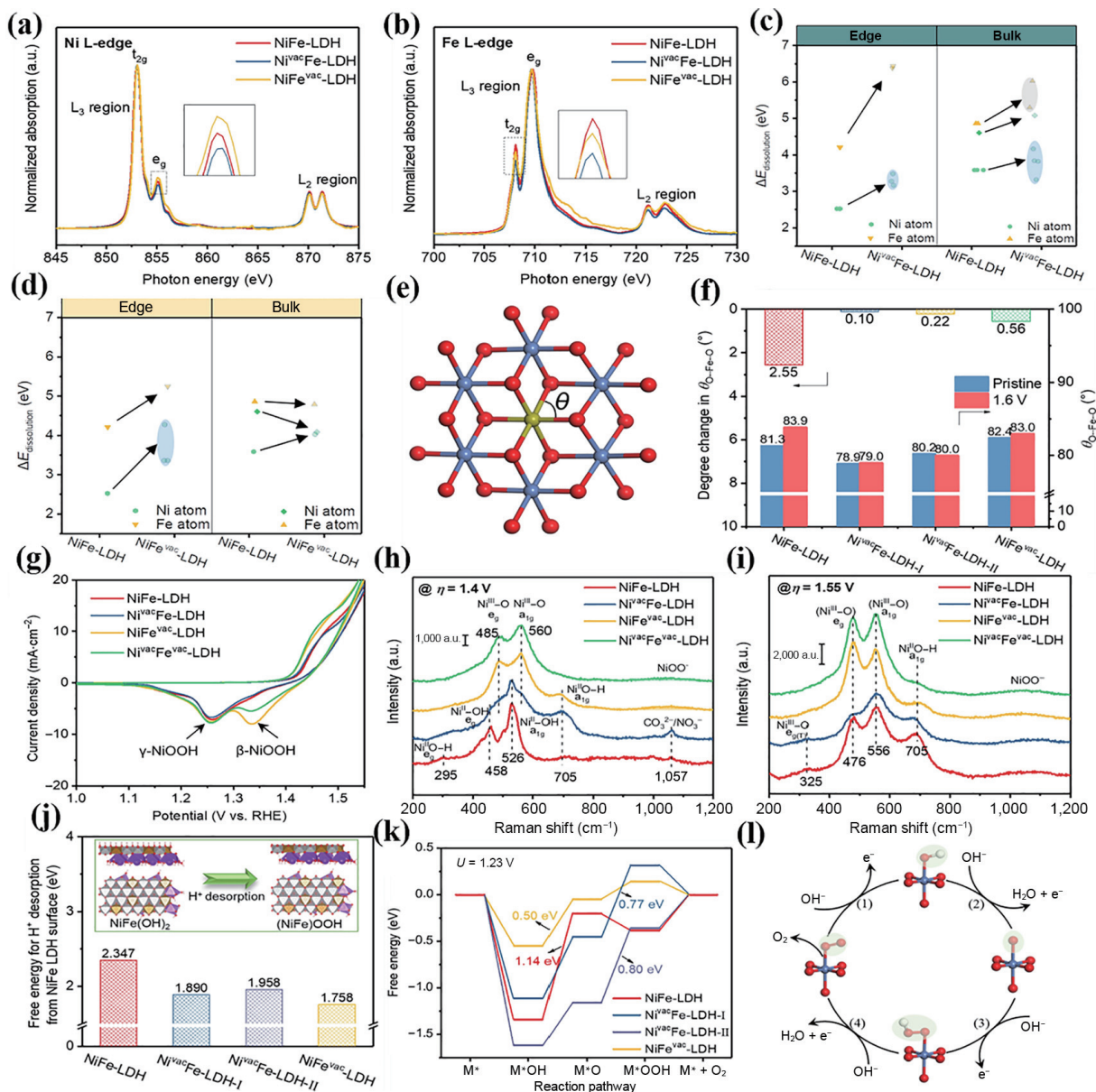


Figure 10 (a) and (b) X-ray absorption spectra. Calculated dissolution energy of metal atoms in NiFe-LDH with different structural configurations: (c) M²⁺ vacancies and (d) M³⁺ vacancies. (e) Schematic of the angles used to determine the local structural changes in NiFe-LDH. (f) The local structure angles of NiFe-LDH. (g) ECSA-normalized CV curves. (h) and (i) Raman spectra at an applied potential of 1.4 and 1.55 V vs. RHE. (j) Calculated free energy of H⁺ desorption from the surface of different NiFe-LDH-based structural models and (k) free energy diagram. (l) Proposed OER mechanism. Reproduced with permission from Ref. [175], © Wiley-VCH GmbH 2021.

OER process more favorable in thermodynamics. DFT calculations showed that the deprotonation free energy (1.76 eV) in the NiFe LDH with trivalent metal ion vacancy is lower than that of the original LDH catalyst (2.34 eV). In the original NiFe LDH catalyst, the introduction of cation vacancies can also reduce the maximum reaction free energy (ΔG_{PDS}) of the potential-determining step. The ΔG_{PDS} of the introduced bivalent cation vacancy at the nickel site is 0.77 or 0.80 eV, while the ΔG_{PDS} of trivalent cation vacancy is 0.50 eV, providing higher OER activity. The introduction of a trivalent metal ion vacancy reduces the binding of the intermediate at the active site. In conclusion, the introduction of vacancies not only increases active sites but also optimizes the binding energy of the reaction intermediates, and ultimately improves the OER activity and stability.

By reducing the size of catalysts, the vacancies can be increased. Zhang et al. synthesized ultrafine porous monolayer NiFe-LDH nanosheets with the thickness less than 3.0 nm by ultrasonic stripping technology, where there were a large number of metal and oxygen vacancies, showing an OER overpotential (η_{10}) of 230 mV [194]. Theoretical calculations showed that the presence of vacancies greatly enhanced the adsorption of water and facilitated the bonding of OH^* intermediates in the OER. Lang et al. synthesized porous ultra-thin NiFe LDH with cationic and anionic vacancies by assisted etching method [195]. The porous structure, nickel ion vacancy, and oxygen vacancy together improved the OER performance, and the catalyst had a low overpotential ($\eta_{10} = 170$ mV). DFT calculations indicated that the OER performance was significantly improved because the oxygen vacancy inhibited the $3d-e_g$ of the nickel site around it and facilitated the d-band center to move towards the direction of small electron energy barrier.

Cationic and anion vacancies are usually simple metal and oxygen vacancies, which can activate surrounding metal sites to act as new active sites. However, for defects, they are unstable and can be transformed into other types of vacancy defects, such as V_{MOH} and $V_{\text{MOH-H}}$ at certain applied voltages. Li et al. reported that cation dissolution was made by cation coordination between N,N-dimethylformamide (DMF) and NiFe-LDH to form NiFe-LDH

with cation vacancy [196]. In NiFe-LDH, the absence of cations elongated the Fe–Ni bond, resulting in the formation of highly oxidizing $\text{Fe}^{(3+\delta)}$. Under alkaline conditions, the evolution of cationic defect structure in the OER process is as follows $V_{\text{M}} \rightarrow V_{\text{MOH}} \rightarrow V_{\text{MOH-H}}$ (Figs. 11(a) and 11(b)). According to the formation energy of different defects, the difficulty of their formation can be obtained, and the energy required for the formation of $V_{\text{M}} \rightarrow V_{\text{MOH}} \rightarrow V_{\text{MOH-H}}$ defects increases gradually. Compared with the original NiFe-LDH, the adsorption strength of oxygen-containing substances on the defective NiFe-LDH was improved. The negative adsorption energy of the catalysts with V_{MOH} and $V_{\text{MOH-H}}$ vacancies for oxygen species is greater than that of V_{M} . The variation of Gibbs free energy in the four-step OER reaction shows that the vacancy configuration affects the OER activity, and the ΔG_3 is smaller in the structures with V_{MOH} and $V_{\text{MOH-H}}$. The basic steps based on the calculation of the hydrogen electrode model and the maximum ΔG show that the thermodynamic limiting step is related to the oxidation of $^*\text{OH}$ to $^*\text{O}$ (Figs. 11(c)–11(g)).

5.1.3 Hybrid structure of LDHs

LDHs have the structure of transition metal oxides, and due to their inherent catalytic activity, the catalysis of OER under alkaline conditions has attracted extensive attention. Layered structure has good compatibility and flexibility, and many kinds of transition metal LDHs have been prepared, among which iron group elements have been widely studied due to their unique interactions [197]. However, small specific surface area, poor electrical conductivity, and less active site would affect their applications in the field of electrocatalysis. To improve the catalytic properties of LDHs, they can be hybridized with other 2D materials, such as carbon nanotubes, graphene, MOFs, and COFs, making full use of the synergy between these materials to improve OER performance.

The assembly between hydroxides and graphene can solve the problems of low specific surface area and low conductivity of LDHs. Theoretically, graphene has a specific surface area of $2,600 \text{ m}^2\text{g}^{-1}$ and a conductivity of $\sim 10^6 \text{ S}\cdot\text{cm}^{-1}$, which provides a

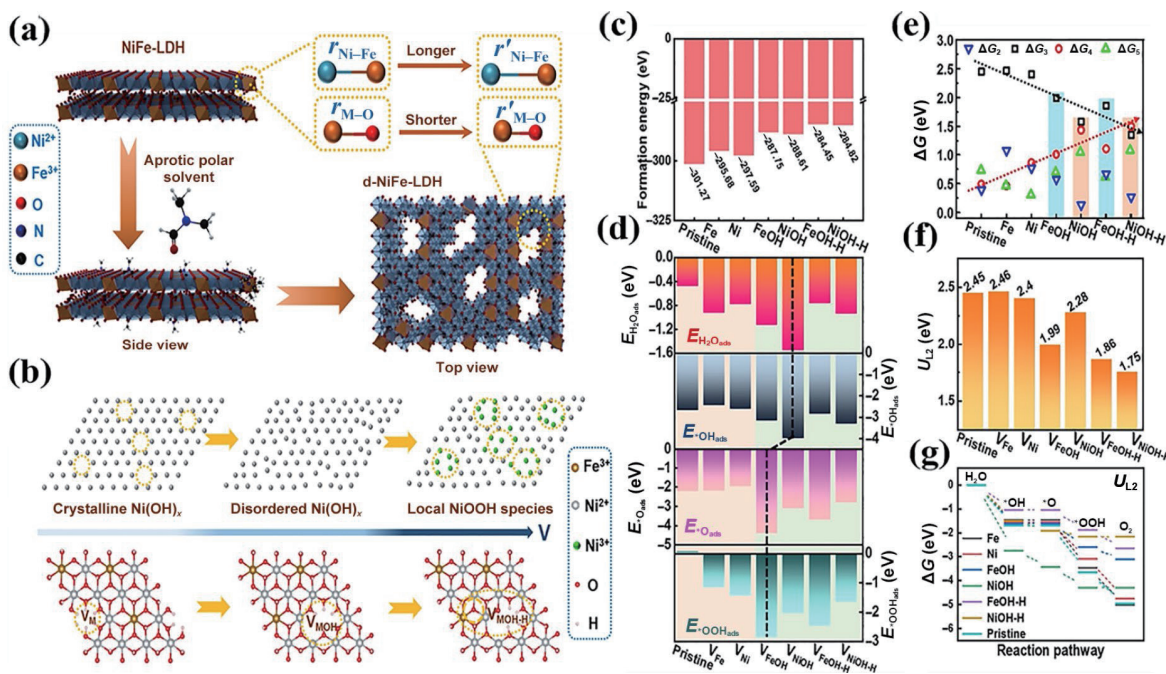


Figure 11 (a) The coordination between the aprotic polar solvent DMF and cations in NiFe-LDH. (b) Local conversion of crystalline $\text{Ni}(\text{OH})_x$ species. (c) Formation energy of DFT-optimized NiFe-LDH. (d) Adsorption energies of various intermediates. (e) Comparison of ΔG_i ($i = 2, 3, 4,$ and 5) for the four elementary steps in the OER process and (f) the corresponding thermodynamic limiting potential U_{L2} . (g) Gibbs free energy diagram. Reproduced with permission from Ref. [196], © Wiley-VCH GmbH 2021.

platform for charge transfer and mass transfer in catalytic reactions. Direct interfacial contact between 3d is possible when the positively charged LDH is alternated with the negatively charged graphene. Zhou et al. synthesized 3d transition metal LDH with different Ni/Fe ratios by uniform precipitation. Subsequently, the Ni-Fe LDH nanosheets were hybridized with graphene oxide (GO) to form a superlattice heterostructure [198]. In the whole structure, the nanosheets with different charges were successively arranged to enhance the conductivity of the material. The presence of GO can effectively prevent the aggregation of LDH nanosheets and increase the specific surface area of the material (Figs. 12(a)–12(d)). The assembled catalyst showed good OER performance with the overpotential (η_{10}) of 0.21 V. The combination of LDH and carbon nanotubes can form an interconnected conduction grid to promote electron transfer within the catalyst. Gong et al. reported the mechanism when NiFe-LDH and carbon nanotubes cooperated in the OER [199]. Near the edge of carbon, there was a significant π^* peak compared with that without NiFe-LDH in NiFe-LDH/CNT. When M-O-C was formed inside the catalyst, the carbon atom of carbonyl group was greatly disturbed (Figs. 12(e)–12(g)).

Hybrid materials show high electrocatalytic OER activity due to excellent structural characteristics and synergistic effect. The flawless 2D materials usually show poor OER activity, low adsorption energy, few active sites, and poor electrical conductivity. However, their electrocatalytic performance can be significantly improved by modifying them. Hybrid of LDHs with

other 2D materials can improve the electrocatalytic performance significantly. The weak van der Waals forces between layers of 2D materials make them possible for modifying the active sites. Wang et al. reported a 2D/2D heterojunction catalyst using lowtoxic solvent [200], which not only effectively avoided the aggregation of NiFe, but also promoted the formation of NiFe nanoflakes. DFT calculations proved that the existence of NiFe increased the stability of MoS₂. From the adsorption diagram, the binding energy of the Ni atom in the plane is very large. DOS showed that the catalytic effect of Ni/MoS₂ on OER was much lower than that of NiFe/MoS₂ because the electron mobility in the latter was greatly increased. Furthermore, the free energy of *OOH on the NiFe/MoS₂ was significantly reduced (Figs. 13(a)–13(d)). Jia et al. prepared NiFe LDH/graphene heterojunction. Theoretical calculations revealed that the internal electrons were rearranged during the synthesis of heterojunction catalyst. The electrons in NiFe LDH aggregated on the graphene, resulting in NiFe LDH holes, which enhanced the catalytic ability of OER (Figs. 13(e)–13(g)) [201].

Zhao et al. synthesized Co(OH)₂ derived from ZIF-67 by ion exchange method, and FeCo-LDH/Co(OH)₂ electrocatalyst was prepared by electrodeposition. FeCo-LDH and Co(OH)₂ layer acted as transportation hubs for accelerating electron transfer and material exchange [202]. In addition, bimetallic FeCo alloys can promote electron transfer at newly formed interfaces and enhance stability. Chu et al. reported the transfer of the electrochemical active center from Fe to Ni after ZnO deposition on NiFe-LDH by

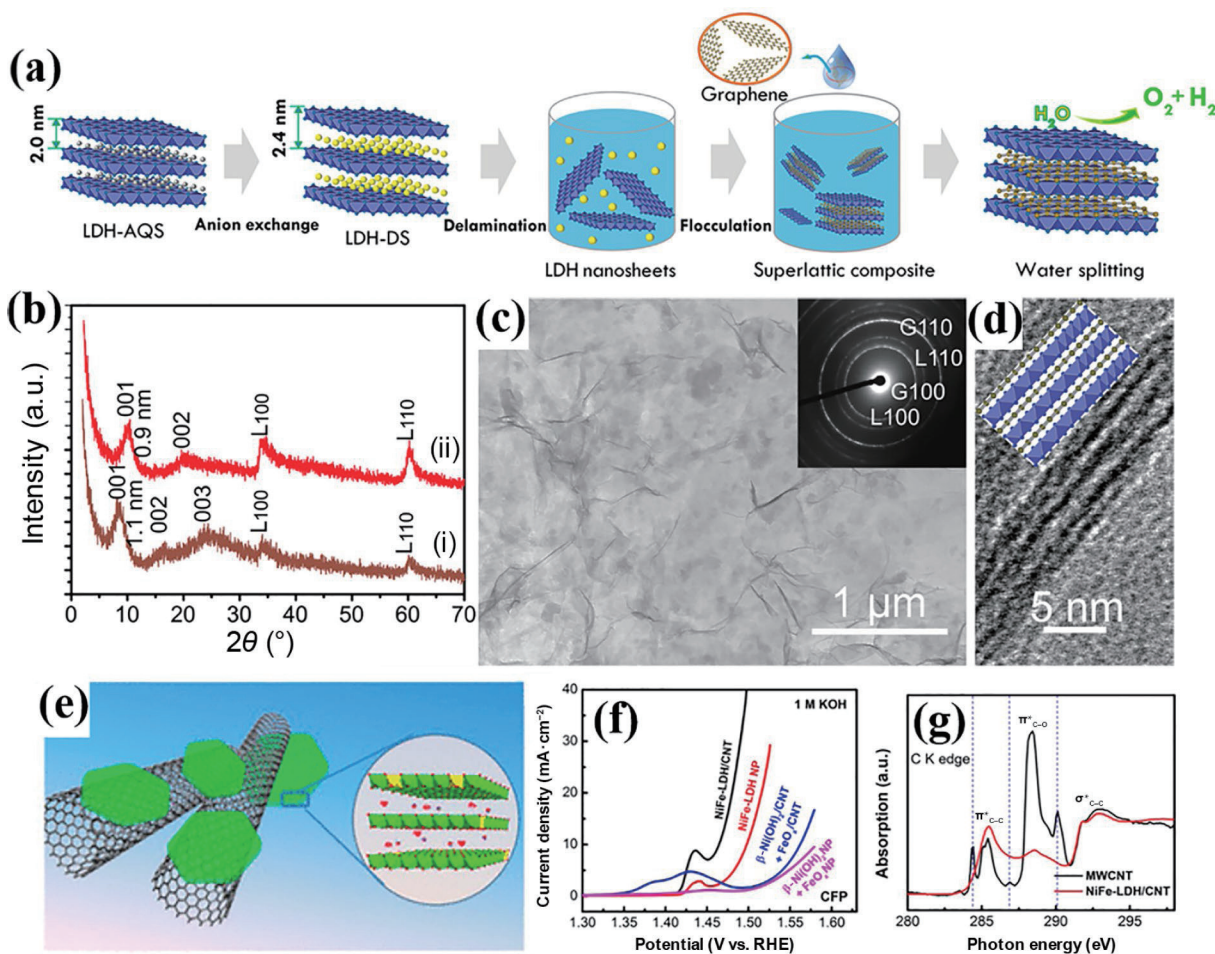


Figure 12 (a) Procedures of hetero-assembling Ni-Fe LDH nanosheets and graphene for water splitting. (b) XRD patterns of superlattice composites of Ni₂₃Fe₁₃-NS and (i) GO and (ii) reduced graphene oxide (rGO). (c) TEM image. (d) High-resolution TEM (HRTEM) and schematic illustration of alternately stacked LDH nanosheets and graphene. (e) Schematic showing the hybrid architecture and LDH crystal structure. (f) Polarization curves. (g) C K-edge XANES spectra of NiFe-LDH/CNT (black) and pure MWCNT (red) without coupling to LDH. (a)–(d) Reproduced with permission from Ref. [198], © American Chemical Society 2015. (e)–(g) Reproduced with permission from Ref. [199], © American Chemical Society 2013.

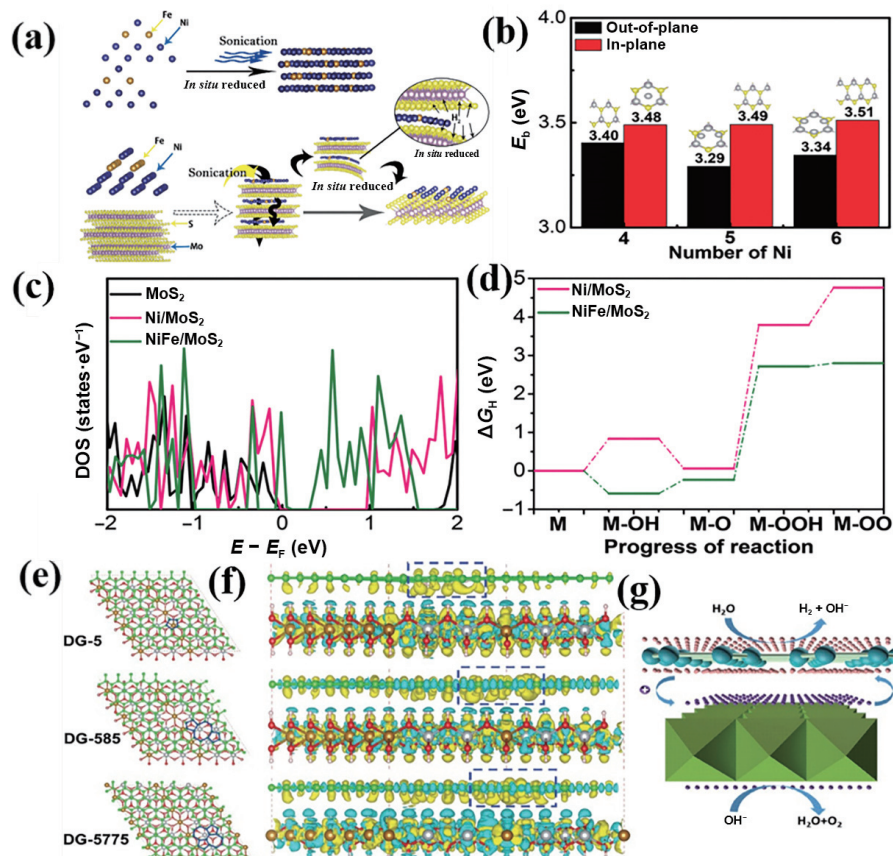


Figure 13 (a) Synthesis of NiFe/MoS₂. (b) Histogram of binding energy (E_b). (c) Corresponding DOS illustrations. (d) Free-energy diagram. (e) The top views of optimized Ni-Fe LDH-NS@DG based composite interfaces. (f) The side views. (g) The probable electrocatalytic mechanism on Ni-Fe LDH-NS@DG. (a)–(d) Reproduced with permission from Ref. [200], © WILEY-VCH Verlag GmbH & Co. KGaA, Weinheim 2019. (e)–(g) Reproduced with permission from Ref. [201], © WILEY-VCH Verlag GmbH & Co. KGaA, Weinheim 2017.

Raman spectra [203]. ZnO nanoparticles were deposited by plasma sputtering. The advantage of this deposition method is that the distribution of ZnO nanoparticles in LDH is uniform. Moreover, ZnO alone has poor OER electrochemical activity, which confirmed the electrochemical influence of the heterogeneous structure.

The transfer of electrons from NiTe to NiFeOOH was confirmed by DFT calculations. Decomposition of the active intermediate OOH^* is a decisive step in OER. Reasonable design and modification of 2D materials can significantly reduce the Gibbs free energy and accelerate the OER (Figs. 14(a)–14(c)). The NiFeOOH/NiTe catalyst showed a low overpotential ($\eta_{10} = 228$ mV) due to strong electron coupling and arrival channel planning, showing excellent OER performance in LDH based catalysts (Figs. 14(d)–14(f)) [204]. The thickness of LDHs can be effectively controlled by tuning reaction time, which affects the catalytic efficiency. The structure of LDHs usually undergoes a series of phase transitions during the reaction process, and hydroxides were recognized as the active species [205, 206]. The preparation of FeNi-LDH/Ti₃C₂-MXene nanohybrid composite electrocatalyst is based on the co-precipitation of bimetal ions [206]. During the synthesis process, Al layers were selectively etched, after which hydrophilic functional groups were introduced. XPS spectra revealed strong electron interactions between 2D nanomaterials. The optimized layer spacing calculated by DFT was 1.74 Å, and the binding energy of each cell was 0.36 eV, which indicates that there is a strong interaction between FeNi-LDH and MXene (Figs. 14(g)–14(i)).

Han et al. used FeOOH to modulate the electronic structure of NiFe LDH. The modulation of electrons at FeOOH and NiFe LDH interface was confirmed by various characterization

methods. The size of FeOOH particles had a significant effect on OER activity [207]. MOFs have been widely studied due to their structural diversity, electronic adjustability, and large specific surface area. Chen et al. prepared QD@NC@RGO by pyrolysis of MOF precursor at low temperature [90]. DFT calculations revealed that there is a strong electronic interaction between Ni and H⁺. Peng studied the active components of NiFe LDH, and found that when Fe ion occupied the lattice of Ni ion in NiFe LDH, the activation energy decreased [208]. However, the specific catalytic mechanism on NiFe LDH catalyst is not clear. They used acid corrosion technology to maximize the active center. Theoretical calculations showed that the Fe site at the edge had a smaller Gibbs free energy and the activity of internal Ni in NiFe LDH was higher than that of marginal Ni. Cao et al. prepared EG/Co(OH)₂/ZIF-67 electrocatalyst with core-shell structure. XPS spectra showed that the binding energy of pyridine nitrogen in the composite catalyst moved negatively, which confirmed the strong coupling between the interface of Co(OH)₂ and ZIF-67. When the ultra-thin ZIF-67 was coated with Co(OH)₂, it showed excellent electrocatalytic OER activity due to the strong coupling between them [209]. The OER performance of LDH-based catalysts is summarized in Table 2.

5.2 Covalent organic frameworks

Covalent organic skeleton is composed of organic molecules connected by strong valence bonds and arranged in a specific geometry and space. Due to the diversity of organic molecules, different sizes of connecting units can be used for the precise design of COFs. In recent years, COFs have been widely studied in photocatalysis, electrocatalysis, biomedicine, and other fields. The first 2D COF was synthesized by Yaghi et al. in 2005, and COF-1

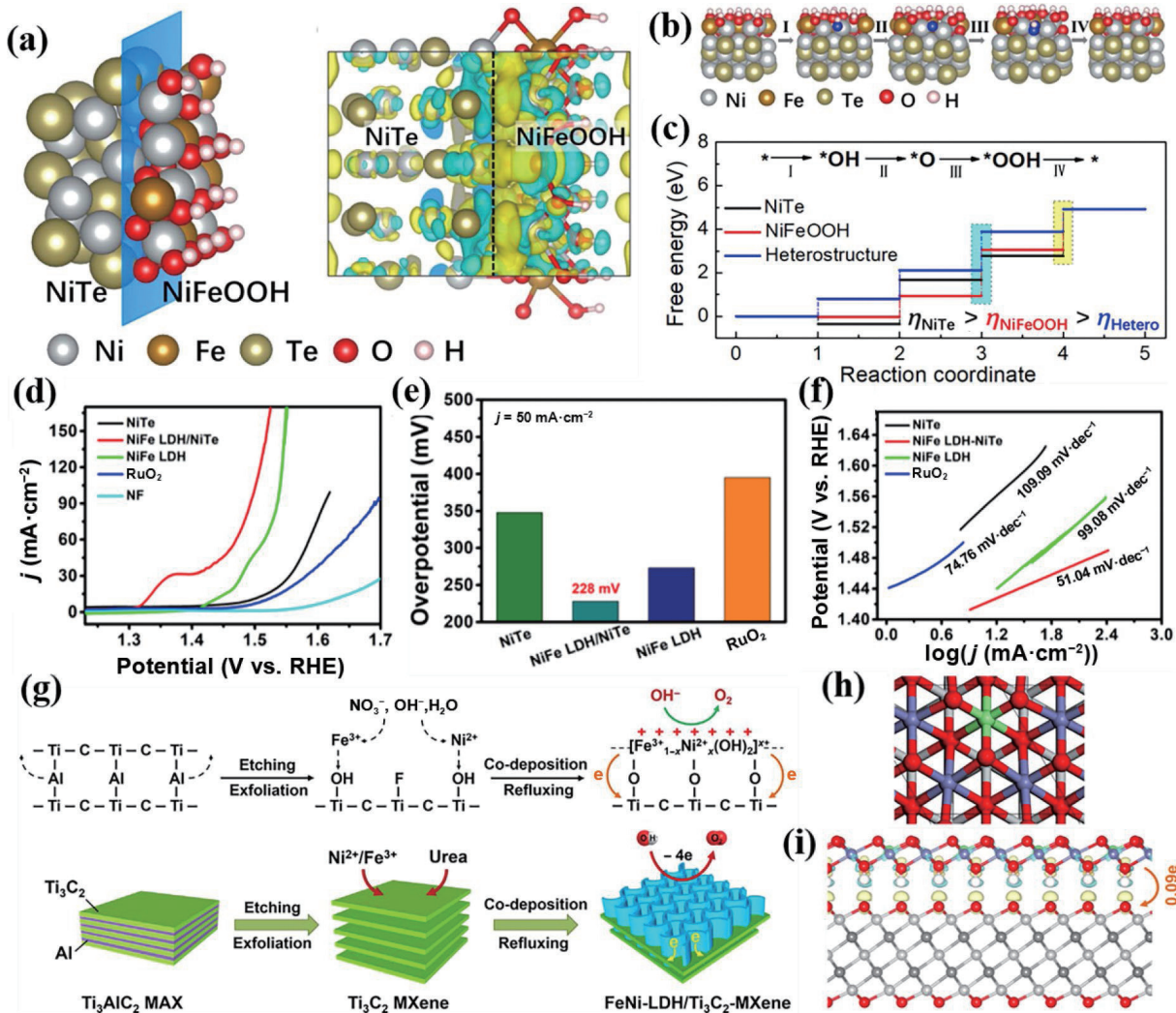


Figure 14 (a) Optimized geometry of NiFeOOH/NiTe heterostructures and charge density difference at the interface of NiFeOOH and NiTe. (b) Proposed 4e⁻ mechanism of OER. (c) Gibbs free energy diagram. (d) Linear sweep voltammetry (LSV) polarization curves. (e) Overpotential. (f) Tafel plots. (g) Illustration of the formation of 2D hierarchic FeNi-LDH/Ti₃C₂-MXene nanohybrids. (h) Top view and (i) side view of model structure. (a)–(f) Reproduced with permission from Ref. [204], © Elsevier B.V. 2020. (g)–(i) Reproduced with permission from Ref. [206], © Elsevier Ltd. 2017.

Table 2 Comparison of OER performance on LDH-based catalysts

Catalyst	Loading mass (mg·cm ⁻²)	Electrolyte	η @10 mA·cm ⁻² (mV)	Tafel slope (mV·dec ⁻¹)	References
Pt-NiFe LDH	0.205	1 M KOH	230	33	[169]
NiFe LDH/Ni-Te	1.0	1 M KOH	—	51.04	[204]
CoNi-LDH/Ti ₃ C ₂ T _x	—	1 M KOH	257.4	68	[210]
FeOOH/LDH	0.02	1 M KOH	174	27	[90]
FeNi-LDH/Ti ₃ C ₂ -MXene	0.2	1 M KOH	298	43	[206]
NiMn LDH/carbon foam	0.425	1 M KOH	220	30	[211]
NiFe LDH/carbon quantum dots	0.2	1 M KOH	235	30	[212]
NiFe-LDH/C	0.28	1 M KOH	210	35	[213]
Fe-Ni hydroxide/GMC	0.147	1 M KOH	320	57	[214]
HPGC@NiFe	0.285	1 M KOH	265	56	[215]
NiFe-LDH@SWNT	0.272	1 M KOH	250	35	[216]
NaBH ₄ -NiFe LDH	—	1 M KOH	280	56	[217]
v-NiFe LDH	—	1 M KOH	210	34.8	[218]
L-NiFe LDH	—	1 M KOH	150	37.1	[218]
NiFe-LDH/NrGO	0.36	0.1 M KOH	258	63	[219]
NiFe-LDH/Co	0.12	0.1 M KOH	312	60	[220]
nNiFe LDH/NGF	0.25	0.1 M KOH	337	45	[221]

and COF-5 showed high thermal stability, permanent porosity, and high surface area [222]. Subsequently, a large number of studies focused on the construction of COFs with different morphologies and their functions [223, 224]. The ordered structure of 2D COFs promotes quick carrier transfer in the stacking direction, which provides a platform for the application of 2D COFs in electrocatalytic OER.

The modification of 2D COFs for catalytic OER has many advantages. First, 2D COFs have adjustable porous structures, which provide a specific surface area for catalytic reactions. Second, a variety of layered stack structures favor the transport of electrons and reaction intermediates. Finally, 2D COFs can be reasonably designed for different reactions. The skeleton of 2D COFs is composed of strong covalent bonds with non-metallic elements, which makes the materials show high stability, low density, and permanent porosity, exhibiting a foundation for the applications of electrocatalysis. Zhang et al. performed theoretical calculations of COFs [225], and pointed out that COFs containing C and N have excellent electrochemical activity. The advantage of covalent connection mode was that it can not only significantly improve the stability of the catalyst, but also give nitrogen a particular position and stoichiometric number. Moreover, the relationships among C,N stoichiometry, pore size, and activity were compared. Smaller band gaps have stronger adsorption capacity for H^+ and OOH^+ and can significantly reduce the OER overpotential [226]. The reaction paths on catalysts with different configurations are significantly different. At present, many 2D COFs have been used as electrocatalysts to promote OER. Here we

briefly summarize the application of modified 2D COFs in OER.

5.2.1 Doping active metals

Due to the lack of active sites, 2D COFs showed poor catalytic OER activity. The OER activity can be improved by introducing reactive metals into the COFs. Thomas et al. synthesized a crystalline COF with uniformly distributed inherent micropores and adjustable macroporous structure by using template assisted strategy (Figs. 15(a) and 15(b)) [227]. They synthesized cobalt-coordinated bipyridyl COF to catalyze OER and demonstrated rapid ion transport in the layered COF structure. Spectral analysis showed that cobalt ions were coordinated with pyridine nitrogen in the COF, and Co–N bond existed in the TPBpy-Co sample (Figs. 15(c)–15(f)). Macroine-tpbpy-co showed better OER catalytic performance ($\eta_{50} = 430$ mV) than cobalt-coordinated microporous COF, which is attributed to the transport characteristics of graded porous COF and the proximity of Co^{2+} -bipyridine active site.

The poor tolerance of COFs in OER leads to leaching and decreased catalytic activity in the long-time reaction. By constructing appropriate topologies and structural units in COFs, they are judiciously tailored to precisely regulate the properties, density, and spatial configuration of the active center. The catalytic activity and stability of COFs in OER can be improved by regulation of the electronic structure. Schiff base modified COFs can undergo proton tautomerism and are chemically stable [228]. Banerjee et al. developed a cobalt-ion modified bipyridine COF (Co-TpBpy), in which the bipyridine N atoms in the framework

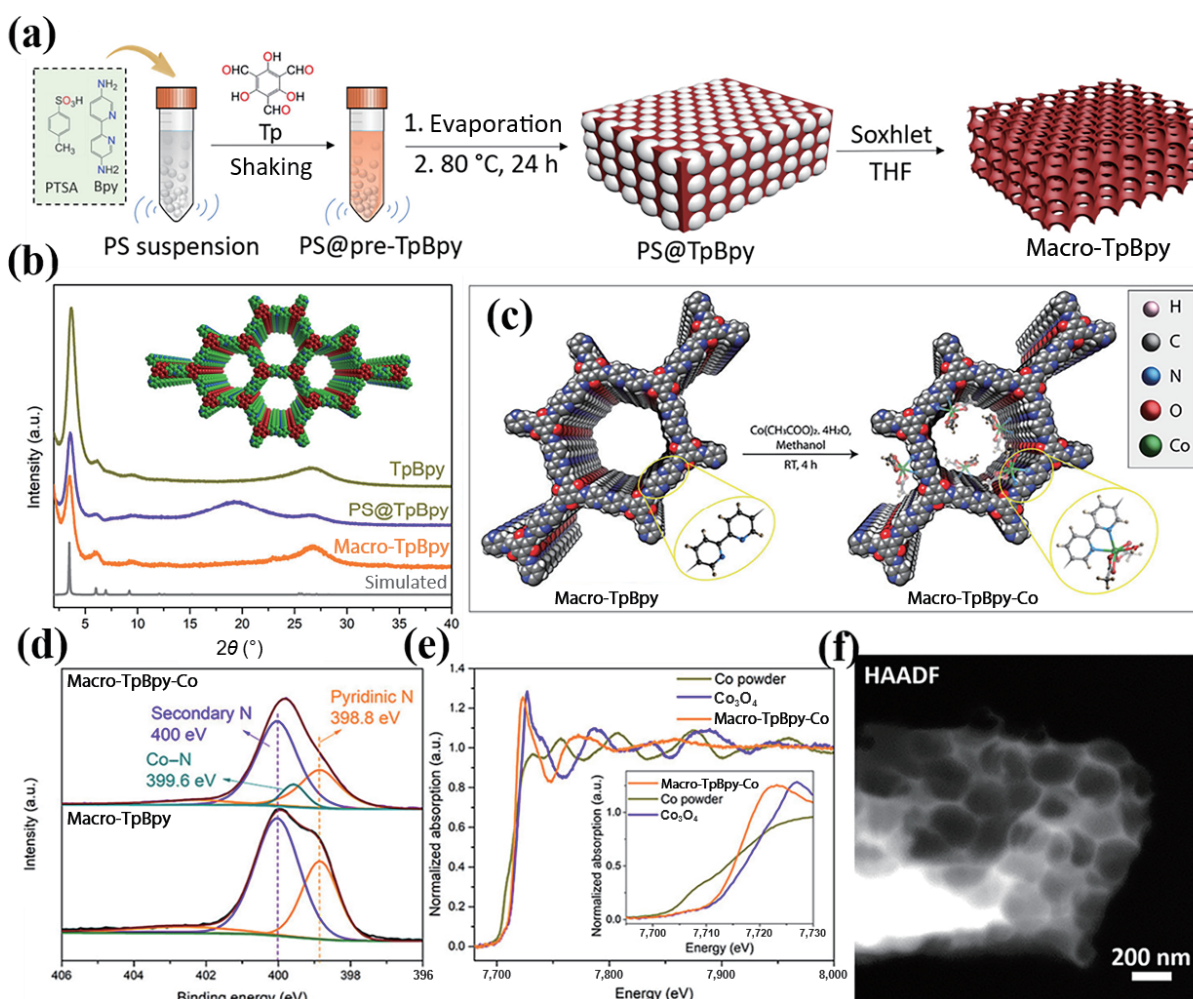


Figure 15 (a) Schematic of macro-TpBpy fabrication. (b) Powder X-Ray diffraction (PXRD) patterns. (c) Schematic of the synthesis of macro-TpBpy-Co. (d) High-resolution N 1s spectra of macro-TpBpy and macro-TpBpy-Co. (e) Normalized Co K-edge XAS spectra. (f) HAADF-STEM images. Reproduced with permission from Ref. [227], © American Chemical Society 2019.

coordinate with Co ions [229]. The modified catalyst had little change in surface area ($450 \text{ m}^2\text{g}^{-1}$) and still retained a strong COF framework. Under neutral conditions, after CV for 1,000 cycles and operation for 24 h, the η_{10} was 400 mV (Figs. 16(a)–16(f)). The high stability is attributed to the interaction of porosity and active coordination units in the COF. Chen et al. developed a metal porphyrin-based GDY analogue (Co-PDY) with unique π conjugated structure by Glaser–Hay coupling reaction on bubbling copper [230]. The stable Co-N₄ in the 2D Co-PDY plane acts as the highly active center of OER, and the conjugation structure in the structure favors electron transfer and maintains continuous OER activity. The increase of aperture is beneficial to mass transfer in vertical direction (Figs. 16(g)–16(k)).

The introduction of metal elements in COFs as catalytic active centers can be combined to the porphyrin unit in COFs, showing good electrocatalytic activity. From the perspective of structure, strong π - π interaction around the porphyrin ring would reduce the utilization rate of metal atoms. Luo et al. designed a simple cation exchange method to synthesize COF electrocatalyst with high utilization rate based on the tunability of organic structural units [231]. DFT calculations showed that oxygen formed coordination bonds with metal in $-\text{SO}_3^-$ unit of COF, and the improvement of OER activity indicated that the cation exchange strategy improved the atom utilization. The synthesized Ni_{0.5}Fe_{0.5}@COF-SO₃ catalyst had a high turnover frequency (TOF) (0.14 s^{-1}) at 300 mV. In addition, theoretical calculations showed that the introduction of bimetal has electron interaction, which further improves the catalytic activity of the active site.

5.2.2 Introducing active molecules

Another strategy is to introduce reactive molecules into the skeleton of COF to adjust the structure to achieve high OER performance. The OER performance of nonmetallic electrocatalysts can be improved by introducing metal ions and regulating N position in COF structure. 2D-COFs with phenazine bonds show good stability and nitrogen rich characteristics because of their rigid structure and the uniform hexagonal holes. Zhang et al. prepared COF-C₄N by solvothermal reaction method, which showed ordered crystal structure with highly conjugate basis plane [225]. The periodic monolayer model of COF-C₄N was established by DFT calculations. The pore size order is $h\text{-C}_5\text{N}_2 > \text{COF-C}_4\text{N} > h\text{-C}_2\text{N}$, and the band gap decreases with the increase of pore size. The smaller the band gap is, the stronger the adsorption of OH* and OOH* in OER is. The calculation results showed that OOH* adsorption is a rate-limiting step in all three structures. The N coordination in the catalyst has an important effect on the OER activity. The larger band gap of $h\text{-C}_2\text{N}$ made the adsorption of the intermediate weak, which is amorphous and unstable under alkaline conditions. In addition, the electron was transferred from N atom to C atom, and the hole was transferred from C atom to N atom. Therefore, the C site on the surface of COF-C₄N should be the active site (Figs. 17(a)–17(f)). COF-C₄N with the pore size of about 10.9 Å showed good catalytic OER performance with small overpotential ($\eta_{10} = 349 \text{ mV}$). Bhaumik et al. synthesized an imide linked thiadiazole group crystal COF (C4-SHz COF) with high specific surface area and crystalline

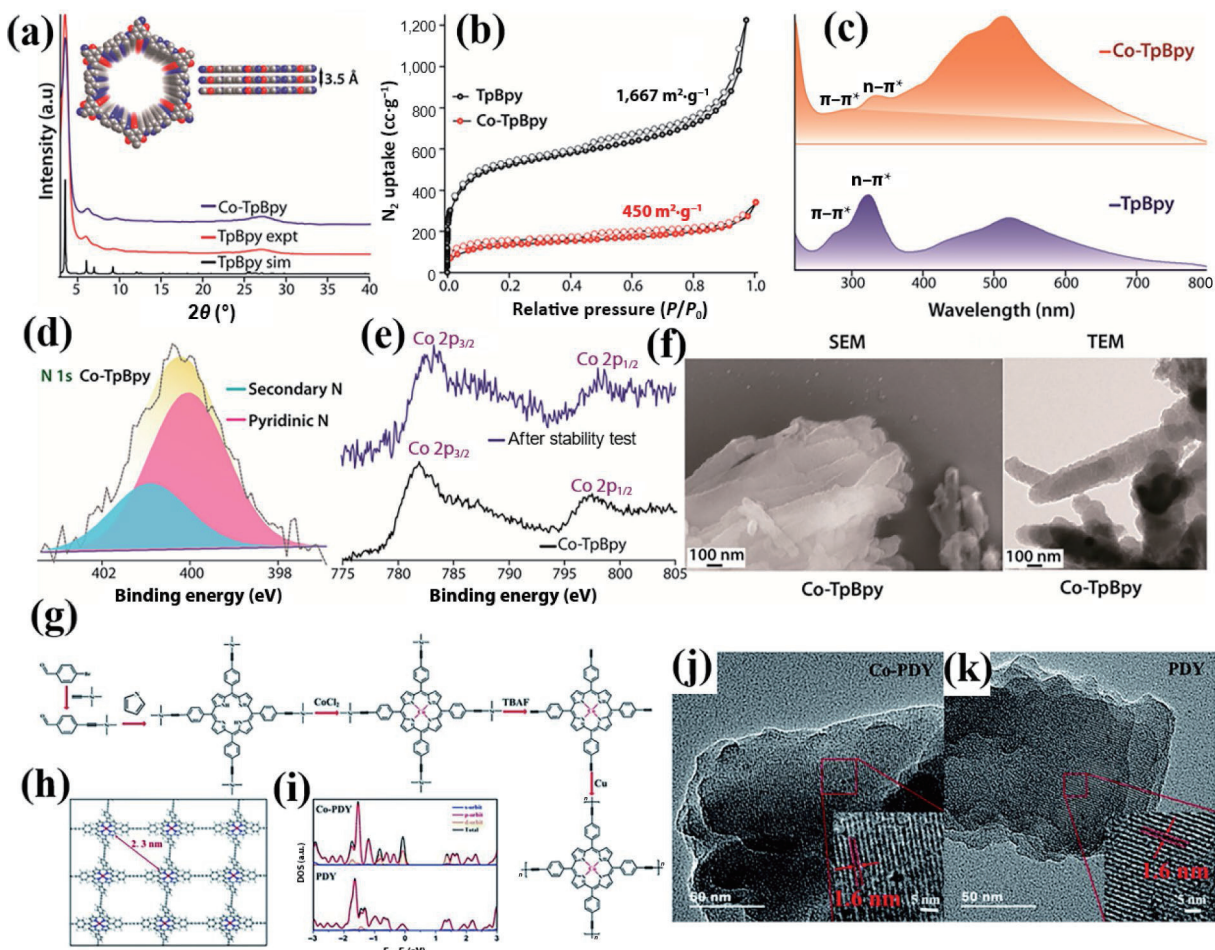


Figure 16 (a) XRD patterns, (b) N₂ adsorption isotherms, and (c) ultraviolet–visible (UV–vis) diffuse reflectance spectroscopy spectra. (d) XPS N 1s spectra of the cobalt-impregnated TPBpy. (e) Co 2p XPS spectra. (f) SEM and TEM images of Co-TPBpy. (g) Synthetic route of Co-PDY. (h) Structure of Co-PDY. (i) Calculated density of states. TEM images of (j) Co-PDY and (k) PDY. (a)–(f) Reproduced with permission from Ref. [229], © American Chemical Society 2016. (g)–(k) Reproduced with permission from Ref. [230], © The Royal Society of Chemistry 2019.

nonmetallic organic skeleton structure by solvothermal synthesis [232]. Nitrogen-rich thiadiazole enhanced the catalytic performance of OER (Figs. 17(g)–17(i)). Theoretical calculations showed that there are multiple adsorption sites for OH⁻ on the surface of C4-CSHz, and the interaction with N3 and S sites is very weak, and therefore, OH⁻ is mainly adsorbed on C2 site. According to the Gibbs free energy, OOH* adsorption is the OER rate-determining step (Fig. 17(j)–17(m)).

5.3 MOF-based electrocatalysts

MOFs are one category of porous materials formed by coordination of inorganic metal ions and organic ligands. MOFs have the characteristics of structural diversity, metal ion coordination uniformity, and high specific surface area. In general, large coordination number of metal sites would make them difficult to react with reactants. Therefore, MOF-derived materials can be used as effective OER catalysts. After high temperature

decomposition, the pores of MOF can be partially preserved to produce porous carbon carriers with high surface area, to expose more active sites, and to accelerate the OER process. The nitrogen atoms in the ligands can be partially contained and evenly dispersed in the whole carbon matrix, so as to adjust the charge density and spin density of the surrounding carbon, thus improving the OER activity. In recent years, 2D ultra-thin MOFs and their derivatives were prepared for the OER. The ultra-thin layered structure of 2D MOFs is conducive to the rapid transfer of electrons, accelerating the reaction kinetics. Most MOF derivatives have hollow or reticular structure, which significantly increases the number of active sites [233]. Moreover, unsaturated metal ions on the surface of MOF derivatives interact with other substances to accelerate the reaction kinetics [234].

5.3.1 MOFs as the electrocatalysts

MOFs have a porous network and are self-assembled using

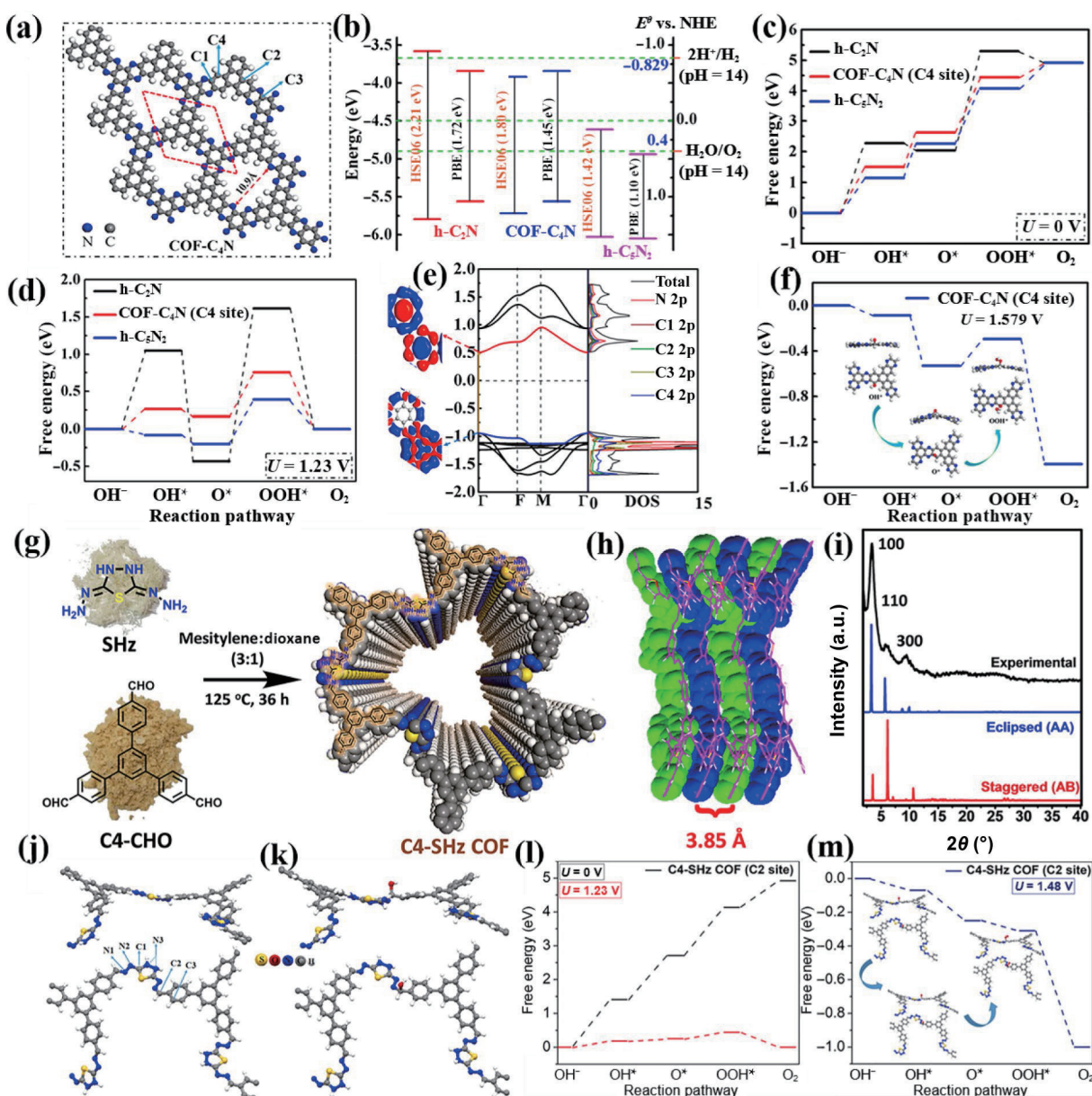


Figure 17 (a) Theoretically optimized COF-C₄N monolayer. (b) Absolute energy of the conduction band minimum (CBM) and valence band maximum (VBM). Free energy profile for the OER pathway at (c) U = 0 V and (d) U = 1.23 V. (e) Band structures, DOS, and wave functions of the CBM and VBM for monolayer COF-C₄N. (f) Free energy profile at 1.579 V. Schematic of the COF (g) proposed structure and (h) packing diagram. (i) PXRD patterns. (j) Theoretically optimized structure of the C4-SHz monolayer and (k) most stable structure of the OH* adsorbed C4-SHz surface. (l) Free-energy profile. (m) Free-energy profile at the experimentally determined onset potential. (a)–(f) Reproduced with permission from Ref. [225], © American Chemical Society 2019. (g)–(m) Reproduced with permission from Ref. [232], © American Chemical Society 2020.

inorganic metal ions and organic ligands. Due to high surface area, they have been widely used in molecular separation, catalysis, and chemical sensing. However, most MOFs do not conduct electricity well, and the active sites encapsulated by organic ligands lead to poor electrocatalytic performance. To improve the conductivity of MOFs, the covalent bond of the coordination polymer can be extended to achieve high charge transfer, and non-covalent interaction can be used to provide charge transfer pathway by π - π stacking between organic ligands. Although many MOFs have been studied in electrochemical applications, these strategies are often not ideal due to the complicated synthesis of MOFs with three-dimensional (3D) network structure. Therefore, 2D MOFs have been fabricated. The nanometer thickness is conducive to the rapid transfer of reaction intermediates and electrons, and the exposure of a large number of surface active metal sites. In addition, the unsaturated coordination of surface metal sites promotes the interaction with the reaction intermediates [233–235].

2D MOFs can not only provide a large number of metal active sites, but also react with other substances to accelerate the reaction kinetics. Thereinto, 2D NiFe-MOFs possess many advantages, including abundant active sites, ultra-thin structure that improves electron transfer rate, interaction between Fe and Ni sites, and unique coordination environment of the active sites [151, 236, 237]. In addition, compared with commercial Ir-based catalysts, 2D NiFe-MOFs exhibited higher catalytic activity and stability in alkaline media, and are superior to other MOF-based catalysts [238]. In NiFe-MOFs, the introduction of Fe can increase the valence of Ni. The high-valence Ni exhibits stronger electron acceptability and thus significantly improves OER activity. Wang et al. prepared a MOF electrocatalyst with uniform size [239]. Since the synergistic action between unsaturated metal active sites on the surface of MOF, they showed excellent electrochemical activity (Figs. 18(a)–18(c)). The presence of iron can improve the valence state of nickel and optimize the e_g orbit, and thus the electrocatalytic activity can be significantly enhanced [240]. The excellent electrochemical activity of NiFe-UMNs was mainly due to the strengthened adsorption of OH^- in the $\Delta G(\text{i})$ step, which is conducive to the formation of intermediates. The addition of Fe improved the valence state of Ni, and the high valence state of Ni had stronger electron acceptance ability in the OER, which is

particularly advantageous in charge transfer between the catalyst and OH^- [241]. In addition, Ni(II) possesses e_g^2 -orbit, while Fe(II) possesses e_g^0 -orbit, and the difference between them can effectively adjust the e_g -orbit. Therefore, the increased OER activity of Fe-Ni electrocatalyst has been explained by Gibbs free energy, orbital theory, and valence state theory (Figs. 18(d) and 18(e)).

To improve the catalytic activity of MOFs, introduction of metal elements in the structure and forming heterojunction or adjusting the structure of MOFs can be adopted, in which strain strategy is an effective way to adjust the MOF structure since the distance between atoms would be changed by lattice strain, thereby modulating the geometry and electronic structure of active sites and improving catalytic OER activity. The lattice strain is easily introduced when organic joints break. Non-bridging ligands partially replace the bridging ligands, while the interlaminar expansion is caused by weak interlaminar interaction at the replaced joint. Yan et al. induced lattice strain in MOF by replacing the multi-coordination bridge connector with a non-bridging ligand using the method of joint fracture [242]. When there was a strain of 6% lattice expansion in the NiFe-MOF, the OER catalytic performance was good under alkaline conditions, and the overpotential (η_{10}) decreased from 320 mV on strain-free NiFe-MOF to 230 mV. The lattice strain did not change the strength of the nearby Ni–O, but weakened the strength of the Fe–O, because the disorder degree increased due to the fracture of the bonding group, while the coordination number and bond length did not change. Therefore, lattice strain did not change the octahedral coordination of the metal, but slightly deformed the configuration of Fe. The strain is often caused by the dangling bonds around the octahedron of FeO_6 . The electrons were transferred from O 2p to Fe 3d t_{2g} in Fe 3d–O 2p hybridization according to the change in peak intensity. To maintain the charge balance, O acts as a linker between Ni and Fe, enhancing the interaction between Ni and Fe. The lattice strain brought by the interaction of Ni–O–Fe will change the valence band structure of MOF. The lattice strain increased the number of vacant orbitals in Ni 3d e_g level and the number of electrons in Fe 3d t_{2g} level. The optimization of electron structure improved the catalytic performance of NiFe-MOFs for the OER (Figs. 19(a)–19(f)). Different cutting sites will increase the layer spacing, and the occupancy rate of Ni 3d e_g orbital is low after lattice strain. Ni was

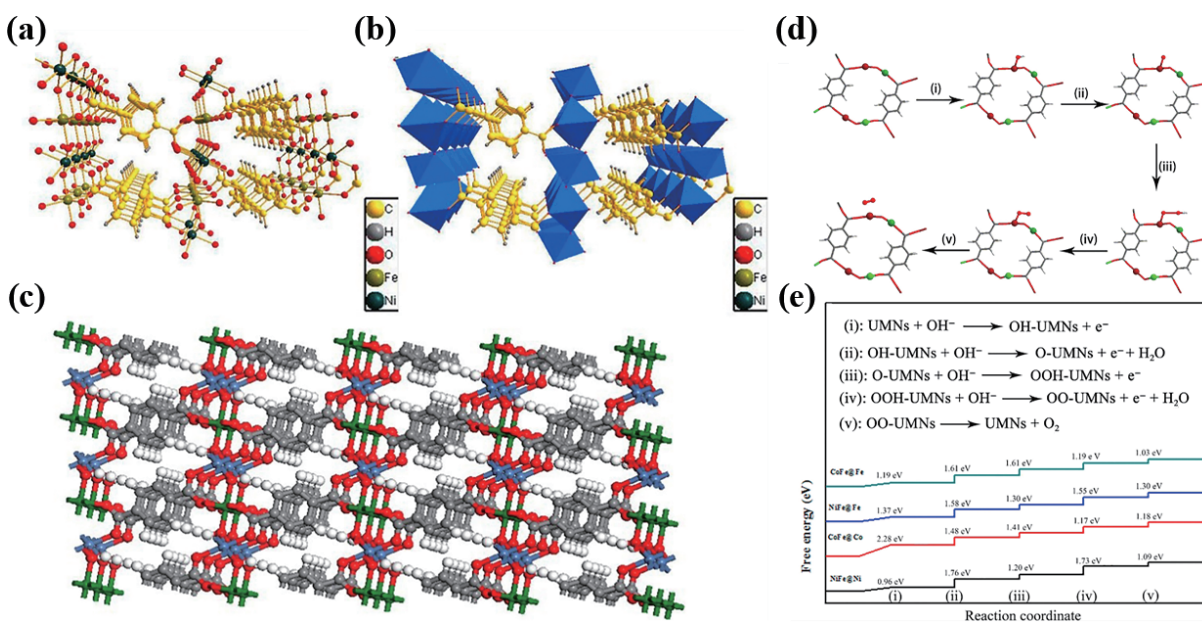


Figure 18 (a) Crystal structure of NiFe-UMNs. (b) Coordination mode of metal atoms. (c) Atomic arrangements of NiFe-UMNs. (d) Reaction steps of the OER processes. (e) Gibbs free energy diagrams. Reproduced with permission from Ref. [239], © Elsevier Ltd. 2017.

the favorable active site, and the formation of $^*\text{OOH}$ was the rate-determining step. The introduction of lattice strain reduced the theoretical overpotential by 0.148 V (Figs. 19(g) and 19(h)).

In order to increase the porosity, conductivity, and catalytic activity, Zhao et al. synthesized nickel-iron nanosheet arrays with organic frameworks using a similar solution-crystallization mechanism (Fig. 20(a)) [243]. The NiFe-MOF material has abundant large pore sizes ranging from 200 to 400 μm . On the surface of the thin film, clear nanosheets with an interval of about 10 nm were grown vertically. Lattice fringes can be clearly observed in the MOF nanosheets, with lattice spacing of about 1.4 nm, and the thickness of nanocrystals obtained by atomic force microscopy (AFM) is about 3.5 nm (Figs. 20(b)–20(d)). The ultra-thin MOF nanosheets showed excellent catalytic performance for OER, and the overpotential (η_{10}) was 240 mV. The excellent electrocatalytic performance is attributed to the ultra-thin nanosheets allowing more active sites to be exposed, as well as improving the combination of conductivity and fractional porosity. Tang et al. synthesized ultra-thin nickel-cobalt organometallic nanosheets, which showed good OER catalytic performance under alkaline conditions with an overpotential (η_{10}) of 250 mV, and the η_{10} was as low as 189 mV when the catalyst was loaded on copper foam. Theoretical calculations showed that there existed unsaturated coordination on the MOF surface, in which coordination unsaturated metal atoms acted as the main active centers, and the interaction between metal atoms Ni and Co enhanced OER activity [234].

5.3.2 MOF derivatives

MOFs can be used precursors to prepare MOF-derived catalysts with good catalytic activity by virtue of controllable morphology

and structure, high porosity, and favourable compatibility with various metal ions. The neatly distributed metal nodes and organic ligands in MOFs are transformed into more complex structures in their derivatives that provide more catalytic active sites. Generally, two kinds of MOF derivatives can be obtained according to different synthesis strategies, namely, single atom-based derivatives and nanoparticle-based derivatives [244]. In MOF derivatives, the kind and content of metal ions can be adjusted, and heteroatom doping can improve the electrical conductivity. In addition, the heteroatom doping broke the complete carbon structure and produced defect structure, further improving the catalytic activity. The morphology and pore structure of MOF derivatives can be obtained by designing the synthesis process of MOF precursors or by selecting appropriate synthesis strategies, such as etching treatment, annealing, and secondary growth strategies [245, 246]. In this section, the regulation of the catalytic performance of single atom-based MOF derivatives and nanoparticle-based MOF derivatives by different strategies is discussed.

5.3.2.1 Single-atom MOF derivatives

Single-atom MOF derivatives can be usually synthesized via three strategies. (i) Metal ions are introduced in MOF precursors, and then annealing treatment is performed. The metal ions can be fixed into the pore structure of porous carbon materials, and the organic ligands can be used as sources of heteroatoms. (ii) Porous carbon materials are obtained by calcination of MOF precursors, which are used to capture metal ions. (iii) Metal salts are mixed with MOF precursors, which are annealed to dope metal into the porous carbon materials. Atom-dispersed active sites in MOF derivatives can improve the catalytic activity [247–250]. In this section, three strategies are proposed for improving the OER

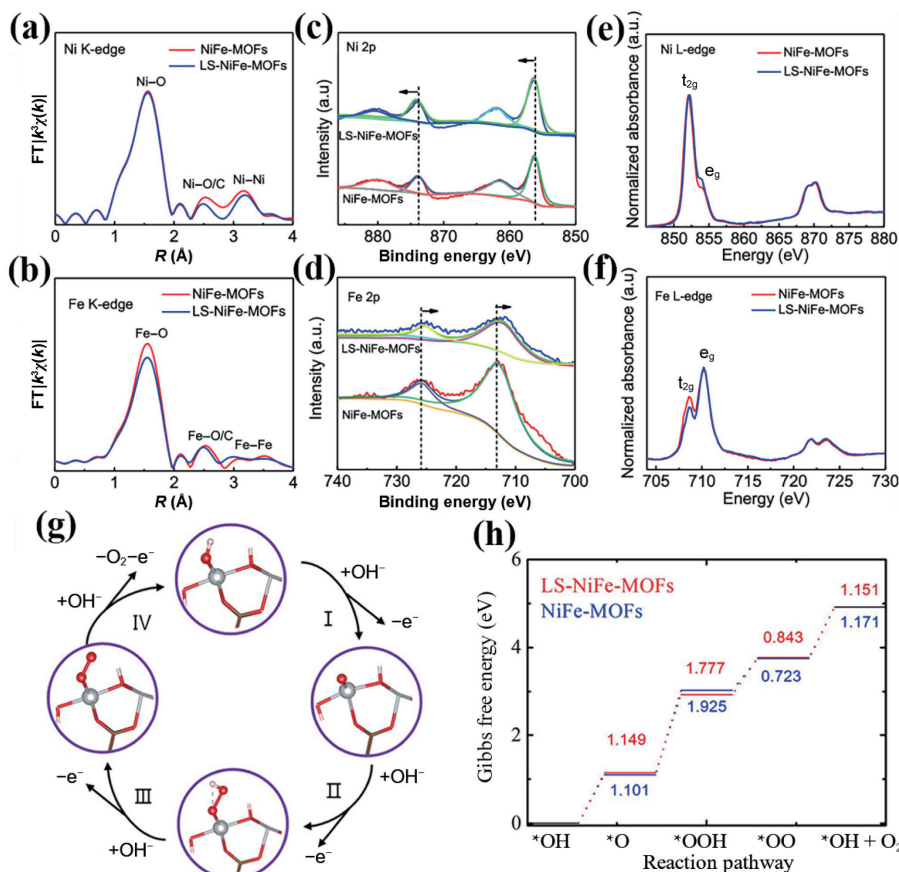


Figure 19 (a) Ni K-edge Fourier transform (FT) curves of the EXAFS $k^2\chi(k)$ functions. (b) Fe K-edge FT curves of the EXAFS $k^2\chi(k)$ functions. (c) Ni 2p XPS of the NiFe-MOFs and LS-NiFe-MOFs. (d) Fe 2p XPS of the NiFe-MOFs and LS-NiFe-MOFs. (e) Ni L-edge XAS spectra. (f) Fe L-edge XAS spectra. (g) OER mechanism on the LS-NiFe-MOF. (h) Gibbs free energy diagram. Reproduced with permission from Ref. [242], © American Chemical Society 2020.

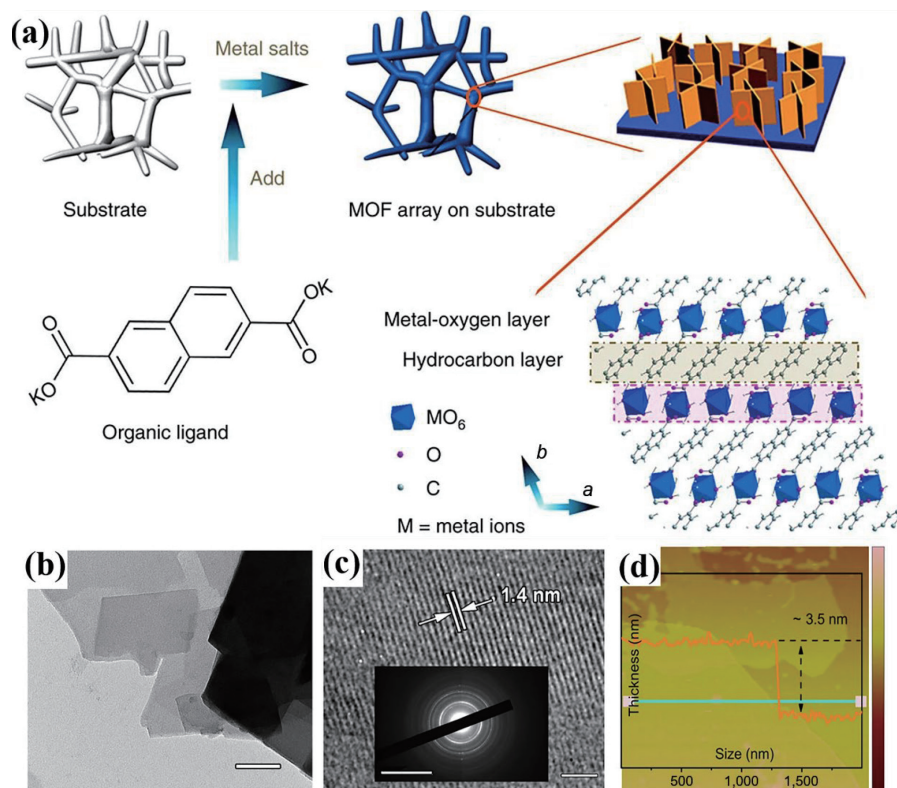


Figure 20 (a) Synthetic process of MOF nanosheet array. (b) TEM image (100 nm). (c) HRTEM image (5 nm) and selected area electron diffraction (SAED) pattern (10/1 nm). (d) AFM image. Reproduced with permission from Ref. [243], © Duan, J. J. et al. 2017.

performance of monatomic MOF derivatives, namely, adjusting the coordination environment of central metal ions, constructing bimetal monatomic sites, and modifying carbon structures.

5.3.2.1.1 Adjusting the coordination environment of central metal ions

In single-atom MOF derivatives, the active sites are usually made of metal and heteroatomic ligands. By adjusting the number and type of heteroatoms, the electronic structure and the geometric configuration of active sites can be optimized, which will affect the adsorption of reaction intermediates and improve OER activity. In MOF derivatives, N atoms with lone pair electrons can activate π electrons of adjacent carbon atoms, which can delocalize the charge of carbon atoms and promote the catalytic OER activity [251, 252]. In addition, the abundance of covalent and metallic bonds in single-atom MOF derivatives can accelerate the formation of OER intermediates and oxygen adsorption.

Lei et al. assembled 2D MOF using alternate strategy and synthesized hollow well-defined Co-N-C nanoleaf (HP-CON-L) [253]. Figures 21(a)–21(c) show the synthesis of HP-CoNC-L, NC-Co-L, and Co-NC-L. The difference between OER ($E_{j=10}$) and ORR ($E_{1/2}$) (ΔE) was used to evaluate the overall oxygen activity. The smaller the ΔE is, the better the activity is. The ΔE of HP-CoNC-L was 0.64 V, which was much lower than most catalysts (Fig. 21(d)). The stratification and interconnection of the pores ensured rapid mass transfer and provided a shorter ion transport path. From Fig. 21(e), the pyridine nitrogen with electron-withdrawing property can accept electrons from neighboring carbon atoms, which facilitated the adsorption of OH^* and OOH^* and increased the kinetics of OER.

5.3.2.1.2 Constructing bimetal monatomic sites

By introducing a second metal atom into the catalyst and constructing bimetal single-atom sites, the number of active sites can be increased and the synergy between the adjacent two kinds

of metals is an important factor to improve the catalytic activity [237, 254]. The construction of bimetallic sites is helpful for the OER application of MOF derivatives. Non-noble metals Fe and Co, which have the advantages of high reserves and variable structure, have been widely concerned in electrochemical OER. Li et al. synthesized iron and cobalt co-doped nanosheets ($\text{Fe-Co}_4\text{N@N-C}$) derived from MOF precursors on carbon cloth, which exhibited bifunctionality [255]. There is a strong coordination effect between $\text{Fe-Co}_4\text{N}$ and N-C , in which M-N acts as the active site. The enriched single cobalt sites can promote charge transfer and the formation of key intermediates in OER, and reduce the charge transfer resistance (Fig. 22). Feng et al. synthesized FeCo fluoride catalyst derived from ZIF-FeCo MOFs using MOF derivatization and fluorination strategies, and found that bimetals have synergistic effects [256]. Compared with mono-metal MOF derivatized fluoride, the kinetics, charge transfer capacity, and active site efficiency of the FeCo fluoride catalyst were improved, which may be attributed to higher chemical surface area, more active site exposure, and improved electrical conductivity produced by fluorination etching.

5.3.2.1.3 Modifying carbon structures

Although single metal atom is the active site, the structure of carbon substrate has an influence on the electronic structure of the active site. In addition, the carbon base plane also affects charge transfer and mass transfer. The introduction of heteroatoms on the carbon base plane or the manufacture of defects can modify the carbon structure. It is important to design suitable strategy to construct carbon base to obtain high catalytic performance. Xu et al. constructed abundant defects in the structure by using thermally decomposed MOF materials. The vacancy defect structure was conducive to *in situ* derivatization and uniform formation of vacancy interfaces along the skeleton. Through controlled heat treatment, metal phosphide was combined with defect MOF to generate CoP hybrid structure with high activity. The presence of defects can provide more active sites and regulate

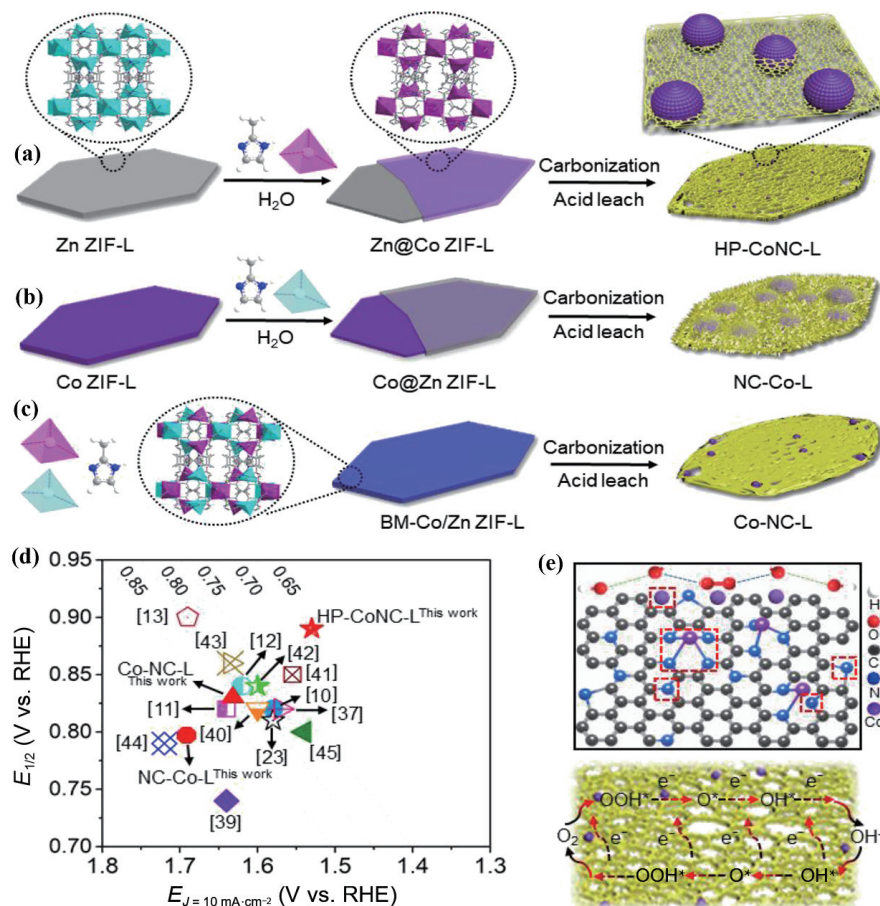


Figure 21 (a) The synthesis of HP-CoNC-L. (b) The synthesis of NC-Co-L. (c) The synthesis of Co-NC-L. (d) The overall comparison of ORR and OER overpotentials for HP-CoNC-L with recently reported catalysts. (e) Mechanism of ORR and OER for synergistic effects in HP-CoNC-L. Reproduced with permission from Ref. [253], © Elsevier Ltd. 2020.

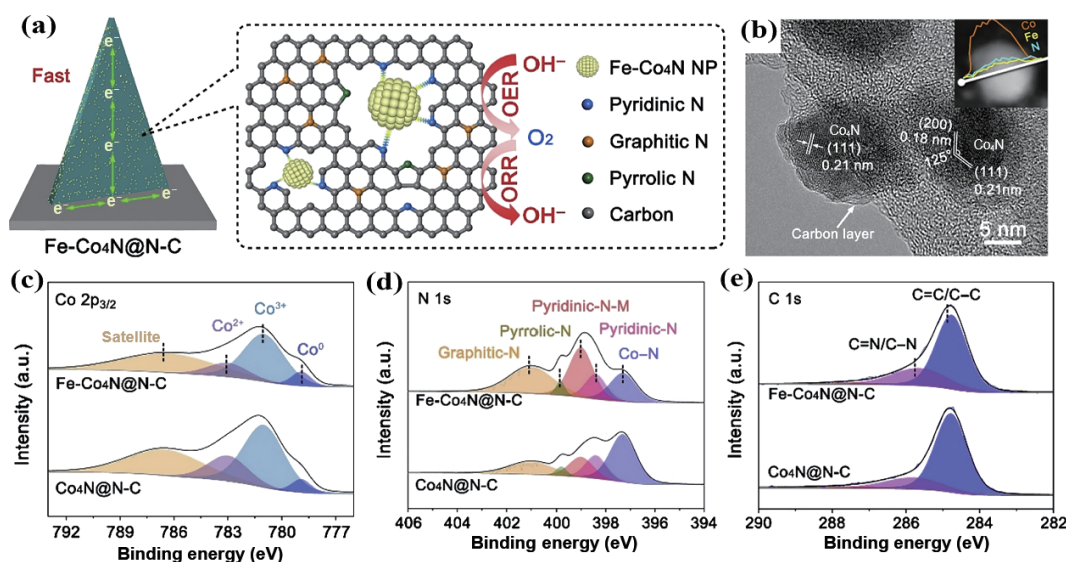


Figure 22 (a) Schematic of the Fe-Co₄N@N-C nanosheet grown on carbon cloth for dual-functional oxygen reaction. (b) High-resolution TEM image. (c)–(e) High-resolution XPS spectra. Reproduced with permission from Ref. [255], © Elsevier B.V. 2019.

the electronic structure while preserving the structure, while phosphating further enhances the catalytic activity of the mixed material. The defects of the substrate material and the unique hybrid structure provide large electrochemical active surface area and fast electron transfer rate together promote the OER activity of the catalyst [257].

5.3.2.2 Nanoparticle-based MOF derivatives

Besides single-atom MOF derivatives, there is another kind of

electrocatalysts with metal nanoparticles in MOF derivatives, which can also show good electrocatalytic OER activity after reasonable regulation. The structure can be optimized by introducing different metal elements, constructing heterogeneous structures, and constructing functional composite materials. MOFs and MOF-derived materials with mesoporous nanostructures usually have a large active surface area, which can provide more active sites for electrocatalytic reactions. In addition, the internal pore structure can reduce ion transport onto the

active site and accelerate the kinetic OER process [258, 259]. In addition, the diffusion of ions towards active sites in MOF derivatives can be reduced by reducing the size of the catalyst, thus increasing the utilization rate of active sites and improving the reaction kinetics [260]. The metal nodes of MOFs can be changed and the MOFs with mixed metal nodes can be synthesized. The mixed metals can interact to adjust the electrocatalytic activity [261]. Compared with single-metal MOF-derived materials, bimetallic MOF derivatives usually have better electrocatalytic activity [262]. In addition to the construction of heterojunction, the construction of composite materials can reduce the inherent defects and improve the electrocatalytic activity.

Ultra-thin 2D MOFs allow them to maximize the exposure of active sites, and the relationship between structure and performance can be obtained. An electrolyte-assisted technology for stripping MOF was reported by Zhang et al. [263]. In the process of synthesis, the catalyst consists of bimetallic Ni and Ce as the metal center and water molecules as the ligands. The anion moves near the cation under the drive of applied voltage. The electrolyte and solvent tend to enter into the interlayer and expand the hydrogen bond to break (Figs. 23(a) and 23(b)). Therefore, appropriate electrolytes can effectively improve the stripping effect. From Figs. 23(c)–23(e), the highest occupied molecular orbital (HOMO) is occupied by Ni and therefore, Ni is the active site for the OER.

The electrocatalytic activity of MOF derivatives can be improved by constructing heterojunction and functional

composite materials. Wei et al. prepared a MOF derivative ($\text{Co}_3\text{O}_4@\text{C-N NSA/NiF}$) by electrochemical deposition method and high-temperature inert gas treatment method (Fig. 24) [264]. The synergistic effect of 2D nanosheets with ultra-thin and large specific surface and Co_3O_4 NPs dispersed uniformly on the nanosheets resulted in the synthesis of $\text{Co}_3\text{O}_4@\text{C-N NSA/NiF}$ catalyst with abundant active sites and good OER activity, with η_{25} of 245 mV. The electron transfer between Co and Ni ions was analyzed by XPS measurement. The Co^{2+} in the hybrid material accepted the electrons from Ni^{2+} , which increased the stability. The OER performance of MOFs and MOF derivatives is summarized in Table 3.

5.4 Hybrid electrocatalysts

Hybrid composite materials show excellent catalytic performance due to synergistic effect between different components. For example, the low conductivity of LDH materials and the agglomeration can be overcome by constructing conductive framework [277]. Graphene, carbon nanotubes, MXenes, and black phosphorus can act as conductive substrates to construct hybrid catalysts with excellent properties [278–280]. In addition to binary heterozygotes, ternary heterozygotes can also be fabricated. Li et al. *in situ* synthesized layered ZIF-67/ CoNiAl-LDH/NF electrocatalyst by combining the properties of LDH, MOF, and nickel foam. The lamellar structure, large electrochemical surface area, porous skeleton, and interfacial coupling effect of the

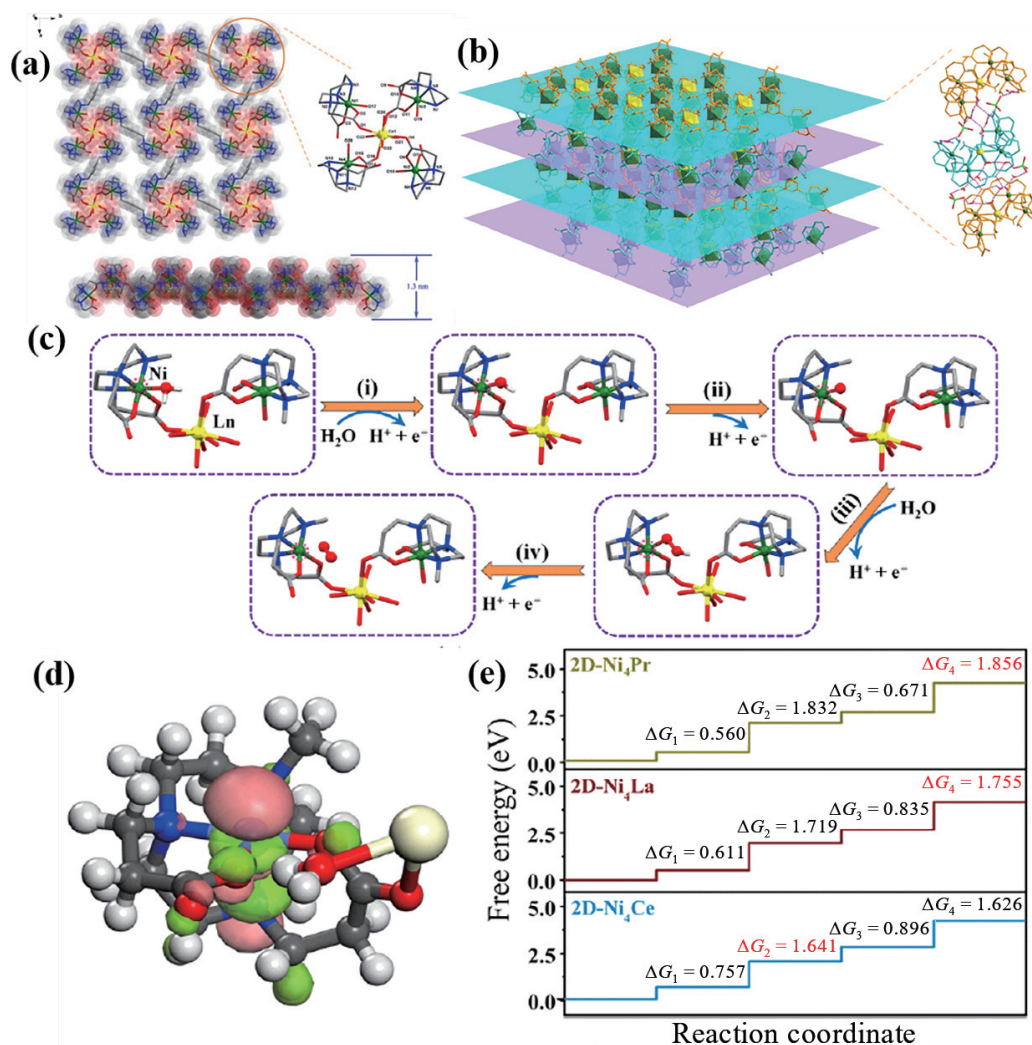


Figure 23 (a) Top and side views of the 2D cationic layer of 2D-Ni₄Ce. (b) Left: packing diagram of 2D cationic layers along *a* axis. Right: the interlayer hydrogen bonds between the adjacent 2D cationic layers. Interlayer forces of 2D-Ni₄Ce. (c) Four elementary OER steps. (d) HOMO of the Ni-Ln cluster model. (e) Standard free energy diagrams. Reproduced with permission from Ref. [263], © American Chemical Society 2020.

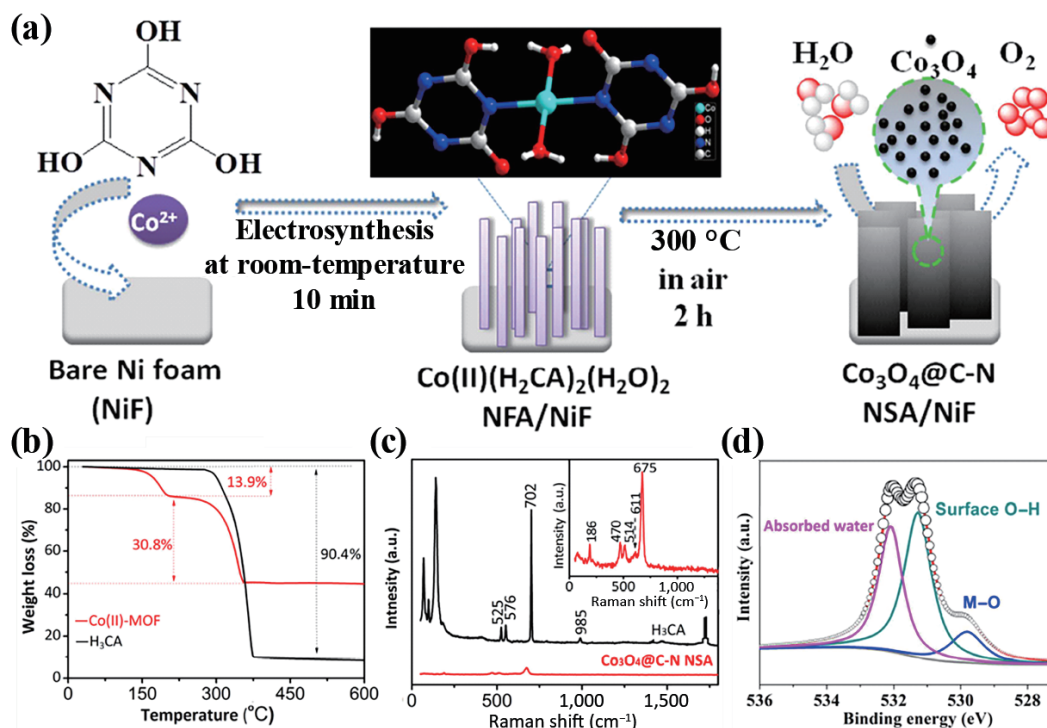


Figure 24 (a) Electrocatalytic oxygen production on Co_3O_4 @C-N NSA/NiF. (b) Thermal gravimetric (TG). (c) Raman spectra. (d) O 1s XPS spectra of Co_3O_4 @C-N NSA. Reproduced with permission from Ref. [264], © Elsevier Ltd. 2018.

catalyst together determined the electrocatalytic OER performance ($\eta_{10} = 303$ mV) [281]. Heumann et al. synthesized a layered composite material (CoTFBDC/EG) by using graphite with good electrical conductivity and MOF with chemical regularity. In the composite material, hydroxyl cobalt fluoride nanoparticles were immobilized on graphite nanomaterials by thermal decomposition of 2D cobalt tetrafluorobenate MOF nanocrystals, which showed good OER performance with an initial overpotential of 310 mV [282]. Electron paramagnetic resonance (EPR) showed that the introduction of cobalt increased the electron spin relaxation rate, indicating that there is an effective electron contact at the junction of the two materials. Stacked graphene nanosheets provided a pathway for mass transfer without big gap between the two materials.

Qiu et al. prepared Fe-CoOOH/G with graphene as support (Fig. 25(a)) [283]. The metal ions were combined with graphene by electrostatic action, and then the surface of the metal ions was refluxed to form LDH. DFT calculations pointed out that Co was the active center of OER without Fe doping. When Co was partially replaced by Fe, the structure of CoOOH/G surface was changed. Moreover, the Fe–O bond of Co–O bond were distorted, leading to increased adsorption energy and decreased Gibbs free energy (Fig. 25(b)). Sun et al. prepared bimetallic NiFe(II, III)-LDH with a few Fe^{2+} by hydrothermal method, showing excellent OER activity ($\eta_{10} = 140$ mV) [284]. Metal ions are easy to precipitate by adding urea due to hydrolysis, while fluoride ions improve the adhesion between the carbon carrier and the generated hydroxide. The formation mechanism of bilayer

Table 3 Comparison of OER performance on 2D MOFs and MOF-derived catalysts

Catalyst	Loading mass ($\text{mg}\cdot\text{cm}^{-2}$)	Electrolyte	η_{10} at $10\text{ mA}\cdot\text{cm}^{-2}$ (mV)	Tafel slope ($\text{mV}\cdot\text{dec}^{-1}$)	References
Ni-MOF@Fe-MOF	0.2	1 M KOH	265	82	[265]
NiFe-BDC	—	1 M KOH	223	37.3	[266]
NiFe-MOF/OM-NFH	0.4	1 M KOH	270	123	[120]
Fe_2Ni_1 -BDC	0.255	1 M KOH	260	35	[267]
Ni-Fe-MOF NSs	—	1 M KOH	221	56	[238]
NFN-MOF	0.6	1 M KOH	240	58.8	[268]
Ni@NC	0.31	1 M KOH	280	45	[269]
Co- Mo_2N	0.7077	1 M KOH	302	90	[270]
Fe_1Co_2 -P/C	—	1 M KOH	360	50.1	[271]
Fe-CoP	4.2	1 M KOH	190	36	[272]
$\text{Co}_4\text{Ni}_1\text{P}$	0.19	1 M KOH	245	61	[273]
$\text{Zn}_{0.2}\text{Co}_{0.8}\text{OOH}$	0.204	1 M KOH	235	34.7	[274]
NiFe-MOF	0.3	0.1 M KOH	240	34	[243]
FeCo-MNS	0.36	0.1 M KOH	298	21.6	[275]
NCNTFs	0.2	0.1 M KOH	370	93	[276]

hydroxides is based on the redox reaction of Ni(II) and Fe(III), where partial Fe(II) will be oxidized to Fe(III) by oxygen (Figs. 25(c) and 25(d)). Wang et al. prepared 2D/2D NiS/graphene heterojunction electrocatalyst using pyrolysis and vulcanization processes, exhibiting ultra-thin lamellar structure [285]. The unique 2D heterostructure provided more electron interactions for NiS and graphene, thus showing good OER and HER activity under alkaline conditions. The rapid transfer of electrons between heterojunction layers effectively promoted the OER process. Compared with NiS and graphene alone, the Gibbs free energy of the heterojunction was significantly reduced. Ishihara et al. prepared Ni-Fe nitride/nitrogen-doped graphene hybrid by calcination of Ni-Fe LDH/GO hybrid. There is a strong coupling between metal-doped nitride nanosheets and graphene. During the hybridization of the two materials, the electronic structure of the nitride changed, which made the catalyst have good OER activity with an initial overpotential of 150 mV [286].

2D MXene family mainly includes transition metal carbides, nitrides, and carbonitrides. In general, MXene is prepared by selectively etching of element A from the MAX phase by strong acid and stripping. The weaker hydrogen bonds of OH, O, or F can replace the relatively strong metallic bonds between M and A in the MAX phase by using aqueous hydrofluoric acid (HF) as an etching agent. MXene has unique properties such as high electrical conductivity, high surface area, large layer spacing, excellent thermal stability, and easy to adjust structure [287–290]. Some MXenes showed excellent electrocatalytic performance on both their edge and basal planes due to abundant metal and functional group sites. However, MXenes usually exhibit poor OER activity due to the lack of active metal sites. In addition, the metallic properties, poor conductivity, and poor stability of MXenes greatly limit their direct application in the OER. MXene can be combined with other materials to significantly improve their electrical conductivity. The excellent electrochemical activity of MXenes is

due to the strong coordination between cations and anions in electrolyte. Zhu et al. developed S-NiFe₂O₄@Ti₃C₂@NF by thiourea assisted electrodeposition and low temperature calcination treatment [291], which exhibited good OER performance with η_{20} of 270 mV. The thin substrate and network structure of Ti₃C₂ facilitated rapid electron transport, while S-NiFe₂O₄ nanosheets provided abundant active sites. Hu et al. synthesized a hybrid catalyst (CoFe-LDH/MXene) by growing CoFe-LDH on the surface of Ti₃C₂ MXene nanosheets, covering the MXene plane with a densely arranged array of very small CoFe-LDH nanosheets (Figs. 26(a)–26(c)) [292]. The η_{10} of the catalyst was 319 mV for the OER, and the improvement of catalytic performance may be due to the interaction between the antioxidant capacity of CoFe-LDH and good conductivity of Ti₃C₂. DFT calculations showed that the oxidized iron and cobalt ions in the CoFe-LDH/MXene system acted as electrophilic centers during OER. High electron density at the interface of LDH reduced the resistance, effectively improved the conductivity, and promoted the electron transfer between the two materials (Figs. 26(d)–26(f)).

Similar to graphene, MXenes are excellent catalyst carrier [293], which can be used to improve the stability of other 2D catalysts. As mentioned above, MOF materials can adjust the electronic structure and surface structure of their derivatives. However, these derivatives often accumulate during the formation process, which not only reduces the active area but also affects the electron transfer rate. As a unique electronic structure and geometric configuration, MXene can be used to solve the problems faced by MOF derivatives. Ultra-thin MXene nanosheets have large active surface area, high electrical conductivity, and strong coupling at the interface, and therefore, the combination of MOF derivatives and MXene to construct the hybrid shows high catalytic activity. For example, Fan et al. reported loaded MOF on MXene to stabilize it [294]. Although 2D MOFs have adjustable structure

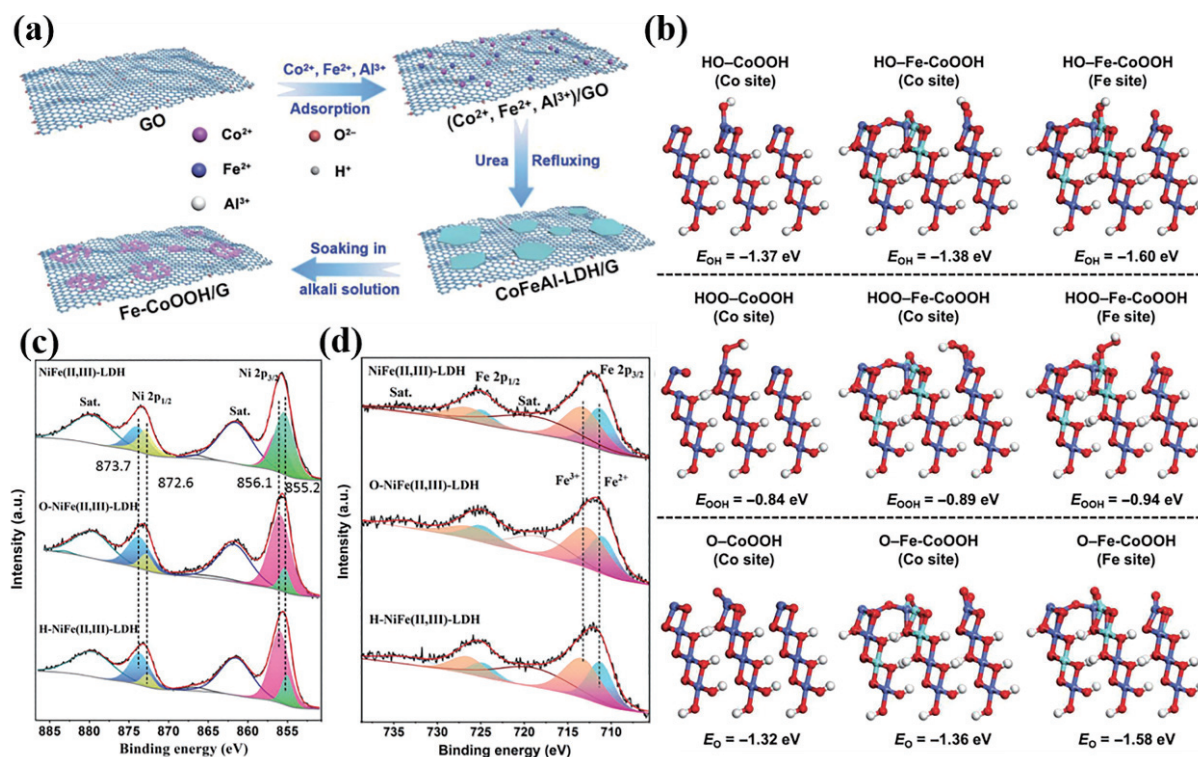


Figure 25 (a) Schematic fabrication process for Fe-CoOOH nanoparticles assembled on graphene. (b) Structures and adsorption energies. (c) and (d) XPS spectra Ni 2p and Fe 2p of NiFe(II,III)-LDH, O-NiFe(II,III)-LDH, and H-NiFe(II,III)-LDH, respectively. (a) and (b) Reproduced with permission from Ref. [283], © WILEY-VCH Verlag GmbH & Co. KGaA, Weinheim 2017. (c) and (d) Reproduced with permission from Ref. [284], © WILEY-VCH Verlag GmbH & Co. KGaA, Weinheim 2019.

and abundant channels, their conductivity is poor. MXenes are a kind of 2D materials with high conductivity. The MXene/MOF heterostructure electrocatalyst was constructed by a special interdiffusion assisted method [295]. 2D MXenes nanosheets not only have large specific surface area and fast electron transfer rate, but also have strong hydrophilicity [296]. As electrocatalysts with ultra-low electronegativity surface, MXenes are expected to change the active center of composite electrocatalysts, so as to effectively adjust the electronic structure and change their electrocatalytic performance [297, 298].

Hybridization of MXenes and metal oxide nanoparticles is an effective way to achieve high-performance OER activity. Routa et al. decorated 2D Ti_3C_2 nanosheets with spinel NiFe_2O_4 nanoparticles ($\text{NiFe}_2\text{O}_4/\text{Ti}_3\text{C}_2$) using one-pot hydrothermal technique [299]. The composite showed superior OER catalytic activity with an η_{10} of 266 mV. DFT calculations showed that the interaction between the spinel NiFe_2O_4 and 2D MXene contained not only the van der Waals force but also the chemical interaction. The charge transfer between NiFe_2O_4 and MXene enhanced the electronic states near the Fermi level due to the interaction between the Ni and Fe 3d orbitals and the C 2p orbitals. A large number of experiments have shown that the enhanced OER activity is mainly due to the increased surface area and strong interface interaction between MXenes and hybrid nanomaterials, which is conducive to promoting gas diffusion and electron conduction. In addition, the electrostatic interaction between

MXenes and hybrid nanomaterials can attract more anionic intermediates and accelerate the OER kinetics [292, 299–302].

In interface engineering, reasonable heterogeneous structure design is an important strategy to improve electrocatalytic OER performance. Composite catalysts can be reasonably constructed by integrating black phosphorus (BP) and graphene. Xu et al. supported red phosphorus (RP) and BP on expanded graphite (EG) using ball milling technique [303]. Under the action of high temperature and shear force during the synthesis process, part of the RP can be converted into chemically active BP, and the RP–BP heterostructure was obtained. EG was treated to produce defect-rich graphene nanosheets. The hybridization of RP–BP heterojunctions with EG provided a large number of active sites and increased the electrical conductivity, showing a good OER activity ($\eta_{10} = 328$ mV). Low cost, adjustable electronic structure, and excellent electrical conductivity make BP/graphene composite receive much attention in OER. Dai et al. used an exudation technique to couple ultra-thin and low-layer exudated black phosphorus (EBP) nanosheets with N-doped graphene (NG) at high Fermi levels to obtain metal-free 2D/2D heterostructures (EBP@NG) (Figs. 27(a)–27(e)) [304]. The catalyst exhibited unique interfacial structure and electronic structure. Direct contact on all sides and large interface area are conducive to charge separation and transfer. The Fermi energy level of the two hybrid materials is different. NG is higher than EBP, and the electron interaction can promote the transfer from NG to EBP, which

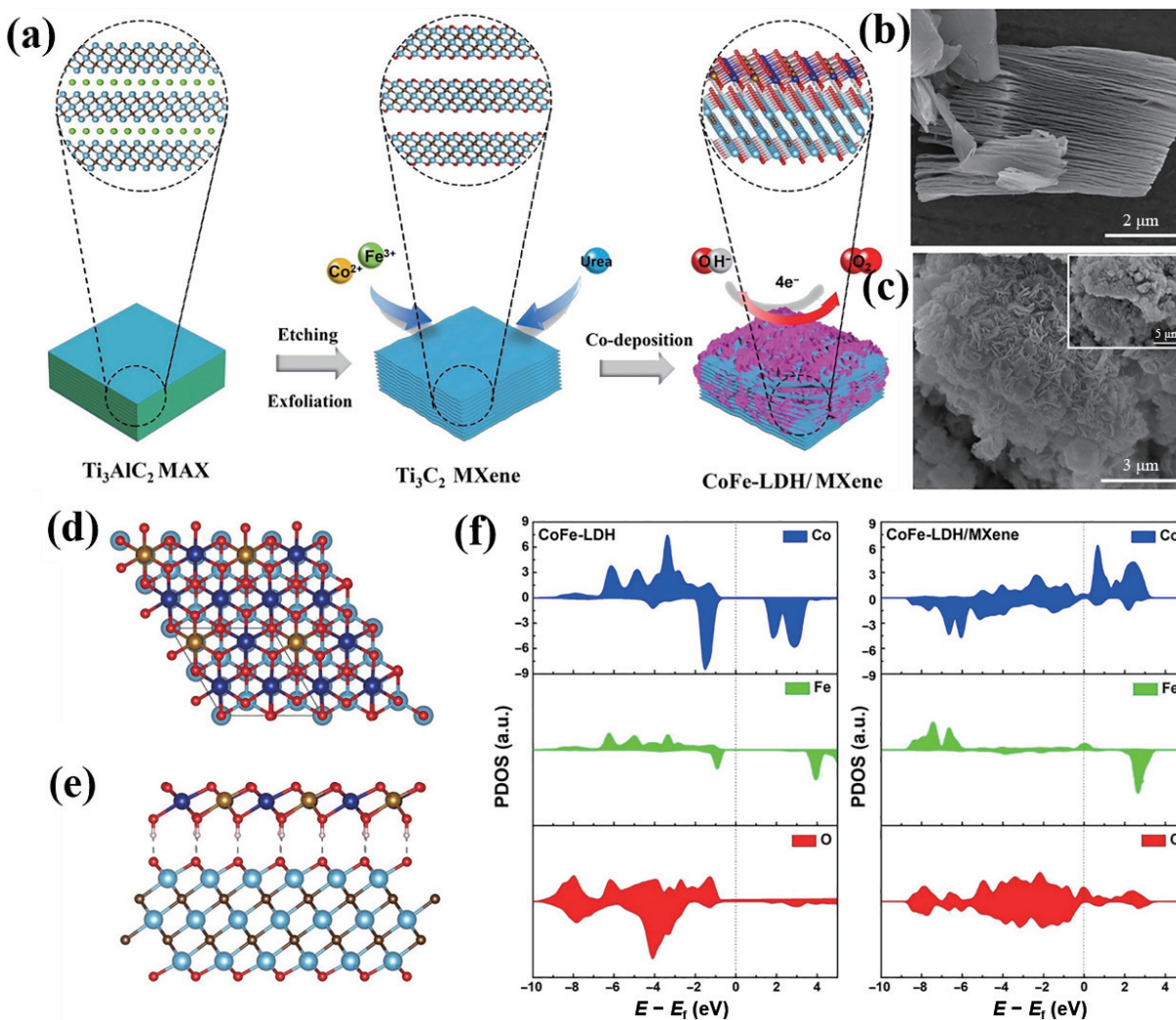


Figure 26 (a) Scheme of the formation process of CoFe-LDH/MXene. SEM images of (b) MXene and (c) CoFe-LDH/MXene nanohybrids. (d) Top view and (e) side view of model structure of CoFe-LDH/MXene hybrid system. (f) Projected density of states (PDOS) of CoFe-LDH and CoFe-LDH/MXene. Reproduced with permission from Ref. [292], © Elsevier Ltd. 2019.

adjusted the adsorption energy of OER intermediates and optimized H adsorption and desorption, making the reaction easier (Figs. 27(f)–27(h)).

6 Conclusions and outlook

In the face of the continuous reduction of global non-renewable energy, hydrogen as a green and clean energy has attracted much attention in recent years, and electrocatalytic OER plays a key role in the large-scale production of hydrogen. Therefore, it is urgent to develop efficient, cheap, and abundant OER electrocatalysts. Although 2D materials have made good progress in electrocatalytic OER, there are still great challenges in designing low-cost catalysts for industrial applications. This review systematically summarizes the synthesis strategies of 2D materials in recent years, including hydrothermal/solvothermal, exfoliation, coprecipitation, electrochemical deposition, wet chemistry, and other synthesis methods. OER mechanism under acidic and alkaline conditions and characterization techniques of 2D materials are summarized and theoretical studies on Gibbs free energy diagram, state density, band structure, and charge analysis are introduced. The modification and regulation of LDHs, COFs, MOFs, and hybrids by different strategies to improve the OER performance are emphasized, including metal/nonmetal doping, defect engineering, interface engineering, lattice strain, and fabrication of heterojunction. The relationship between 2D structure and OER performance is discussed by theoretical analysis.

Compared with other materials, 2D materials have many

characteristics, for example, LDHs have the advantages of low cost, simple synthesis process, plasticity of metal ions in the substrate, and tunability of interlayer anions. COFs have excellent physical and chemical stability, easy synthesis method, controllable structure, and functionalization. MOFs have abundant nanopores and channels, and the metal distribution are relatively uniform and exhibit good stability. Hybrids can be designed with the required structure and properties according to various properties of 2D materials. For 2D materials with ordered layered atomic structure, the strong chemical bonds in the plane are conducive to charge transfer. The ultra-thin nanosheets are favorable for surface modification the formation of surface defects caused by atomic doping and escaping, and the improvement of conductivity. The modification of the surface structure of 2D materials provides more effective active sites, which can optimize the adsorption energy and reduce the gibbs free energy, thus improving OER activity.

Although many synthesis strategies of 2D materials have been developed, the high cost of precursors, high temperature treatment, and complex synthesis limit their large-scale acquisition of high-quality 2D materials. Therefore, more economical, efficient, and green synthesis strategies need to be developed. In addition, there is still a long way to go for the surface optimization of 2D materials. The surface area can be increased and more edged active sites will be generated by reducing the thickness of 2D nanosheets, but the nanosheets in the current research are mainly limited at the nanoscale. Reducing the thickness of 2D nanosheets to atomic level will be more conducive

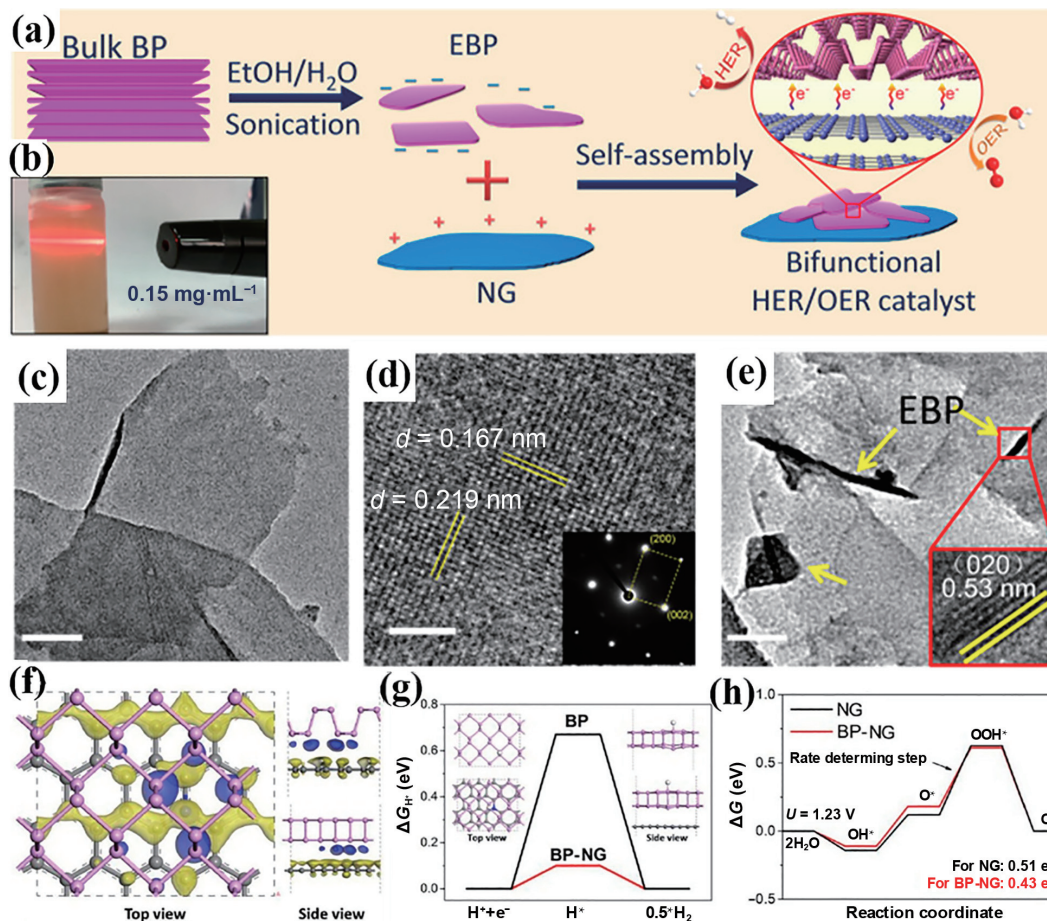


Figure 27 (a) Schematic for the liquid exfoliation of bulk BP and construction of EBP@NG. (b) Photograph of an EBP dispersion. (c) TEM image (50 nm) and (d) HRTEM image of EBP (1 nm). (e) Bright-field TEM image of EBP@NG (1:8) (500 nm). (f) Illustration of the differential charge density of NG and EBP. Calculated free energy diagrams of (g) the HER on BP and BP-NG and (h) OER on NG and BP-NG at the potential of 1.23 V. Reproduced with permission from Ref. [304], © American Chemical Society 2019.

to the application of 2D materials in the field of electrocatalysis. Doping strategy and defect engineering are often used in surface modification. However, there are still some problems in accurately doping and controlling the location and content of defects. Theoretical study is the current main means for predicting OER mechanism, adsorption behavior on active sites, electron transfer path, and the change of the structure during OER. It is needed to develop *in situ* characterization techniques for accurately capturing reaction intermediates for a better understanding of OER process. In addition, most of the studies focused on alkaline solutions, and the stability of 2D materials in OER under acidic conditions has not been thoroughly studied. In theoretical calculations, the OER catalytic performance can be analyzed from multiple dimensions, which provide guidance for researchers to seek appropriate catalysts and optimize them according to the volcanic peaks. Although theoretical calculations provide a bridge for the relationship between catalyst structure and performance, the calculation models are relatively simple, which are different from the actual complicated system, resulting in some inaccuracy.

In situ XAS can provide effective dynamic information for understanding the structure change of catalysts during OER. For example, transition metal oxide radicals can be obtained by the change of the valence state of metal ions at the active sites. However, XAS is a volume sensitive characterization instrument, which reflects the average valence state of the catalyst body and the surface, and cannot monitor the change of specified active sites. Moreover, many researchers face difficulties due to equipment cost constraints and complicated operation. Therefore, there is an urgent need to develop more easy-to-use *in situ* techniques to better understand the relationship between structure and activity. Despite all the difficulties, controllable synthesis of atomic 2D materials with excellent OER performance is hortative in the future work.

Acknowledgements

This work was supported by the National Natural Science Foundation of China (No. 22075099) and the Education Department of Jilin Province (Nos. JJKH20220967KJ and JJKH20220968CY).

References

- Yang, A. Z.; Li, T. C.; Jiang, S.; Wang, X. R.; Qiu, X. Y.; Lei, W.; Tang, Y. W. High-density growth of ultrafine PdIr nanowires on graphene: Reducing the graphene wrinkles and serving as efficient bifunctional electrocatalysts for water splitting. *Nanoscale* **2019**, *11*, 14561–14568.
- Wu, X. J.; Feng, B. M.; Li, W.; Niu, Y. L.; Yu, Y. N.; Lu, S. Y.; Zhong, C. Y.; Liu, P. Y.; Tian, Z. Q.; Chen, L. et al. Metal-support interaction boosted electrocatalysis of ultrasmall iridium nanoparticles supported on nitrogen doped graphene for highly efficient water electrolysis in acidic and alkaline media. *Nano Energy* **2019**, *62*, 117–126.
- Du, Z. G.; Yang, S. B.; Li, S. M.; Lou, J.; Zhang, S. Q.; Wang, S.; Li, B.; Gong, Y. J.; Song, L.; Zou, X. L. et al. Conversion of non-van der Waals solids to 2D transition-metal chalcogenides. *Nature* **2020**, *577*, 492–496.
- Wu, H.; Chen, Z. M.; Wang, Y.; Cao, E. P.; Xiao, F.; Chen, S.; Du, S. C.; Wu, Y. Q.; Ren, Z. Y. Regulating the allocation of N and P in codoped graphene via supramolecular control to remarkably boost hydrogen evolution. *Energy Environ. Sci.* **2019**, *12*, 2697–2705.
- Levinas, R.; Tsyntaru, N.; Cesulius, H. Insights into electrodeposition and catalytic activity of MoS₂ for hydrogen evolution reaction electrocatalysis. *Electrochim. Acta* **2019**, *317*, 427–436.
- Liu, Z. P.; Zhao, L.; Liu, Y. H.; Gao, Z. C.; Yuan, S. S.; Li, X. T.; Li, N.; Miao, S. D. Vertical nanosheet array of 1T phase MoS₂ for efficient and stable hydrogen evolution. *Appl. Catal. B* **2019**, *246*, 296–302.
- Zhang, L. N.; Wu, L. L.; Li, J.; Lei, J. L. Electrodeposition of amorphous molybdenum sulfide thin film for electrochemical hydrogen evolution reaction. *BMC Chem.* **2019**, *13*, 88.
- Xie, Q. X.; Zhou, D. J.; Li, P. S.; Cai, Z.; Xie, T. H.; Gao, T. F.; Chen, R. D.; Kuang, Y.; Sun, X. M. Enhancing oxygen evolution reaction by cationic surfactants. *Nano Res.* **2019**, *12*, 2302–2306.
- Najafi, L.; Bellani, S.; Oropesa-Nuñez, R.; Martín-García, B.; Prato, M.; Bonaccorso, F. Single-/few-layer graphene as long-lasting electrocatalyst for hydrogen evolution reaction. *ACS Appl. Energy Mater.* **2019**, *2*, 5373–5379.
- Wang, W. C.; Zhu, S.; Cao, Y. N.; Tao, Y.; Li, X.; Pan, D. L.; Phillips, D. L.; Zhang, D. Q.; Chen, M.; Li, G. S. et al. Edge-enriched ultrathin MoS₂ embedded yolk-shell TiO₂ with boosted charge transfer for superior photocatalytic H₂ evolution. *Adv. Funct. Mater.* **2019**, *29*, 1901958.
- Ding, Y.; Cao, K. W.; He, J. W.; Li, F. M.; Huang, H.; Chen, P.; Chen, Y. Nitrogen-doped graphene aerogel-supported ruthenium nanocrystals for pH-universal hydrogen evolution reaction. *Chin. J. Catal.* **2022**, *43*, 1535–1543.
- Xue, Q.; Bai, X. Y.; Zhao, Y.; Li, Y. N.; Wang, T. J.; Sun, H. Y.; Li, F. M.; Chen, P.; Jin, P. J.; Yin, S. B. et al. Au core–PtAu alloy shell nanowires for formic acid electrolysis. *J. Energy Chem.* **2022**, *65*, 94–102.
- Guan, J. Q.; Bai, X.; Tang, T. M. Recent progress and prospect of carbon-free single-site catalysts for the hydrogen and oxygen evolution reactions. *Nano Res.* **2022**, *15*, 818–837.
- Zhang, Q. Q.; Guan, J. Q. Applications of atomically dispersed oxygen reduction catalysts in fuel cells and zinc-air batteries. *Energy Environ. Mater.* **2021**, *4*, 307–335.
- Lopes, P. P.; Chung, D. Y.; Rui, X.; Zheng, H.; He, H. Y.; Martins, P. F. B. D.; Strmcnik, D.; Stamenkovic, V. R.; Zapol, P.; Mitchell, J. F. et al. Dynamically stable active sites from surface evolution of perovskite materials during the oxygen evolution reaction. *J. Am. Chem. Soc.* **2021**, *143*, 2741–2750.
- Li, S. S.; Gao, Y. Q.; Li, N.; Ge, L.; Bu, X. H.; Feng, P. Y. Transition metal-based bimetallic MOFs and MOF-derived catalysts for electrochemical oxygen evolution reaction. *Energy Environ. Sci.* **2021**, *14*, 1897–1927.
- Feng, C.; Faheem, M. B.; Fu, J.; Xiao, Y. Q.; Li, C. L.; Li, Y. B. Fe-based electrocatalysts for oxygen evolution reaction: Progress and perspectives. *ACS Catal.* **2020**, *10*, 4019–4047.
- Tahir, M.; Pan, L.; Idrees, F.; Zhang, X. W.; Wang, L.; Zou, J. J.; Wang, Z. L. Electrocatalytic oxygen evolution reaction for energy conversion and storage: A comprehensive review. *Nano Energy* **2017**, *37*, 136–157.
- Busch, M.; Halck, N. B.; Kramm, U. I.; Siahrostami, S.; Krtil, P.; Rossmeisl, J. Beyond the top of the volcano? —A unified approach to electrocatalytic oxygen reduction and oxygen evolution. *Nano Energy* **2016**, *29*, 126–135.
- Zhang, C. L.; Wang, B. W.; Shen, X. C.; Liu, J. W.; Kong, X. K.; Chuang, S. S. C.; Yang, D.; Dong, A. G.; Peng, Z. M. A nitrogen-doped ordered mesoporous carbon/graphene framework as bifunctional electrocatalyst for oxygen reduction and evolution reactions. *Nano Energy* **2016**, *30*, 503–510.
- Zhu, C. Z.; Fu, S. F.; Shi, Q. R.; Du, D.; Lin, Y. H. Single-atom electrocatalysts. *Angew. Chem., Int. Ed.* **2017**, *56*, 13944–13960.
- Kong, X. K.; Xu, K.; Zhang, C. L.; Dai, J.; Olliaee, S. N.; Li, L. Y.; Zeng, X. C.; Wu, C. Z.; Peng, Z. M. Free-standing two-dimensional Ru nanosheets with high activity toward water splitting. *ACS Catal.* **2016**, *6*, 1487–1492.
- Cherevko, S.; Geiger, S.; Kasian, O.; Kulyk, N.; Grote, J. P.; Savan, A.; Shrestha, B. R.; Merzlikin, S.; Breitbach, B.; Ludwig, A. et al. Oxygen and hydrogen evolution reactions on Ru, RuO₂, Ir, and IrO₂ thin film electrodes in acidic and alkaline electrolytes: A comparative study on activity and stability. *Catal. Today* **2016**, *262*,

- 170–180.
- [24] Huo, J. M.; Wang, Y.; Meng, J.; Zhao, X. Y.; Zhai, Q. G.; Jiang, Y. C.; Hu, M. C.; Li, S. N.; Chen, Y. π - π interaction directed 2D FeNi-LDH nanosheets from 2D Hofmann-MOFs for the oxygen evolution reaction. *J. Mater. Chem. A* **2022**, *10*, 1815–1820.
- [25] Han, L.; Dong, S. J.; Wang, E. K. Transition-metal (Co, Ni, and Fe)-based electrocatalysts for the water oxidation reaction. *Adv. Mater.* **2016**, *28*, 9266–9291.
- [26] Seitz, L. C.; Dickens, C. F.; Nishio, K.; Hikita, Y.; Montoya, J.; Doyle, A.; Kirk, C.; Vojvodic, A.; Hwang, H. Y.; Nørskov, J. K. et al. A highly active and stable $\text{IrO}_2/\text{SrIrO}_3$ catalyst for the oxygen evolution reaction. *Science* **2016**, *353*, 1011–1014.
- [27] Ma, C. L.; Sun, W.; Zaman, W. Q.; Zhou, Z. H.; Zhang, H.; Shen, Q. C.; Cao, L. M.; Yang, J. Lanthanides regulated the amorphization-crystallization of IrO_2 for outstanding OER performance. *ACS Appl. Mater. Interfaces* **2020**, *12*, 34980–34989.
- [28] Over, H. Fundamental studies of planar single-crystalline oxide model electrodes (RuO_2 , IrO_2) for acidic water splitting. *ACS Catal.* **2021**, *11*, 8848–8871.
- [29] Qin, Y. C.; Yang, M.; Deng, C. F.; Shen, W.; He, R. X.; Li, M. Theoretical insight into single Rh atoms anchored on N-doped γ -graphyne as an excellent bifunctional electrocatalyst for the OER and ORR: Electronic regulation of graphitic nitrogen. *Nanoscale* **2021**, *13*, 5800–5808.
- [30] Novoselov, K. S.; Geim, A. K.; Morozov, S. V.; Jiang, D.; Zhang, Y.; Dubonos, S. V.; Grigorieva, I. V.; Firsov, A. A. Electric field effect in atomically thin carbon films. *Science* **2004**, *306*, 666–669.
- [31] Nicolosi, V.; Chhowalla, M.; Kanatzidis, M. G.; Strano, M. S.; Coleman, J. N. Liquid exfoliation of layered materials. *Science* **2013**, *340*, 1226419.
- [32] Yang, W. L.; Zhang, X. D.; Xie, Y. Advances and challenges in chemistry of two-dimensional nanosheets. *Nano Today* **2016**, *11*, 793–816.
- [33] Huang, J.; Li, Y.; Huang, R. K.; He, C. T.; Gong, L.; Hu, Q.; Wang, L. S.; Xu, Y. T.; Tian, X. Y.; Liu, S. Y. et al. Electrochemical exfoliation of pillared-layer metal-organic framework to boost the oxygen evolution reaction. *Angew. Chem., Int. Ed.* **2018**, *57*, 4632–4636.
- [34] Ortiz, D. G.; Pochat-Bohatier, C.; Cambedouzou, J.; Bechelany, M.; Miele, P. Exfoliation of hexagonal boron nitride (h-BN) in liquid phase by ion intercalation. *Nanomaterials* **2018**, *8*, 716.
- [35] Rafiq, M.; Hu, X. Z.; Ye, Z. L.; Qayum, A.; Xia, H.; Hu, L. S.; Lu, F. S.; Chu, P. K. Recent advances in structural engineering of 2D hexagonal boron nitride electrocatalysts. *Nano Energy* **2022**, *91*, 106661.
- [36] Sun, M. M.; Dong, J. C.; Lv, Y.; Zhao, S. Q.; Meng, C. X.; Song, Y. J.; Wang, G. X.; Li, J. F.; Fu, Q.; Tian, Z. Q. et al. Pt@h-BN core-shell fuel cell electrocatalysts with electrocatalysis confined under outer shells. *Nano Res.* **2018**, *11*, 3490–3498.
- [37] Wang, Y. H.; Liu, L. Z.; Ma, T. Y.; Zhang, Y. H.; Huang, H. W. 2D graphitic carbon nitride for energy conversion and storage. *Adv. Funct. Mater.* **2021**, *31*, 2102540.
- [38] Yin, T.; Long, L. Y.; Tang, X.; Qiu, M.; Liang, W. Y.; Cao, R.; Zhang, Q. Z.; Wang, D. H.; Zhang, H. Advancing applications of black phosphorus and BP-analog materials in photo/electrocatalysis through structure engineering and surface modulation. *Adv. Sci.* **2020**, *7*, 2001431.
- [39] Wang, X.; Raghupathy, R. K. M.; Querebillo, C. J.; Liao, Z. Q.; Li, D. Q.; Lin, K.; Hantusch, M.; Sofer, Z.; Li, B. H.; Zschech, E. et al. Interfacial covalent bonds regulated electron-deficient 2D black phosphorus for electrocatalytic oxygen reactions. *Adv. Mater.* **2021**, *33*, 2008752.
- [40] Lee, M. K.; Shokouhimehr, M.; Kim, S. Y.; Jang, H. W. Two-dimensional metal-organic frameworks and covalent-organic frameworks for electrocatalysis: Distinct merits by the reduced dimension. *Adv. Energy Mater.* **2022**, *12*, 2003990.
- [41] Li, Z. D.; Attanayake, N. H.; Blackburn, J. L.; Miller, E. M. Carbon dioxide and nitrogen reduction reactions using 2D transition metal dichalcogenide (TMDC) and carbide/nitride (MXene) catalysts. *Energy Environ. Sci.* **2021**, *14*, 6242–6286.
- [42] Cheng, J. L.; Wang, D. S. 2D materials modulating layered double hydroxides for electrocatalytic water splitting. *Chin. J. Catal.* **2022**, *43*, 1380–1398.
- [43] Chen, W. B.; Wang, C. S.; Su, S. B.; Wang, H.; Cai, D. D. Synthesis of ZIF-9(III)/Co LDH layered composite from ZIF-9(I) based on controllable phase transition for enhanced electrocatalytic oxygen evolution reaction. *Chem. Eng. J.* **2021**, *414*, 128784.
- [44] Vikraman, D.; Hussain, S.; Karuppasamy, K.; Feroze, A.; Kathalingam, A.; Sanmugam, A.; Chun, S. H.; Jung, J.; Kim, H. S. Engineering the novel MoSe_2 - Mo_2C hybrid nanoarray electrodes for energy storage and water splitting applications. *Appl. Catal. B* **2020**, *264*, 118531.
- [45] Zhang, L.; Khan, K.; Zou, J. F.; Zhang, H.; Li, Y. C. Recent advances in emerging 2D material-based gas sensors: Potential in disease diagnosis. *Adv. Mater. Interfaces* **2019**, *6*, 1901329.
- [46] Munteanu, R. E.; Moreno, P. S.; Bramini, M.; Gáspár, S. 2D materials in electrochemical sensors for *in vitro* or *in vivo* use. *Anal. Bioanal. Chem.* **2021**, *413*, 701–725.
- [47] Neema, P. M.; Tomy, A. M.; Cyriac, J. Chemical sensor platforms based on fluorescence resonance energy transfer (FRET) and 2D materials. *TrAC Trends Anal. Chem.* **2020**, *124*, 115797.
- [48] Chen, J. H.; Pu, H. H.; Hersam, M. C.; Westerhoff, P. Molecular engineering of 2D nanomaterial field-effect transistor sensors: Fundamentals and translation across the innovation spectrum. *Adv. Mater.* **2022**, *34*, 2106975.
- [49] Kim, Y.; Lee, S.; Song, J. G.; Ko, K. Y.; Woo, W. J.; Lee, S. W.; Park, M.; Lee, H.; Lee, Z.; Choi, H. et al. 2D transition metal dichalcogenide heterostructures for p- and n-type photovoltaic self-powered gas sensor. *Adv. Funct. Mater.* **2020**, *30*, 2003360.
- [50] Evans, A. M.; Bradshaw, N. P.; Litchfield, B.; Strauss, M. J.; Seckman, B.; Ryder, M. R.; Castano, I.; Gilmore, C.; Gianneschi, N. C.; Mulzer, C. R. et al. High-sensitivity acoustic molecular sensors based on large-area, spray-coated 2D covalent organic frameworks. *Adv. Mater.* **2020**, *32*, 2004205.
- [51] Kumar, R.; Liu, X. H.; Zhang, J.; Kumar, M. Room-temperature gas sensors under photoactivation: From metal oxides to 2D materials. *Nano-Micro Lett.* **2020**, *12*, 164.
- [52] Li, S. S.; Sun, J. R.; Guan, J. Q. Strategies to improve electrocatalytic and photocatalytic performance of two-dimensional materials for hydrogen evolution reaction. *Chin. J. Catal.* **2021**, *42*, 511–556.
- [53] Tang, L.; Meng, X. G.; Deng, D. H.; Bao, X. H. Confinement catalysis with 2D materials for energy conversion. *Adv. Mater.* **2019**, *31*, 1901996.
- [54] Fan, F. R.; Wang, R. X.; Zhang, H.; Wu, W. Z. Emerging beyond-graphene elemental 2D materials for energy and catalysis applications. *Chem. Soc. Rev.* **2021**, *50*, 10983–11031.
- [55] Li, Z.; Wu, Y. 2D early transition metal carbides (MXenes) for catalysis. *Small* **2019**, *15*, 1804736.
- [56] Liu, D. Q.; Barbar, A.; Najam, T.; Javed, M. S.; Shen, J.; Tsiakaras, P.; Cai, X. K. Single noble metal atoms doped 2D materials for catalysis. *Appl. Catal. B* **2021**, *297*, 120389.
- [57] Heard, C. J.; Čejka, J.; Opanasenko, M.; Nachtigall, P.; Centi, G.; Perathoner, S. 2D oxide nanomaterials to address the energy transition and catalysis. *Adv. Mater.* **2019**, *31*, 1801712.
- [58] Wang, H.; Chen, J. M.; Lin, Y. P.; Wang, X. H.; Li, J. M.; Li, Y.; Gao, L. J.; Zhang, L. B.; Chao, D. L.; Xiao, X. et al. Electronic modulation of non-van der Waals 2D electrocatalysts for efficient energy conversion. *Adv. Mater.* **2021**, *33*, 2008422.
- [59] Bie, C. B.; Cheng, B.; Fan, J. J.; Ho, W.; Yu, J. G. Enhanced solar-to-chemical energy conversion of graphitic carbon nitride by two-dimensional cocatalysts. *EnergyChem* **2021**, *3*, 100051.
- [60] Wang, Z. Q.; Qi, L.; Zheng, Z. Q.; Xue, Y. R.; Li, Y. L. 2D graphdiyne: A rising star on the horizon of energy conversion. *Chem. Asian J.* **2021**, *16*, 3259–3271.
- [61] Zheng, Y.; Li, X. X.; Pi, C. R.; Song, H.; Gao, B.; Chu, P. K.; Huo, K. F. Recent advances of two-dimensional transition metal nitrides for energy storage and conversion applications. *FlatChem* **2020**, *19*,

- 100149.
- [62] Liao, F. F.; Zhao, X.; Yang, G. Y.; Cheng, Q. H.; Mao, L.; Chen, L. Y. Recent advances on two-dimensional NiFe-LDHs and their composites for electrochemical energy conversion and storage. *J. Alloys Compd.* **2021**, *872*, 159649.
- [63] Wang, Y. M.; Feng, W.; Chen, Y. Chemistry of two-dimensional MXene nanosheets in theranostic nanomedicine. *Chin. Chem. Lett.* **2020**, *31*, 937–946.
- [64] Di, S. H.; Qian, Y. H.; Wang, L.; Li, Z. Biofunctionalization of graphene and its two-dimensional analogues and synthesis of biomimetic materials: A review. *J. Mater. Sci.* **2022**, *57*, 3085–3113.
- [65] Ouyang, J.; Rao, S. Y.; Liu, R. C.; Wang, L. Q.; Chen, W.; Tao, W.; Kong, N. 2D materials-based nanomedicine: From discovery to applications. *Adv. Drug Delivery Rev.* **2022**, *185*, 114268.
- [66] Lu, B. B.; Zhu, Z. Y.; Ma, B. Y.; Wang, W.; Zhu, R. S.; Zhang, J. H. 2D MXene nanomaterials for versatile biomedical applications: Current trends and future prospects. *Small* **2021**, *17*, 2100946.
- [67] Huang, H.; Feng, W.; Chen, Y. Two-dimensional biomaterials: Material science, biological effect and biomedical engineering applications. *Chem. Soc. Rev.* **2021**, *50*, 11381–11485.
- [68] Wang, X. J.; Han, X. J.; Li, C. Z.; Chen, Z.; Huang, H.; Chen, J. D.; Wu, C. S.; Fan, T. J.; Li, T. Z.; Huang, W. C. et al. 2D materials for bone therapy. *Adv. Drug Delivery Rev.* **2021**, *178*, 113970.
- [69] Hu, R.; Liao, G. C.; Huang, Z. Y.; Qiao, H.; Liu, H. T.; Shu, Y. Q.; Wang, B.; Qi, X. Recent advances of monoelemental 2D materials for photocatalytic applications. *J. Hazard. Mater.* **2021**, *405*, 124179.
- [70] Zheng, Y. S.; Sun, F. Z.; Han, X.; Xu, J. L.; Bu, X. H. Recent progress in 2D metal-organic frameworks for optical applications. *Adv. Opt. Mater.* **2020**, *8*, 2000110.
- [71] Zhang, A. J.; Wang, Z. H.; Ouyang, H.; Lyu, W. H.; Sun, J. X.; Cheng, Y.; Fu, B. Recent progress of two-dimensional materials for ultrafast photonics. *Nanomaterials* **2021**, *11*, 1778.
- [72] Wang, F. K.; Pei, K.; Li, Y.; Li, H. Q.; Zhai, T. Y. 2D homojunctions for electronics and optoelectronics. *Adv. Mater.* **2021**, *33*, 2005303.
- [73] Yu, H. H.; Cao, Z. H.; Zhang, Z.; Zhang, X. K.; Zhang, Y. Flexible electronics and optoelectronics of 2D van der Waals materials. *Int. J. Miner. Metall. Mater.* **2022**, *29*, 671–690.
- [74] Pham, P. V.; Bodepudi, S. C.; Shehzad, K.; Liu, Y.; Xu, Y.; Yu, B.; Duan, X. F. 2D heterostructures for ubiquitous electronics and optoelectronics: Principles, opportunities, and challenges. *Chem. Rev.* **2022**, *122*, 6514–6613.
- [75] Xie, J. F.; Zhang, X. D.; Xie, Y. Preferential microstructure design of two-dimensional electrocatalysts for boosted oxygen evolution reaction. *ChemCatChem* **2019**, *11*, 4662–4670.
- [76] Zhang, W.; Zhou, K. Ultrathin two-dimensional nanostructured materials for highly efficient water oxidation. *Small* **2017**, *13*, 1700806.
- [77] Yang, C.; Cai, W. J.; Yu, B. B.; Qiu, H.; Li, M. L.; Zhu, L. W.; Yan, Z.; Hou, L.; Wang, Y. Y. Performance enhancement of oxygen evolution reaction through incorporating bimetallic electrocatalysts in two-dimensional metal-organic frameworks. *Catal. Sci. Technol.* **2020**, *10*, 3897–3903.
- [78] Tang, T. M.; Wang, Z. L.; Guan, J. Q. A review of defect engineering in two-dimensional materials for electrocatalytic hydrogen evolution reaction. *Chin. J. Catal.* **2022**, *43*, 636–678.
- [79] Kim, S. C.; Islam, S.; Hwang, S. J. Application of exfoliated inorganic nanosheets for strongly-coupled hybrid photocatalysts. *Sol. RRL* **2018**, *2*, 1800092.
- [80] Oh, S. M.; Patil, S. B.; Jin, X. Y.; Hwang, S. J. Recent applications of 2D inorganic nanosheets for emerging energy storage system. *Chem.—Eur. J.* **2018**, *24*, 4757–4773.
- [81] Ma, R. Z.; Liu, Z. P.; Li, L.; Iyi, N.; Sasaki, T. Exfoliating layered double hydroxides in formamide: A method to obtain positively charged nanosheets. *J. Mater. Chem.* **2006**, *16*, 3809–3813.
- [82] Lee, J. M.; Kang, B.; Jo, Y. K.; Hwang, S. J. Organic intercalant-free liquid exfoliation route to layered metal-oxide nanosheets via the control of electrostatic interlayer interaction. *ACS Appl. Mater. Interfaces* **2019**, *11*, 12121–12132.
- [83] Feng, X.; Ding, X. S.; Jiang, D. L. Covalent organic frameworks. *Chem. Soc. Rev.* **2012**, *41*, 6010–6022.
- [84] Stock, N.; Biswas, S. Synthesis of metal-organic frameworks (MOFs): Routes to various MOF topologies, morphologies, and composites. *Chem. Rev.* **2012**, *112*, 933–969.
- [85] Huang, Y. J.; Liang, J.; Wang, C.; Yin, S. J.; Fu, W. Y.; Zhu, H. W.; Wan, C. L. Hybrid superlattices of two-dimensional materials and organics. *Chem. Soc. Rev.* **2020**, *49*, 6866–6883.
- [86] Qin, C. L.; Fan, A. X.; Zhang, X.; Wang, S. Q.; Yuan, X. L.; Dai, X. P. Interface engineering: Few-layer MoS₂ coupled to a NiCo-sulfide nanosheet heterostructure as a bifunctional electrocatalyst for overall water splitting. *J. Mater. Chem. A* **2019**, *7*, 27594–27602.
- [87] Chen, Z. L.; Xu, H. B.; Ha, Y.; Li, X. Y.; Liu, M.; Wu, R. B. Two-dimensional dual carbon-coupled defective nickel quantum dots towards highly efficient overall water splitting. *Appl. Catal. B* **2019**, *250*, 213–223.
- [88] Niyitanga, T.; Jeong, H. K. Hydrogen and oxygen evolution reactions of molybdenum disulfide synthesized by hydrothermal and plasma method. *J. Electroanal. Chem.* **2019**, *849*, 113383.
- [89] Shah, S. A.; Shen, X. P.; Xie, M. H.; Zhu, G. X.; Ji, Z. Y.; Zhou, H. B.; Xu, K. Q.; Yue, X. Y.; Yuan, A. H.; Zhu, J. et al. Nickel@nitrogen-doped carbon@MoS₂ nanosheets: An efficient electrocatalyst for hydrogen evolution reaction. *Small* **2019**, *15*, 1804545.
- [90] Chen, J. D.; Zheng, F.; Zhang, S. J.; Fisher, A.; Zhou, Y.; Wang, Z. Y.; Li, Y. Y.; Xu, B. B.; Li, J. T.; Sun, S. G. Interfacial interaction between FeOOH and Ni-Fe LDH to modulate the local electronic structure for enhanced OER electrocatalysis. *ACS Catal.* **2018**, *8*, 11342–11351.
- [91] Ye, X. Q.; Fan, J. C.; Min, Y. L.; Shi, P. H.; Xu, Q. J. Synergistic effects of Co/CoO nanoparticles on imine-based covalent organic frameworks for enhanced OER performance. *Nanoscale* **2021**, *13*, 14854–14865.
- [92] Li, H. H.; Tan, M. Y.; Huang, C.; Luo, W. P.; Yin, S. F.; Yang, W. J. Co₂(OH)₂Cl and MOF mediated synthesis of porous Co₃O₄/NC nanosheets for efficient OER catalysis. *Appl. Surf. Sci.* **2021**, *542*, 148739.
- [93] Chen, Y. Z.; Pang, W. K.; Bai, H. H.; Zhou, T. F.; Liu, Y. N.; Li, S.; Guo, Z. P. Enhanced structural stability of nickel-cobalt hydroxide via intrinsic pillar effect of metaborate for high-power and long-life supercapacitor electrodes. *Nano Lett.* **2017**, *17*, 429–436.
- [94] Lv, L.; Yang, Z. X.; Chen, K.; Wang, C. D.; Xiong, Y. J. 2D layered double hydroxides for oxygen evolution reaction: From fundamental design to application. *Adv. Energy Mater.* **2019**, *9*, 1803358.
- [95] Hernandez, Y.; Nicolosi, V.; Lotya, M.; Blighe, F. M.; Sun, Z. Y.; De, S.; McGovern, I. T.; Holland, B.; Byrne, M.; Gun'ko, Y. K. et al. High-yield production of graphene by liquid-phase exfoliation of graphite. *Nat. Nanotechnol.* **2008**, *3*, 563–568.
- [96] Lukowski, M. A.; Daniel, A. S.; Meng, F.; Forticaux, A.; Li, L. S.; Jin, S. Enhanced hydrogen evolution catalysis from chemically exfoliated metallic MoS₂ nanosheets. *J. Am. Chem. Soc.* **2013**, *135*, 10274–10277.
- [97] Benabdallah, I.; Kara, A.; Benaissa, M. Exfoliation and re-aggregation mechanisms of black phosphorus: A molecular dynamics study. *Appl. Surf. Sci.* **2020**, *507*, 144826.
- [98] Hu, W. H.; Han, G. Q.; Dai, F. N.; Liu, Y. R.; Shang, X.; Dong, B.; Chai, Y. M.; Liu, Y. Q.; Liu, C. G. Effect of pH on the growth of MoS₂ (002) plane and electrocatalytic activity for HER. *Int. J. Hydrogen Energy* **2016**, *41*, 294–299.
- [99] De-Mello, G. B.; Smith, L.; Rowley-Neale, S. J.; Gruber, J.; Hutton, S. J.; Banks, C. E. Surfactant-exfoliated 2D molybdenum disulfide (2D-MoS₂): The role of surfactant upon the hydrogen evolution reaction. *RSC Adv.* **2017**, *7*, 36208–36213.
- [100] Le, T. H.; Oh, Y.; Kim, H.; Yoon, H. Exfoliation of 2D materials

- for energy and environmental applications. *Chem.—Eur. J.* **2020**, *26*, 6360–6401.
- [101] Song, F.; Hu, X. L. Exfoliation of layered double hydroxides for enhanced oxygen evolution catalysis. *Nat. Commun.* **2014**, *5*, 4477.
- [102] Shen, J.; Zhang, P.; Xie, R. S.; Chen, L.; Li, M. T.; Li, J. P.; Ji, B. Q.; Hu, Z. Y.; Li, J. J.; Song, L. X. et al. Controlled self-assembled nife layered double hydroxides/reduced graphene oxide nanohybrids based on the solid-phase exfoliation strategy as an excellent electrocatalyst for the oxygen evolution reaction. *ACS Appl. Mater. Interfaces* **2019**, *11*, 13545–13556.
- [103] Wang, Y. Y.; Zhang, Y. Q.; Liu, Z. J.; Xie, C.; Feng, S.; Liu, D. D.; Shao, M. F.; Wang, S. Y. Layered double hydroxide nanosheets with multiple vacancies obtained by dry exfoliation as highly efficient oxygen evolution electrocatalysts. *Angew. Chem., Int. Ed.* **2017**, *56*, 5867–5871.
- [104] Xing, J.; Chen, J. F.; Li, Y. H.; Yuan, W. T.; Zhou, Y.; Zheng, L. R.; Wang, H. F.; Hu, P.; Wang, Y.; Zhao, H. J. et al. Stable isolated metal atoms as active sites for photocatalytic hydrogen evolution. *Chem.—Eur. J.* **2014**, *20*, 2138–2144.
- [105] Qiao, B. T.; Lin, J.; Wang, A. Q.; Chen, Y.; Zhang, T.; Liu, J. Y. Highly active Au₁/Co₃O₄ single-atom catalyst for CO oxidation at room temperature. *Chin. J. Catal.* **2015**, *36*, 1505–1511.
- [106] Zhang, K.; Wang, W. H.; Kuai, L.; Geng, B. Y. A facile and efficient strategy to gram-scale preparation of composition-controllable Ni-Fe LDHs nanosheets for superior OER catalysis. *Electrochim. Acta* **2017**, *225*, 303–309.
- [107] Gao, R.; Yan, D. P. Fast formation of single-unit-cell-thick and defect-rich layered double hydroxide nanosheets with highly enhanced oxygen evolution reaction for water splitting. *Nano Res.* **2018**, *11*, 1883–1894.
- [108] Zhou, Y.; Zhang, W. B.; Hu, J. L.; Li, D.; Yin, X.; Gao, Q. S. Inherent oxygen vacancies boost surface reconstruction of ultrathin Ni-Fe layered-double-hydroxides toward efficient electrocatalytic oxygen evolution. *ACS Sustainable Chem. Eng.* **2021**, *9*, 7390–7399.
- [109] Arif, M.; Yasin, G.; Shakeel, M.; Fang, X. Y.; Gao, R.; Ji, S. F.; Yan, D. P. Coupling of bifunctional CoMn-layered double hydroxide@graphitic C₃N₄ nanohybrids towards efficient photoelectrochemical overall water splitting. *Chem. Asian J.* **2018**, *13*, 1045–1052.
- [110] Li, R.; Xu, J. S.; Ba, J. W.; Li, Y. R.; Liang, C. H.; Tang, T. Facile synthesis of nanometer-sized NiFe layered double hydroxide/nitrogen-doped graphite foam hybrids for enhanced electrocatalytic oxygen evolution reactions. *Int. J. Hydrogen Energy* **2018**, *43*, 7956–7963.
- [111] Zhang, W.; Wu, Y. Z.; Qi, J.; Chen, M. X.; Cao, R. A thin NiFe hydroxide film formed by stepwise electrodeposition strategy with significantly improved catalytic water oxidation efficiency. *Adv. Energy Mater.* **2017**, *7*, 1602547.
- [112] Li, W. J.; Xue, S.; Watzel, S.; Hou, S. J.; Fichtner, J.; Semrau, A. L.; Zhou, L. J.; Welle, A.; Bandarenka, A. S.; Fischer, R. A. Advanced bifunctional oxygen reduction and evolution electrocatalyst derived from surface-mounted metal-organic frameworks. *Angew. Chem., Int. Ed.* **2020**, *59*, 5837–5843.
- [113] Bera, K.; Karmakar, A.; Kumaravel, S.; Sankar, S. S.; Madhu, R.; Dhandapani, H. N.; Nagappan, S.; Kundu, S. Vanadium-doped nickel cobalt layered double hydroxide: A high-performance oxygen evolution reaction electrocatalyst in alkaline medium. *Inorg. Chem.* **2022**, *61*, 4502–4512.
- [114] Kashale, A. A.; Yi, C. H.; Cheng, K. Y.; Guo, J. S.; Pan, Y. H.; Chen, I. W. P. Binder-free heterostructured NiFe₂O₄/NiFe LDH nanosheet composite electrocatalysts for oxygen evolution reactions. *ACS Appl. Energy Mater.* **2020**, *3*, 10831–10840.
- [115] Sankar, S. S.; Keerthana, G.; Manjula, K.; Sharad, J. H.; Kundu, S. Electrospun Fe-incorporated ZIF-67 nanofibers for effective electrocatalytic water splitting. *Inorg. Chem.* **2021**, *60*, 4034–4046.
- [116] Xu, Y. Y.; Cao, H. Z.; Xue, Y. Q.; Li, B.; Cai, W. H. Liquid-phase exfoliation of graphene: An overview on exfoliation media, techniques, and challenges. *Nanomaterials* **2018**, *8*, 942.
- [117] Ahmed, Z.; Krishankant; Rai, R.; Kumar, R.; Maruyama, T.; Bera, C.; Bagchi, V. Unraveling a graphene exfoliation technique analogy in the making of ultrathin nickel-iron oxyhydroxides@nickel foam to promote the OER. *ACS Appl. Mater. Interfaces* **2021**, *13*, 55281–55291.
- [118] Li, J. P.; Zhang, P.; Zhao, X. L.; Chen, L.; Shen, J.; Li, M. T.; Ji, B. Q.; Song, L. X.; Wu, Y. P.; Liu, D. Structure-controlled Co-Al layered double hydroxides/reduced graphene oxide nanomaterials based on solid-phase exfoliation technique for supercapacitors. *J. Colloid Interface Sci.* **2019**, *549*, 236–245.
- [119] Hu, Q.; Huang, X. W.; Wang, Z. Y.; Li, G. M.; Han, Z.; Yang, H. P.; Ren, X. Z.; Zhang, Q. L.; Liu, J. H.; He, C. X. Unconventionally fabricating defect-rich NiO nanoparticles within ultrathin metal-organic framework nanosheets to enable high-output oxygen evolution. *J. Mater. Chem. A* **2020**, *8*, 2140–2146.
- [120] Zhuang, L. Z.; Ge, L.; Liu, H. L.; Jiang, Z. R.; Jia, Y.; Li, Z. H.; Yang, D. J.; Hocking, R. K.; Li, M. R.; Zhang, L. Z. et al. A surfactant-free and scalable general strategy for synthesizing ultrathin two-dimensional metal-organic framework nanosheets for the oxygen evolution reaction. *Angew. Chem., Int. Ed.* **2019**, *58*, 13565–13572.
- [121] Wen, Y. Y.; Wei, Z. T.; Liu, J. H.; Li, R.; Wang, P.; Zhou, B.; Zhang, X.; Li, J.; Li, Z. X. Synergistic cerium doping and MXene coupling in layered double hydroxides as efficient electrocatalysts for oxygen evolution. *J. Energy Chem.* **2021**, *52*, 412–420.
- [122] Zhang, X.; Wan, K.; Subramanian, P.; Xu, M. W.; Luo, J. S.; Fransær, J. Electrochemical deposition of metal-organic framework films and their applications. *J. Mater. Chem. A* **2020**, *8*, 7569–7587.
- [123] Song, S. W.; Yu, L.; Hadjiev, V. G.; Zhang, W. Y.; Wang, D. Z.; Xiao, X.; Chen, S.; Zhang, Q. Y.; Ren, Z. F. New way to synthesize robust and porous Ni_{1-x}Fe_x layered double hydroxide for efficient electrocatalytic oxygen evolution. *ACS Appl. Mater. Interfaces* **2019**, *11*, 32909–32916.
- [124] Li, R. P.; Li, Y.; Yang, P. X.; Wang, D.; Xu, H.; Wang, B.; Meng, F.; Zhang, J. Q.; An, M. Z. Electrodeposition: Synthesis of advanced transition metal-based catalyst for hydrogen production via electrolysis of water. *J. Energy Chem.* **2021**, *57*, 547–566.
- [125] Xu, H.; Shang, H. Y.; Wang, C.; Du, Y. K. Surface and interface engineering of noble-metal-free electrocatalysts for efficient overall water splitting. *Coord. Chem. Rev.* **2020**, *418*, 213374.
- [126] Liu, W.; Zhang, H. X.; Li, C. M.; Wang, X.; Liu, J. Q.; Zhang, X. W. Non-noble metal single-atom catalysts prepared by wet chemical method and their applications in electrochemical water splitting. *J. Energy Chem.* **2020**, *47*, 333–345.
- [127] Cai, Z. Y.; Liu, B. L.; Zou, X. L.; Cheng, H. M. Chemical vapor deposition growth and applications of two-dimensional materials and their heterostructures. *Chem. Rev.* **2018**, *118*, 6091–6133.
- [128] Jung, S. Y.; Kang, S.; Kim, K. M.; Mhin, S.; Kim, J. C.; Kim, S. J.; Enkhtuvshin, E.; Choi, S.; Han, H. Sulfur-incorporated nickel-iron layered double hydroxides for effective oxygen evolution reaction in seawater. *Appl. Surf. Sci.* **2021**, *568*, 150965.
- [129] Rafai, S.; Qiao, C.; Wang, Z. T.; Cao, C. B.; Mahmood, T.; Naveed, M.; Younas, W.; Khalid, S. Cobalt phosphide ultrathin and freestanding sheets prepared through microwave chemical vapor deposition: A highly efficient oxygen evolution reaction catalyst. *ChemElectroChem* **2019**, *6*, 5469–5478.
- [130] Sirisomboonchai, S.; Li, S. S.; Yoshida, A.; Li, X. M.; Samart, C.; Abudula, A.; Guan, G. Q. Fabrication of NiO microflake@NiFe-LDH nanosheet heterostructure electrocatalysts for oxygen evolution reaction. *ACS Sustainable Chem. Eng.* **2019**, *7*, 2327–2334.
- [131] Roy, S.; Mari, S.; Sai, M. K.; Sarma, S. C.; Sarkar, S.; Peter, S. C. Highly efficient bifunctional oxygen reduction/evolution activity of a non-precious nanocomposite derived from a tetrazine-COF. *Nanoscale* **2020**, *12*, 22718–22734.
- [132] Zhuang, G. L.; Gao, Y. F.; Zhou, X.; Tao, X. Y.; Luo, J. M.; Gao, Y. J.; Yan, Y. L.; Gao, P. Y.; Zhong, X.; Wang, J. G. ZIF-67/COF-derived highly dispersed Co₃O₄/N-doped porous carbon with

- excellent performance for oxygen evolution reaction and Li-ion batteries. *Chem. Eng. J.* **2017**, *330*, 1255–1264.
- [133] Zhang, B. W.; Zhu, C. Q.; Wu, Z. S.; Stavitski, E.; Lui, Y. H.; Kim, T. H.; Liu, H.; Huang, L.; Luan, X. C.; Zhou, L. et al. Integrating Rh species with NiFe-layered double hydroxide for overall water splitting. *Nano Lett.* **2020**, *20*, 136–144.
- [134] Kim, J. S.; Kim, B.; Kim, H.; Kang, K. Recent progress on multimetal oxide catalysts for the oxygen evolution reaction. *Adv. Energy Mater.* **2018**, *8*, 1702774.
- [135] Shan, J. Q.; Zheng, Y.; Shi, B. Y.; Davey, K.; Qiao, S. Z. Regulating electrocatalysts via surface and interface engineering for acidic water electrooxidation. *ACS Energy Lett.* **2019**, *4*, 2719–2730.
- [136] Li, M. T.; Zhang, L. P.; Xu, Q.; Niu, J. J.; Xia, Z. H. N-doped graphene as catalysts for oxygen reduction and oxygen evolution reactions: Theoretical considerations. *J. Catal.* **2014**, *314*, 66–72.
- [137] Cai, Z. Y.; Bu, X. M.; Wang, P.; Ho, J. C.; Yang, J. H.; Wang, X. Y. Recent advances in layered double hydroxide electrocatalysts for the oxygen evolution reaction. *J. Mater. Chem. A* **2019**, *7*, 5069–5089.
- [138] Zheng, Y.; Jiao, Y.; Vasileff, A.; Qiao, S. Z. The hydrogen evolution reaction in alkaline solution: From theory, single crystal models, to practical electrocatalysts. *Angew. Chem., Int. Ed.* **2018**, *57*, 7568–7579.
- [139] Cheng, X.; Fabbri, E.; Nachtegaal, M.; Castelli, I. E.; El Kazzi, M.; Haumont, R.; Marzari, N.; Schmidt, T. J. Oxygen evolution reaction on $\text{La}_{1-x}\text{Sr}_x\text{CoO}_3$ perovskites: A combined experimental and theoretical study of their structural, electronic, and electrochemical properties. *Chem. Mater.* **2015**, *27*, 7662–7672.
- [140] Li, P. S.; Wang, M. Y.; Duan, X. X.; Zheng, L. R.; Cheng, X. P.; Zhang, Y. F.; Kuang, Y.; Li, Y. P.; Ma, Q.; Feng, Z. X. et al. Boosting oxygen evolution of single-atomic ruthenium through electronic coupling with cobalt-iron layered double hydroxides. *Nat. Commun.* **2019**, *10*, 1711.
- [141] Wu, G. Y.; Liu, S. C.; Cheng, G. J.; Li, H.; Liu, Y. Ni-Co@carbon nanosheet derived from nickelocene doped Co-BDC for efficient oxygen evolution reaction. *Appl. Surf. Sci.* **2021**, *545*, 148975.
- [142] Zhang, W. D.; Hu, Q. T.; Wang, L. L.; Gao, J.; Zhu, H. Y.; Yan, X. D.; Gu, Z. G. *In-situ* generated Ni-MOF/LDH heterostructures with abundant phase interfaces for enhanced oxygen evolution reaction. *Appl. Catal. B* **2021**, *286*, 119906.
- [143] Yao, N.; Jia, H. N.; Fan, Z. Y.; Bai, L.; Xie, W.; Cong, H. J.; Chen, S. L.; Luo, W. Nitridation-induced metal-organic framework nanosheet for enhanced water oxidation electrocatalysis. *J. Energy Chem.* **2022**, *64*, 531–537.
- [144] Yao, N.; Fan, Z. Y.; Meng, R.; Jia, H. N.; Luo, W. A cobalt hydroxide coated metal-organic framework for enhanced water oxidation electrocatalysis. *Chem. Eng. J.* **2021**, *408*, 127319.
- [145] Yang, J. L.; Xuan, H. C.; Yang, J. T.; Meng, L. X.; Wang, J.; Liang, X. H.; Li, Y. P.; Han, P. D. Metal-organic framework-derived $\text{FeS}_2/\text{CoNiSe}_2$ heterostructure nanosheets for highly-efficient oxygen evolution reaction. *Appl. Surf. Sci.* **2022**, *578*, 152016.
- [146] Zhang, J. F.; Liu, J. Y.; Xi, L. F.; Yu, Y. F.; Chen, N.; Sun, S. H.; Wang, W. C.; Lange, K. M.; Zhang, B. Single-atom Au/NiFe layered double hydroxide electrocatalyst: Probing the origin of activity for oxygen evolution reaction. *J. Am. Chem. Soc.* **2018**, *140*, 3876–3879.
- [147] Sun, Y. T.; Ding, S.; Xu, S. S.; Duan, J. J.; Chen, S. Metallic two-dimensional metal-organic framework arrays for ultrafast water splitting. *J. Power Sources* **2021**, *494*, 229733.
- [148] Liu, Y. X.; Wei, Y. N.; Liu, M. H.; Bai, Y. C.; Wang, X. Y.; Shang, S. C.; Du, C. S.; Gao, W. Q.; Chen, J. Y.; Liu, Y. Q. Face-to-face growth of wafer-scale 2D semiconducting MOF films on dielectric substrates. *Adv. Mater.* **2021**, *33*, 2007741.
- [149] Mu, Q. Q.; Zhu, W.; Li, X.; Zhang, C. F.; Su, Y. H.; Lian, Y. B.; Qi, P. W.; Deng, Z.; Zhang, D.; Wang, S. A. et al. Electrostatic charge transfer for boosting the photocatalytic CO_2 reduction on metal centers of 2D MOF/rGO heterostructure. *Appl. Catal. B* **2020**, *262*, 118144.
- [150] Bu, L. Z.; Zhang, N.; Guo, S. J.; Zhang, X.; Li, J.; Yao, J. L.; Wu, T.; Lu, G.; Ma, J. Y.; Su, D. et al. Biaxially strained Pt/Pb/Pt core/shell nanoplate boosts oxygen reduction catalysis. *Science* **2016**, *354*, 1410–1414.
- [151] Wang, Y. Y.; Xie, C.; Zhang, Z. Y.; Liu, D. D.; Chen, R.; Wang, S. Y. *In situ* exfoliated, N-doped, and edge-rich ultrathin layered double hydroxides nanosheets for oxygen evolution reaction. *Adv. Funct. Mater.* **2018**, *28*, 1703363.
- [152] Islam, S.; Kim, M.; Jin, X. Y.; Oh, S. M.; Lee, N. S.; Kim, H.; Hwang, S. J. Bifunctional 2D superlattice electrocatalysts of layered double hydroxide-transition metal dichalcogenide active for overall water splitting. *ACS Energy Lett.* **2018**, *3*, 952–960.
- [153] Li, Y.; Li, F. M.; Meng, X. Y.; Li, S. N.; Zeng, J. H.; Chen, Y. Ultrathin Co_3O_4 nanomeshes for the oxygen evolution reaction. *ACS Catal.* **2018**, *8*, 1913–1920.
- [154] Li, Y.; Li, F. M.; Meng, X. Y.; Wu, X. R.; Li, S. N.; Chen, Y. Direct chemical synthesis of ultrathin holey iron doped cobalt oxide nanosheets on nickel foam for oxygen evolution reaction. *Nano Energy* **2018**, *54*, 238–250.
- [155] Wang, X. L.; Xiao, H.; Li, A.; Li, Z.; Liu, S. J.; Zhang, Q. H.; Gong, Y.; Zheng, L. R.; Zhu, Y. Q.; Chen, C. et al. Constructing NiCo/Fe₃O₄ heteroparticles within MOF-74 for efficient oxygen evolution reactions. *J. Am. Chem. Soc.* **2018**, *140*, 15336–15341.
- [156] Zhao, Y. F.; Jia, X. D.; Chen, G. B.; Shang, L.; Waterhouse, G. I. N.; Wu, L. Z.; Tung, C. H.; O'Hare, D.; Zhang, T. R. Ultrafine NiO nanosheets stabilized by TiO₂ from monolayer NiTi-LDH precursors: An active water oxidation electrocatalyst. *J. Am. Chem. Soc.* **2016**, *138*, 6517–6524.
- [157] Zhang, W.; Wang, Y.; Zheng, H.; Li, R.; Tang, Y. J.; Li, B. Y.; Zhu, C.; You, L. M.; Gao, M. R.; Liu, Z. et al. Embedding ultrafine metal oxide nanoparticles in monolayered metal-organic framework nanosheets enables efficient electrocatalytic oxygen evolution. *ACS Nano* **2020**, *14*, 1971–1981.
- [158] Liu, R.; Wang, Y. Y.; Liu, D. D.; Zou, Y. Q.; Wang, S. Y. Water-plasma-enabled exfoliation of ultrathin layered double hydroxide nanosheets with multivacancies for water oxidation. *Adv. Mater.* **2017**, *29*, 1701546.
- [159] Cheng, W. R.; Zhao, X.; Su, H.; Tang, F. M.; Che, W.; Zhang, H.; Liu, Q. H. Lattice-strained metal-organic-framework arrays for bifunctional oxygen electrocatalysis. *Nat. Energy* **2019**, *4*, 115–122.
- [160] Chala, S. A.; Tsai, M. C.; Su, W. N.; Ibrahim, K. B.; Duma, A. D.; Yeh, M. H.; Wen, C. Y.; Yu, C. H.; Chan, T. S.; Dai, H. J. et al. Site activity and population engineering of NiRu-layered double hydroxide nanosheets decorated with silver nanoparticles for oxygen evolution and reduction reactions. *ACS Catal.* **2019**, *9*, 117–129.
- [161] Zhou, W.; Yang, L.; Wang, X.; Zhao, W. L.; Yang, J. X.; Zhai, D.; Sun, L.; Deng, W. Q. *In silico* design of covalent organic framework-based electrocatalysts. *JACS Au* **2021**, *1*, 1497–1505.
- [162] Joya, K. S.; Sala, X. *In situ* Raman and surface-enhanced Raman spectroscopy on working electrodes: Spectroelectrochemical characterization of water oxidation electrocatalysts. *Phys. Chem. Chem. Phys.* **2015**, *17*, 21094–21103.
- [163] Deng, Y. L.; Yeo, B. S. Characterization of electrocatalytic water splitting and CO_2 reduction reactions using *in situ/operando* Raman spectroscopy. *ACS Catal.* **2017**, *7*, 7873–7889.
- [164] Sasaki, K.; Wang, J. X.; Naohara, H.; Marinkovic, N.; More, K.; Inada, H.; Adzic, R. R. Recent advances in platinum monolayer electrocatalysts for oxygen reduction reaction: Scale-up synthesis, structure and activity of Pt shells on Pd cores. *Electrochim. Acta* **2010**, *55*, 2645–2652.
- [165] Wang, D. N.; Zhou, J. G.; Hu, Y. F.; Yang, J. L.; Han, N.; Li, Y. G.; Sham, T. K. *In situ* X-ray absorption near-edge structure study of advanced NiFe(OH)_x electrocatalyst on carbon paper for water oxidation. *J. Phys. Chem. C* **2015**, *119*, 19573–19583.
- [166] Friebe, D.; Louie, M. W.; Bajdich, M.; Sanwald, K. E.; Cai, Y.; Wise, A. M.; Cheng, M. J.; Sokaras, D.; Weng, T. C.; Alonso-Mori,

- R. et al. Identification of highly active Fe sites in (Ni, Fe)OOH for electrocatalytic water splitting. *J. Am. Chem. Soc.* **2015**, *137*, 1305–1313.
- [167] Zhu, W. X.; Liu, L. Z.; Yue, Z. H.; Zhang, W. T.; Yue, X. Y.; Wang, J.; Yu, S. X.; Wang, L.; Wang, J. L. Au Promoted nickel-iron layered double hydroxide nanoarrays: A modular catalyst enabling high-performance oxygen evolution. *ACS Appl. Mater. Interfaces* **2017**, *9*, 19807–19814.
- [168] Yu, J.; Yu, F.; Yuen, M. F.; Wang, C. D. Two-dimensional layered double hydroxides as a platform for electrocatalytic oxygen evolution. *J. Mater. Chem. A* **2021**, *9*, 9389–9430.
- [169] Anantharaj, S.; Karthick, K.; Venkatesh, M.; Simha, T. V. S. V.; Salunke, A. S.; Ma, L.; Liang, H.; Kundu, S. Enhancing electrocatalytic total water splitting at few layer Pt-NiFe layered double hydroxide interfaces. *Nano Energy* **2017**, *39*, 30–43.
- [170] Chen, Z. W.; Ju, M.; Sun, M. Z.; Jin, L.; Cai, R. M.; Wang, Z.; Dong, L.; Peng, L. M.; Long, X.; Huang, B. L. et al. TM LDH meets birnessite: A 2D-2D hybrid catalyst with long-term stability for water oxidation at industrial operating conditions. *Angew. Chem., Int. Ed.* **2021**, *60*, 9699–9705.
- [171] Jiang, J.; Zhang, A. L.; Li, L. L.; Ai, L. H. Nickel-cobalt layered double hydroxide nanosheets as high-performance electrocatalyst for oxygen evolution reaction. *J. Power Sources* **2015**, *278*, 445–451.
- [172] Gong, M.; Dai, H. J. A mini review of NiFe-based materials as highly active oxygen evolution reaction electrocatalysts. *Nano Res.* **2015**, *8*, 23–39.
- [173] Fu, L. H.; Cheng, G. Z.; Luo, W. Colloidal synthesis of monodisperse trimetallic IrNiFe nanoparticles as highly active bifunctional electrocatalysts for acidic overall water splitting. *J. Mater. Chem. A* **2017**, *5*, 24836–24841.
- [174] Liu, J.; Wang, J. S.; Zhang, B.; Ruan, Y. J.; Lv, L.; Ji, X.; Xu, K.; Miao, L.; Jiang, J. Hierarchical NiCo₂S₄@NiFe LDH heterostructures supported on nickel foam for enhanced overall-water-splitting activity. *ACS Appl. Mater. Interfaces* **2017**, *9*, 15364–15372.
- [175] Peng, L. S.; Yang, N.; Yang, Y. Q.; Wang, Q.; Xie, X. Y.; Sun-Waterhouse, D.; Shang, L.; Zhang, T. R.; Waterhouse, G. I. N. Atomic cation-vacancy engineering of NiFe-layered double hydroxides for improved activity and stability towards the oxygen evolution reaction. *Angew. Chem., Int. Ed.* **2021**, *60*, 24612–24619.
- [176] Luo, M.; Cai, Z.; Wang, C.; Bi, Y. M.; Qian, L.; Hao, Y. C.; Li, L.; Kuang, Y.; Li, Y. P.; Lei, X. D. et al. Phosphorus oxoanion-intercalated layered double hydroxides for high-performance oxygen evolution. *Nano Res.* **2017**, *10*, 1732–1739.
- [177] Liu, Q. Y.; Wang, H.; Wang, X. N.; Tong, R.; Zhou, X. L.; Peng, X. N.; Wang, H. B.; Tao, H. L.; Zhang, Z. H. Bifunctional Ni_{1-x}Fe_x layered double hydroxides/Ni foam electrodes for high-efficient overall water splitting: A study on compositional tuning and valence state evolution. *Int. J. Hydrogen Energy* **2017**, *42*, 5560–5568.
- [178] Zeng, L. L.; Yang, L. J.; Lu, J.; Jia, J.; Yu, J. Y.; Deng, Y. Q.; Shao, M. F.; Zhou, W. J. One-step synthesis of Fe-Ni hydroxide nanosheets derived from bimetallic foam for efficient electrocatalytic oxygen evolution and overall water splitting. *Chin. Chem. Lett.* **2018**, *29*, 1875–1878.
- [179] Xie, J. F.; Qu, H. C.; Lei, F. C.; Peng, X.; Liu, W. W.; Gao, L.; Hao, P.; Cui, G. W.; Tang, B. Partially amorphous nickel-iron layered double hydroxide nanosheet arrays for robust bifunctional electrocatalysis. *J. Mater. Chem. A* **2018**, *6*, 16121–16129.
- [180] Zhou, D. J.; Cai, Z.; Bi, Y. M.; Tian, W. L.; Luo, M.; Zhang, Q.; Zhang, Q.; Xie, Q. X.; Wang, J. D.; Li, Y. P. et al. Effects of redox-active interlayer anions on the oxygen evolution reactivity of NiFe-layered double hydroxide nanosheets. *Nano Res.* **2018**, *11*, 1358–1368.
- [181] Si, S.; Hu, H. S.; Liu, R. J.; Xu, Z. X.; Wang, C. B.; Feng, Y. Y. Co-NiFe layered double hydroxide nanosheets as an efficient electrocatalyst for the electrochemical evolution of oxygen. *Int. J. Hydrogen Energy* **2020**, *45*, 9368–9379.
- [182] Jiang, J.; Sun, F. F.; Zhou, S.; Hu, W.; Zhang, H.; Dong, J. C.; Jiang, Z.; Zhao, J. J.; Li, J. F.; Yan, W. S. et al. Atomic-level insight into super-efficient electrocatalytic oxygen evolution on iron and vanadium co-doped nickel (oxy)hydroxide. *Nat. Commun.* **2018**, *9*, 2885.
- [183] Wang, T.; Xu, W. C.; Wang, H. X. Ternary NiCoFe layered double hydroxide nanosheets synthesized by cation exchange reaction for oxygen evolution reaction. *Electrochim. Acta* **2017**, *257*, 118–127.
- [184] Dinh, K. N.; Zheng, P. L.; Dai, Z. F.; Zhang, Y.; Dangel, R.; Zheng, Y.; Li, B.; Zong, Y.; Yan, Q. Y. Ultrathin porous NiFeV ternary layer hydroxide nanosheets as a highly efficient bifunctional electrocatalyst for overall water splitting. *Small* **2018**, *14*, 1703257.
- [185] Wang, Z. L.; Liu, W. J.; Hu, Y. M.; Guan, M. L.; Xu, L.; Li, H. P.; Bao, J.; Li, H. M. Cr-doped CoFe layered double hydroxides: Highly efficient and robust bifunctional electrocatalyst for the oxidation of water and urea. *Appl. Catal. B* **2020**, *272*, 118959.
- [186] Choi, S.; Park, Y.; Yang, H.; Jin, H.; Tomboc, G. M.; Lee, K. Vacancy-engineered catalysts for water electrolysis. *CrystEngComm* **2020**, *22*, 1500–1513.
- [187] Yang, M. Q.; Wang, J.; Wu, H.; Ho, G. W. Noble metal-free nanocatalysts with vacancies for electrochemical water splitting. *Small* **2018**, *14*, 1703323.
- [188] Liu, B.; Wang, Y.; Peng, H. Q.; Yang, R. O.; Jiang, Z.; Zhou, X. T.; Lee, C. S.; Zhao, H. J.; Zhang, W. J. Iron vacancies induced bifunctionality in ultrathin ferroxhyte nanosheets for overall water splitting. *Adv. Mater.* **2018**, *30*, 1803144.
- [189] Kim, S. H.; Park, Y. S.; Kim, C.; Kwon, I. Y.; Lee, J.; Jin, H.; Lee, Y. S.; Choi, S. M.; Kim, Y. Self-assembly of Ni-Fe layered double hydroxide at room temperature for oxygen evolution reaction. *Energy Rep.* **2020**, *6*, 248–254.
- [190] Zhou, D. J.; Xiong, X. Y.; Cai, Z.; Han, N. N.; Jia, Y.; Xie, Q. X.; Duan, X. X.; Xie, T. H.; Zheng, X. L.; Sun, X. M. et al. Flame-engraved nickel-iron layered double hydroxide nanosheets for boosting oxygen evolution reactivity. *Small Methods* **2018**, *2*, 1800083.
- [191] Wu, C. C.; Li, H. Q.; Xia, Z. X.; Zhang, X. M.; Deng, R. Y.; Wang, S. L.; Sun, G. Q. NiFe layered double hydroxides with unsaturated metal sites via precovered surface strategy for oxygen evolution reaction. *ACS Catal.* **2020**, *10*, 11127–11135.
- [192] Liu, S. X.; Zhang, H. W.; Hu, E. L.; Zhu, T. Y.; Zhou, C. Y.; Huang, Y. C.; Ling, M.; Gao, X. H.; Lin, Z. Boosting oxygen evolution activity of NiFe-LDH using oxygen vacancies and morphological engineering. *J. Mater. Chem. A* **2021**, *9*, 23697–23702.
- [193] Chen, R.; Hung, S. F.; Zhou, D. J.; Gao, J. J.; Yang, C. J.; Tao, H. B.; Yang, H. B.; Zhang, L. P.; Zhang, L. L.; Xiong, Q. H. et al. Layered structure causes bulk NiFe layered double hydroxide unstable in alkaline oxygen evolution reaction. *Adv. Mater.* **2019**, *31*, 1903909.
- [194] Zhang, X.; Zhao, Y. F.; Zhao, Y. X.; Shi, R.; Waterhouse, G. I. N.; Zhang, T. R. A simple synthetic strategy toward defect-rich porous monolayer NiFe-layered double hydroxide nanosheets for efficient electrocatalytic water oxidation. *Adv. Energy Mater.* **2019**, *9*, 1900881.
- [195] Zhao, Z. Y.; Shao, Q.; Xue, J. Y.; Huang, B. L.; Niu, Z.; Gu, H. W.; Huang, X. Q.; Lang, J. P. Multiple structural defects in ultrathin NiFe-LDH nanosheets synergistically and remarkably boost water oxidation reaction. *Nano Res.* **2022**, *15*, 310–316.
- [196] Wu, Y. J.; Yang, J.; Tu, T. X.; Li, W. Q.; Zhang, P. F.; Zhou, Y.; Li, J. F.; Li, J. T.; Sun, S. G. Evolution of cationic vacancy defects: A motif for surface restructuring of OER precatalyst. *Angew. Chem., Int. Ed.* **2021**, *60*, 26829–26836.
- [197] Wang, Q. X.; Dastafkan, K.; Zhao, C. Design strategies for non-precious metal oxide electrocatalysts for oxygen evolution reactions. *Curr. Opin. Electrochem.* **2018**, *10*, 16–23.
- [198] Ma, W.; Ma, R. Z.; Wang, C. X.; Liang, J. B.; Liu, X. H.; Zhou, K. C.; Sasaki, T. A superlattice of alternately stacked Ni-Fe hydroxide nanosheets and graphene for efficient splitting of water. *ACS Nano*

- 2015, 9, 1977–1984.
- [199] Gong, M.; Li, Y. G.; Wang, H. L.; Liang, Y. Y.; Wu, J. Z.; Zhou, J. G.; Wang, J.; Regier, T.; Wei, F.; Dai, H. J. An advanced Ni-Fe layered double hydroxide electrocatalyst for water oxidation. *J. Am. Chem. Soc.* **2013**, *135*, 8452–8455.
- [200] Wang, Y. Z.; Zhou, Y. Y.; Han, M. Z.; Xi, Y. K.; You, H. H.; Hao, X. F.; Li, Z. P.; Zhou, J. S.; Song, D. D.; Wang, D. et al. Environmentally-friendly exfoliate and active site self-assembly: Thin 2D/2D heterostructure amorphous nickel-iron alloy on 2D materials for efficient oxygen evolution reaction. *Small* **2019**, *15*, 1805435.
- [201] Jia, Y.; Zhang, L. Z.; Gao, G. P.; Chen, H.; Wang, B.; Zhou, J. Z.; Soo, M. T.; Hong, M.; Yan, X. C.; Qian, G. R. et al. A heterostructure coupling of exfoliated Ni-Fe hydroxide nanosheet and defective graphene as a bifunctional electrocatalyst for overall water splitting. *Adv. Mater.* **2017**, *29*, 1700017.
- [202] Kong, F. H.; Zhang, W. W.; Sun, L. P.; Huo, L. H.; Zhao, H. Interface electronic coupling in hierarchical FeLDH(FeCo)/Co(OH)₂ arrays for efficient electrocatalytic oxygen evolution. *ChemSusChem* **2019**, *12*, 3592–3601.
- [203] Luo, Y.; Wu, Y. H.; Wu, D. H.; Huang, C.; Xiao, D. Z.; Chen, H. Y.; Zheng, S. L.; Chu, P. K. NiFe-layered double hydroxide synchronously activated by heterojunctions and vacancies for the oxygen evolution reaction. *ACS Appl. Mater. Interfaces* **2020**, *12*, 42850–42858.
- [204] Hu, L. Y.; Zeng, X.; Wei, X. Q.; Wang, H. J.; Wu, Y.; Gu, W. L.; Shi, L.; Zhu, C. Z. Interface engineering for enhancing electrocatalytic oxygen evolution of NiFe LDH/NiFe heterostructures. *Appl. Catal. B* **2020**, *273*, 119014.
- [205] Dionigi, F.; Strasser, P. NiFe-based (Oxy)hydroxide catalysts for oxygen evolution reaction in non-acidic electrolytes. *Adv. Energy Mater.* **2016**, *6*, 1600621.
- [206] Yu, M. Z.; Zhou, S.; Wang, Z. Y.; Zhao, J. J.; Qiu, J. S. Boosting electrocatalytic oxygen evolution by synergistically coupling layered double hydroxide with MXene. *Nano Energy* **2018**, *44*, 181–190.
- [207] Han, X. T.; Yu, C.; Yang, J.; Zhao, C. T.; Huang, H. W.; Liu, Z. B.; Ajayan, P. M.; Qiu, J. S. Mass and charge transfer coenhanced oxygen evolution behaviors in CoFe-layered double hydroxide assembled on graphene. *Adv. Mater. Interfaces* **2016**, *3*, 1500782.
- [208] Peng, C. L.; Ran, N.; Wan, G.; Zhao, W. P.; Kuang, Z. Y.; Lu, Z.; Sun, C. J.; Liu, J. J.; Wang, L. Z.; Chen, H. R. Engineering active Fe sites on nickel-iron layered double hydroxide through component segregation for oxygen evolution reaction. *ChemSusChem* **2020**, *13*, 811–818.
- [209] Cao, J. H.; Lei, C. J.; Yang, J.; Cheng, X. D.; Li, Z. J.; Yang, B.; Zhang, X. W.; Lei, L. C.; Hou, Y.; Ostrikov, K. An ultrathin cobalt-based zeolitic imidazolate framework nanosheet array with a strong synergistic effect towards the efficient oxygen evolution reaction. *J. Mater. Chem. A* **2018**, *6*, 18877–18883.
- [210] Hu, L. Y.; Li, M. Y.; Wei, X. Q.; Wang, H. J.; Wu, Y.; Wen, J.; Gu, W. L.; Zhu, C. Z. Modulating interfacial electronic structure of CoNi LDH nanosheets with Ti₃C₂T_x MXene for enhancing water oxidation catalysis. *Chem. Eng. J.* **2020**, *398*, 125605.
- [211] Li, X. J.; Zhou, J.; Li, X. C.; Xin, M. Y.; Cai, T. H.; Xing, W.; Chai, Y. M.; Xue, Q. Z.; Yan, Z. F. Bifunctional petaloid nickel manganese layered double hydroxides decorated on a freestanding carbon foam for flexible asymmetric supercapacitor and oxygen evolution. *Electrochim. Acta* **2017**, *252*, 275–285.
- [212] Tang, D.; Liu, J.; Wu, X. Y.; Liu, R. H.; Han, X.; Han, Y. Z.; Huang, H.; Liu, Y.; Kang, Z. H. Carbon quantum dot/NiFe layered double-hydroxide composite as a highly efficient electrocatalyst for water oxidation. *ACS Appl. Mater. Interfaces* **2014**, *6*, 7918–7925.
- [213] Yin, S. M.; Tu, W. G.; Sheng, Y.; Du, Y. H.; Kraft, M.; Borgna, A.; Xu, R. A highly efficient oxygen evolution catalyst consisting of interconnected nickel-iron-layered double hydroxide and carbon nanodomains. *Adv. Mater.* **2018**, *30*, 1705106.
- [214] Wang, L.; Huang, X. L.; Xue, J. M. Graphitic mesoporous carbon loaded with iron-nickel hydroxide for superior oxygen evolution reactivity. *ChemSusChem* **2016**, *9*, 1835–1842.
- [215] Ni, Y. M.; Yao, L. H.; Wang, Y.; Liu, B.; Cao, M. H.; Hu, C. W. Construction of hierarchically porous graphitized carbon-supported NiFe layered double hydroxides with a core-shell structure as an enhanced electrocatalyst for the oxygen evolution reaction. *Nanoscale* **2017**, *9*, 11596–11604.
- [216] Liu, H. J.; Zhou, J.; Wu, C. Q.; Wang, C. D.; Zhang, Y. K.; Liu, D. B.; Lin, Y. X.; Jiang, H. L.; Song, L. Integrated flexible electrode for oxygen evolution reaction: Layered double hydroxide coupled with single-walled carbon nanotubes film. *ACS Sustainable Chem. Eng.* **2018**, *6*, 2911–2915.
- [217] Wang, Y. Q.; Tao, S.; Lin, H.; Han, S. B.; Zhong, W. H.; Xie, Y. S.; Hu, J.; Yang, S. H. NaBH₄ induces a high ratio of Ni³⁺/Ni²⁺ boosting OER activity of the NiFe LDH electrocatalyst. *RSC Adv.* **2020**, *10*, 33475–33482.
- [218] Wang, Y. Q.; Tao, S.; Lin, H.; Wang, G. P.; Zhao, K. N.; Cai, R. M.; Tao, K. W.; Zhang, C. X.; Sun, M. Z.; Hu, J. et al. Atomically targeting NiFe LDH to create multivacancies for OER catalysis with a small organic anchor. *Nano Energy* **2021**, *81*, 105606.
- [219] Zhan, T. R.; Liu, X. L.; Lu, S. S.; Hou, W. G. Nitrogen doped NiFe layered double hydroxide/reduced graphene oxide mesoporous nanosphere as an effective bifunctional electrocatalyst for oxygen reduction and evolution reactions. *Appl. Catal. B* **2017**, *205*, 551–558.
- [220] Wang, Q.; Shang, L.; Shi, R.; Zhang, X.; Zhao, Y. F.; Waterhouse, G. I. N.; Wu, L. Z.; Tung, C. H.; Zhang, T. R. NiFe layered double hydroxide nanoparticles on Co,N-codoped carbon nanoframes as efficient bifunctional catalysts for rechargeable zinc-air batteries. *Adv. Energy Mater.* **2017**, *7*, 1700467.
- [221] Tang, C.; Wang, H. S.; Wang, H. F.; Zhang, Q.; Tian, G. L.; Nie, J. Q.; Wei, F. Spatially confined hybridization of nanometer-sized NiFe hydroxides into nitrogen-doped graphene frameworks leading to superior oxygen evolution reactivity. *Adv. Mater.* **2015**, *27*, 4516–4522.
- [222] Côté, A. P.; Benin, A. I.; Ockwig, N. W.; O’Keeffe, M.; Matzger, A. J.; Yaghi, O. M. Porous, crystalline, covalent organic frameworks. *Science* **2005**, *310*, 1166–1170.
- [223] Guo, X. X.; Mao, T. H.; Wang, Z. F.; Cheng, P.; Chen, Y.; Ma, S. Q.; Zhang, Z. J. Fabrication of photoresponsive crystalline artificial muscles based on PEGylated covalent organic framework membranes. *ACS Cent. Sci.* **2020**, *6*, 787–794.
- [224] Bi, S.; Thiruvengadam, P.; Wei, S. C.; Zhang, W.; Zhang, F.; Gao, L. S.; Xu, J. S.; Wu, D. Q.; Chen, J. S.; Zhang, F. Vinylene-bridged two-dimensional covalent organic frameworks via Knoevenagel condensation of tricyanomesitylene. *J. Am. Chem. Soc.* **2020**, *142*, 11893–11900.
- [225] Yang, C. H.; Yang, Z. D.; Dong, H.; Sun, N.; Lu, Y.; Zhang, F. M.; Zhang, G. L. Theory-driven design and targeting synthesis of a highly-conjugated basal-plane 2D covalent organic framework for metal-free electrocatalytic OER. *ACS Energy Lett.* **2019**, *4*, 2251–2258.
- [226] Wang, Q. C.; Ji, Y. J.; Lei, Y. P.; Wang, Y. B.; Wang, Y. D.; Li, Y. Y.; Wang, S. Y. Pyridinic-N-dominated doped defective graphene as a superior oxygen electrocatalyst for ultrahigh-energy-density Zn-air batteries. *ACS Energy Lett.* **2018**, *3*, 1183–1191.
- [227] Zhao, X. J.; Pachfule, P.; Li, S.; Langenhahn, T.; Ye, M. Y.; Schlesiger, C.; Praetz, S.; Schmidt, J.; Thomas, A. Macro/microporous covalent organic frameworks for efficient electrocatalysis. *J. Am. Chem. Soc.* **2019**, *141*, 6623–6630.
- [228] Shinde, D. B.; Aiyappa, H. B.; Bhadra, M.; Biswal, B. P.; Wadge, P.; Kandambeth, S.; Garai, B.; Kundu, T.; Kurungot, S.; Banerjee, R. A mechanochemically synthesized covalent organic framework as a proton-conducting solid electrolyte. *J. Mater. Chem. A* **2016**, *4*, 2682–2690.
- [229] Aiyappa, H. B.; Thote, J.; Shinde, D. B.; Banerjee, R.; Kurungot, S. Cobalt-modified covalent organic framework as a robust water oxidation electrocatalyst. *Chem. Mater.* **2016**, *28*, 4375–4379.
- [230] Huang, H.; Li, F. M.; Zhang, Y.; Chen, Y. Two-dimensional graphdiyne analogue Co-coordinated porphyrin covalent organic framework nanosheets as a stable electrocatalyst for the oxygen

- evolution reaction. *J. Mater. Chem. A* **2019**, *7*, 5575–5582.
- [231] Gao, Z.; Gong, L. L.; He, X. Q.; Su, X. M.; Xiao, L. H.; Luo, F. General strategy to fabricate metal-incorporated pyrolysis-free covalent organic framework for efficient oxygen evolution reaction. *Inorg. Chem.* **2020**, *59*, 4995–5003.
- [232] Mondal, S.; Mohanty, B.; Nurhuda, M.; Dalapati, S.; Jana, R.; Addicoat, M.; Datta, A.; Jena, B. K.; Bhaumik, A. A thiadiazole-based covalent organic framework: A metal-free electrocatalyst toward oxygen evolution reaction. *ACS Catal.* **2020**, *10*, 5623–5630.
- [233] Xie, J. F.; Zhang, X. D.; Zhang, H.; Zhang, J. J.; Li, S.; Wang, R. X.; Pan, B. C.; Xie, Y. Intralayered ostwald ripening to ultrathin nanomesh catalyst with robust oxygen-evolving performance. *Adv. Mater.* **2017**, *29*, 1604765.
- [234] Zhao, S. L.; Wang, Y.; Dong, J. C.; He, C. T.; Yin, H. J.; An, P. F.; Zhao, K.; Zhang, X. F.; Gao, C.; Zhang, L. J. et al. Ultrathin metal-organic framework nanosheets for electrocatalytic oxygen evolution. *Nat. Energy* **2016**, *1*, 16184.
- [235] Wang, Y. X.; Zhao, M. T.; Ping, J. F.; Chen, B.; Cao, X. H.; Huang, Y.; Tan, C. L.; Ma, Q. L.; Wu, S. X.; Yu, Y. F. et al. Bioinspired design of ultrathin 2D bimetallic metal-organic-framework nanosheets used as biomimetic enzymes. *Adv. Mater.* **2016**, *28*, 4149–4155.
- [236] Lu, X. F.; Liao, P. Q.; Wang, J. W.; Wu, J. X.; Chen, X. W.; He, C. T.; Zhang, J. P.; Li, G. R.; Chen, X. M. An alkaline-stable, metal hydroxide mimicking metal-organic framework for efficient electrocatalytic oxygen evolution. *J. Am. Chem. Soc.* **2016**, *138*, 8336–8339.
- [237] Wang, J.; Gan, L. Y.; Zhang, W. Y.; Peng, Y. C.; Yu, H.; Yan, Q. Y.; Xia, X. H.; Wang, X. *In situ* formation of molecular Ni-Fe active sites on heteroatom-doped graphene as a heterogeneous electrocatalyst toward oxygen evolution. *Sci. Adv.* **2018**, *4*, eaap7970.
- [238] Li, F. L.; Wang, P. T.; Huang, X. Q.; Young, D. J.; Wang, H. F.; Braunstein, P.; Lang, J. P. Large-scale, bottom-up synthesis of binary metal-organic framework nanosheets for efficient water oxidation. *Angew. Chem., Int. Ed.* **2019**, *58*, 7051–7056.
- [239] Hai, G. T.; Jia, X. L.; Zhang, K. Y.; Liu, X.; Wu, Z. Y.; Wang, G. High-performance oxygen evolution catalyst using two-dimensional ultrathin metal-organic frameworks nanosheets. *Nano Energy* **2018**, *44*, 345–352.
- [240] Grimaud, A.; Diaz-Morales, O.; Han, B. H.; Hong, W. T.; Lee, Y. L.; Giordano, L.; Stoerzinger, K. A.; Koper, M. T. M.; Shao-Horn, Y. Activating lattice oxygen redox reactions in metal oxides to catalyze oxygen evolution. *Nat. Chem.* **2017**, *9*, 457–465.
- [241] Görlin, M.; Chernev, P.; De Araújo, J. F.; Reier, T.; Drespe, S.; Paul, B.; Krähnert, R.; Dau, H.; Strasser, P. Oxygen evolution reaction dynamics, faradaic charge efficiency, and the active metal redox states of Ni-Fe oxide water splitting electrocatalysts. *J. Am. Chem. Soc.* **2016**, *138*, 5603–5614.
- [242] Ji, Q. Q.; Kong, Y.; Wang, C.; Tan, H.; Duan, H. L.; Hu, W.; Li, G. N.; Lu, Y.; Li, N.; Wang, Y. et al. Lattice strain induced by linker scission in metal-organic framework nanosheets for oxygen evolution reaction. *ACS Catal.* **2020**, *10*, 5691–5697.
- [243] Duan, J. J.; Chen, S.; Zhao, C. Ultrathin metal-organic framework array for efficient electrocatalytic water splitting. *Nat. Commun.* **2017**, *8*, 15341.
- [244] Li, Z. Q.; Yin, L. W. Sandwich-like reduced graphene oxide wrapped MOF-derived ZnCo₂O₄-ZnO-C on nickel foam as anodes for high performance lithium ion batteries. *J. Mater. Chem. A* **2015**, *3*, 21569–21577.
- [245] Bavykina, A.; Kolobov, N.; Khan, I. S.; Bau, J. A.; Ramirez, A.; Gascon, J. Metal-organic frameworks in heterogeneous catalysis: Recent progress, new trends, and future perspectives. *Chem. Rev.* **2020**, *120*, 8468–8535.
- [246] Meng, J. S.; Liu, X.; Niu, C. J.; Pang, Q.; Li, J. T.; Liu, F.; Liu, Z. A.; Mai, L. Q. Advances in metal-organic framework coatings: Versatile synthesis and broad applications. *Chem. Soc. Rev.* **2020**, *49*, 3142–3186.
- [247] Yang, D. X.; Chen, Y. F.; Su, Z.; Zhang, X. J.; Zhang, W. L.; Srinivas, K. Organic carboxylate-based MOFs and derivatives for electrocatalytic water oxidation. *Coord. Chem. Rev.* **2021**, *428*, 213619.
- [248] Du, J.; Li, F.; Sun, L. C. Metal-organic frameworks and their derivatives as electrocatalysts for the oxygen evolution reaction. *Chem. Soc. Rev.* **2021**, *50*, 2663–2695.
- [249] Qin, X. Y.; Kim, D.; Piao, Y. Z. Metal-organic frameworks-derived novel nanostructured electrocatalysts for oxygen evolution reaction. *Carbon Energy* **2021**, *3*, 66–100.
- [250] Guan, J. Q. Effect of coordination surroundings of isolated metal sites on electrocatalytic performances. *J. Power Sources* **2021**, *506*, 230143.
- [251] Zhang, W. M.; Yao, X. Y.; Zhou, S. N.; Li, X. W.; Li, L.; Yu, Z.; Gu, L. ZIF-8/ZIF-67-derived Co-N_x-embedded 1D porous carbon nanofibers with graphitic carbon-encased Co nanoparticles as an efficient bifunctional electrocatalyst. *Small* **2018**, *14*, 1800423.
- [252] Zhao, J. J.; Hu, H. B.; Wu, M. Z. N-doped-carbon/cobalt-nanoparticle/N-doped-carbon multi-layer sandwich nanohybrids derived from cobalt MOFs having 3D molecular structures as bifunctional electrocatalysts for on-chip solid-state Zn-air batteries. *Nanoscale* **2020**, *12*, 3750–3762.
- [253] Wang, J. M.; Liu, D.; Zhang, L. Z.; Qian, Y. J.; Chen, C.; Wang, L. F.; Lei, W. W. Rational design of 2D super holey metal carbonitride leaf-like nanostructure for efficient oxygen electrocatalysis. *Carbon* **2020**, *164*, 287–295.
- [254] Wang, J.; Huang, Z. Q.; Liu, W.; Chang, C. R.; Tang, H. L.; Li, Z. J.; Chen, W. X.; Jia, C. J.; Yao, T.; Wei, S. Q. et al. Design of N-coordinated dual-metal sites: A stable and active Pt-free catalyst for acidic oxygen reduction reaction. *J. Am. Chem. Soc.* **2017**, *139*, 17281–17284.
- [255] Xu, Q. C.; Jiang, H.; Li, Y. H.; Liang, D.; Hu, Y. J.; Li, C. Z. *In-situ* enriching active sites on co-doped Fe-Co₄N@N-C nanosheet array as air cathode for flexible rechargeable Zn-air batteries. *Appl. Catal. B* **2019**, *256*, 117893.
- [256] Gu, X. C.; Ji, Y. G.; Tian, J. Q.; Wu, X.; Feng, L. G. Combined MOF derivation and fluorination imparted efficient synergism of Fe-Co fluoride for oxygen evolution reaction. *Chem. Eng. J.* **2022**, *427*, 131576.
- [257] Zou, Z. H.; Wang, J. L.; Pan, H. R.; Li, J.; Guo, K. L.; Zhao, Y. Q.; Xu, C. L. Enhanced oxygen evolution reaction of defective CoP/MOF-integrated electrocatalyst by partial phosphating. *J. Mater. Chem. A* **2020**, *8*, 14099–14105.
- [258] Liu, G. H.; Li, J. D.; Fu, J.; Jiang, G. P.; Lui, G.; Luo, D.; Deng, Y. P.; Zhang, J.; Cano, Z. P.; Yu, A. P. et al. An oxygen-vacancy-rich semiconductor-supported bifunctional catalyst for efficient and stable zinc-air batteries. *Adv. Mater.* **2019**, *31*, 1806761.
- [259] Deng, Y. P.; Jiang, Y.; Luo, D.; Fu, J.; Liang, R. L.; Cheng, S. B.; Bai, Z. Y.; Liu, Y. S.; Lei, W.; Yang, L. et al. Hierarchical porous double-shelled electrocatalyst with tailored lattice alkalinity toward bifunctional oxygen reactions for metal-air batteries. *ACS Energy Lett.* **2017**, *2*, 2706–2712.
- [260] Lin, Y. F.; Wan, H.; Wu, D.; Chen, G.; Zhang, N.; Liu, X. H.; Li, J. H.; Cao, Y. J.; Qiu, G. Z.; Ma, R. Z. Metal-organic framework hexagonal nanoplates: Bottom-up synthesis, topotactic transformation, and efficient oxygen evolution reaction. *J. Am. Chem. Soc.* **2020**, *142*, 7317–7321.
- [261] Zhu, J. B.; Xiao, M. L.; Li, G. R.; Li, S.; Zhang, J.; Liu, G. H.; Ma, L.; Wu, T. P.; Lu, J.; Yu, A. P. et al. A triphasic bifunctional oxygen electrocatalyst with tunable and synergetic interfacial structure for rechargeable Zn-air batteries. *Adv. Energy Mater.* **2020**, *10*, 1903003.
- [262] Zhong, Y. T.; Pan, Z. H.; Wang, X. S.; Yang, J.; Qiu, Y. C.; Xu, S. Y.; Lu, Y. T.; Huang, Q. M.; Li, W. S. Hierarchical Co₃O₄ nano-micro arrays featuring superior activity as cathode in a flexible and rechargeable zinc-air battery. *Adv. Sci.* **2019**, *6*, 1802243.
- [263] Huang, J.; Wu, J. Q.; Shao, B.; Lan, B. L.; Yang, F. J.; Sun, Y.; Tan, X. Q.; He, C. T.; Zhang, Z. Ion-induced delamination of layered bulk metal-organic frameworks into ultrathin nanosheets for boosting the oxygen evolution reaction. *ACS Sustainable Chem. Eng.* **2020**, *8*, 10554–10563.

- [264] Kuang, X.; Luo, Y. C.; Kuang, R.; Wang, Z. L.; Sun, X.; Zhang, Y.; Wei, Q. Metal organic framework nanofibers derived Co_3O_4 -doped carbon-nitrogen nanosheet arrays for high efficiency electrocatalytic oxygen evolution. *Carbon* **2018**, *137*, 433–441.
- [265] Rui, K.; Zhao, G. Q.; Chen, Y. P.; Lin, Y.; Zhou, Q.; Chen, J. Y.; Zhu, J. X.; Sun, W. P.; Huang, W.; Dou, S. X. Hybrid 2D dual-metal-organic frameworks for enhanced water oxidation catalysis. *Adv. Funct. Mater.* **2018**, *28*, 1801554.
- [266] Yue, K. H.; Liu, J. L.; Xia, C. F.; Zhan, K.; Wang, P.; Wang, X. Y.; Yan, Y.; Xia, B. Y. Controllable synthesis of multidimensional carboxylic acid-based NiFe MOFs as efficient electrocatalysts for oxygen evolution. *Mater. Chem. Front.* **2021**, *5*, 7191–7198.
- [267] Li, J. T.; Huang, W. Z.; Wang, M. M.; Xi, S. B.; Meng, J. S.; Zhao, K. N.; Jin, J.; Xu, W. W.; Wang, Z. Y.; Liu, X. et al. Low-crystalline bimetallic metal-organic framework electrocatalysts with rich active sites for oxygen evolution. *ACS Energy Lett.* **2019**, *4*, 285–292.
- [268] Gu, X. G.; Zhang, X. Y.; Ma, H. L.; Jia, S. R.; Zhang, P. F.; Zhao, Y. J.; Liu, Q.; Wang, J. G.; Zheng, X. Y.; Lam, J. W. Y. et al. Corannulene-incorporated AIE nanodots with highly suppressed nonradiative decay for boosted cancer phototheranostics *in vivo*. *Adv. Mater.* **2018**, *30*, 1801065.
- [269] Xu, Y.; Tu, W. G.; Zhang, B. W.; Yin, S. M.; Huang, Y. Z.; Kraft, M.; Xu, R. Nickel nanoparticles encapsulated in few-layer nitrogen-doped graphene derived from metal-organic frameworks as efficient bifunctional electrocatalysts for overall water splitting. *Adv. Mater.* **2017**, *29*, 1605957.
- [270] Shi, X.; Wu, A. P.; Yan, H. J.; Zhang, L.; Tian, C. G.; Wang, L.; Fu, H. G. A “MOFs plus MOFs” strategy toward Co-Mo₂N tubes for efficient electrocatalytic overall water splitting. *J. Mater. Chem. A* **2018**, *6*, 20100–20109.
- [271] Hong, W.; Kitta, M.; Xu, Q. Bimetallic MOF-derived FeCo-P/C nanocomposites as efficient catalysts for oxygen evolution reaction. *Small Methods* **2018**, *2*, 1800214.
- [272] Cao, L. M.; Hu, Y. W.; Tang, S. F.; Iljin, A.; Wang, J. W.; Zhang, Z. M.; Lu, T. B. Fe-CoP electrocatalyst derived from a bimetallic prussian blue analogue for large-current-density oxygen evolution and overall water splitting. *Adv. Sci.* **2018**, *5*, 1800949.
- [273] Yan, L. T.; Cao, L.; Dai, P. C.; Gu, X.; Liu, D. D.; Li, L. J.; Wang, Y.; Zhao, X. B. Metal-organic frameworks derived nanotube of nickel-cobalt bimetal phosphides as highly efficient electrocatalysts for overall water splitting. *Adv. Funct. Mater.* **2017**, *27*, 1703455.
- [274] Huang, Z. F.; Song, J. J.; Du, Y. H.; Xi, S. B.; Dou, S.; Nsanzimana, J. M. V.; Wang, C.; Xu, Z. J.; Wang, X. Chemical and structural origin of lattice oxygen oxidation in Co-Zn oxyhydroxide oxygen evolution electrocatalysts. *Nat. Energy* **2019**, *4*, 329–338.
- [275] Zhan, G. W.; Fan, L. L.; Zhao, F. G.; Huang, Z. L.; Chen, B.; Yang, X.; Zhou, S. F. Fabrication of ultrathin 2D Cu-BDC nanosheets and the derived integrated MOF nanocomposites. *Adv. Funct. Mater.* **2019**, *29*, 1806720.
- [276] Xia, B. Y.; Yan, Y.; Li, N.; Wu, H. B.; Lou, X. W.; Wang, X. A metal-organic framework-derived bifunctional oxygen electrocatalyst. *Nat. Energy* **2016**, *1*, 15006.
- [277] Shao, M. F.; Ning, F. Y.; Zhao, J. W.; Wei, M.; Evans, D. G.; Duan, X. Hierarchical layered double hydroxide microspheres with largely enhanced performance for ethanol electrooxidation. *Adv. Funct. Mater.* **2013**, *23*, 3513–3518.
- [278] Yu, X. W.; Zhang, M.; Yuan, W. J.; Shi, G. Q. A high-performance three-dimensional Ni-Fe layered double hydroxide/graphene electrode for water oxidation. *J. Mater. Chem. A* **2015**, *3*, 6921–6928.
- [279] Liu, Z. B.; Yu, C.; Han, X. T.; Yang, J.; Zhao, C. T.; Huang, H. W.; Qiu, J. S. CoMn layered double hydroxides/carbon nanotubes architectures as high-performance electrocatalysts for the oxygen evolution reaction. *ChemElectroChem* **2016**, *3*, 850.
- [280] Cheng, Y. W.; Zhang, Y. M.; Li, Y.; Dai, J. H.; Song, Y. Hierarchical Ni₂P/Cr₂CT_x (MXene) composites with oxidized surface groups as efficient bifunctional electrocatalysts for overall water splitting. *J. Mater. Chem. A* **2019**, *7*, 9324–9334.
- [281] Xu, J. J.; Zhao, Y. J.; Li, M. Y.; Fan, G. L.; Yang, L.; Li, F. A strong coupled 2D metal-organic framework and ternary layered double hydroxide hierarchical nanocomposite as an excellent electrocatalyst for the oxygen evolution reaction. *Electrochim. Acta* **2019**, *307*, 275–284.
- [282] Rodenas, T.; Beeg, S.; Spanos, I.; Neugebauer, S.; Girgsdies, F.; Algara-Siller, G.; Schleker, P. P. M.; Jakes, P.; Pfänder, N.; Willinger, M. et al. 2D metal organic framework-graphitic carbon nanocomposites as precursors for high-performance O₂-evolution electrocatalysts. *Adv. Energy Mater.* **2018**, *8*, 1802404.
- [283] Han, X. T.; Yu, C.; Zhou, S.; Zhao, C. T.; Huang, H. W.; Yang, J.; Liu, Z. B.; Zhao, J. J.; Qiu, J. S. Ultrasensitive iron-triggered nanosized Fe-CoOOH integrated with graphene for highly efficient oxygen evolution. *Adv. Energy Mater.* **2017**, *7*, 1602148.
- [284] Meng, X. Y.; Han, J. X.; Lu, L.; Qiu, G. R.; Wang, Z. L.; Sun, C. W. Fe³⁺-doped layered double (Ni, Fe) hydroxides as efficient electrocatalysts for water splitting and self-powered electrochemical systems. *Small* **2019**, *15*, 1902551.
- [285] Zhang, D. L.; Mou, H. Y.; Lu, F.; Song, C. X.; Wang, D. B. A novel strategy for 2D/2D NiS/graphene heterostructures as efficient bifunctional electrocatalysts for overall water splitting. *Appl. Catal. B* **2019**, *254*, 471–478.
- [286] Fan, Y. C.; Ida, S.; Staykov, A.; Akbay, T.; Hagiwara, H.; Matsuda, J.; Kaneko, K.; Ishihara, T. Ni-Fe nitride nanoplates on nitrogen-doped graphene as a synergistic catalyst for reversible oxygen evolution reaction and rechargeable Zn-air battery. *Small* **2017**, *13*, 1700099.
- [287] Seh, Z. W.; Fredrickson, K. D.; Anasori, B.; Kibsgaard, J.; Strickler, A. L.; Lukatskaya, M. R.; Gogotsi, Y.; Jaramillo, T. F.; Vojvodic, A. Two-dimensional molybdenum carbide (MXene) as an efficient electrocatalyst for hydrogen evolution. *ACS Energy Lett.* **2016**, *1*, 589–594.
- [288] Ma, T. Y.; Cao, J. L.; Jaroniec, M.; Qiao, S. Z. Interacting carbon nitride and titanium carbide nanosheets for high-performance oxygen evolution. *Angew. Chem., Int. Ed.* **2016**, *55*, 1138–1142.
- [289] Gao, G. P.; O’Mullane, A. P.; Du, A. J. 2D MXenes: A new family of promising catalysts for the hydrogen evolution reaction. *ACS Catal.* **2017**, *7*, 494–500.
- [290] Anasori, B.; Lukatskaya, M. R.; Gogotsi, Y. 2D metal carbides and nitrides (MXenes) for energy storage. *Nat. Rev. Mater.* **2017**, *2*, 16098.
- [291] Tang, Y.; Yang, C. H.; Yang, Y. W.; Yin, X. T.; Que, W. X.; Zhu, J. F. Three dimensional hierarchical network structure of S-NiFe₂O₄ modified few-layer titanium carbides (MXene) flakes on nickel foam as a high efficient electrocatalyst for oxygen evolution. *Electrochim. Acta* **2019**, *296*, 762–770.
- [292] Hao, C. Y.; Wu, Y.; An, Y. J.; Cui, B. H.; Lin, J. N.; Li, X. N.; Wang, D. H.; Jiang, M. H.; Cheng, Z. X.; Hu, S. Interface-coupling of CoFe-LDH on MXene as high-performance oxygen evolution catalyst. *Mater. Today Energy* **2019**, *12*, 453–462.
- [293] Li, Q.; Zhou, J.; Li, F.; Sun, Z. M. Novel MXene-based hierarchically porous composite as superior electrodes for Li-ion storage. *Appl. Surf. Sci.* **2020**, *530*, 147214.
- [294] Zou, H. Y.; He, B. W.; Kuang, P. Y.; Yu, J. G.; Fan, K. Metal-organic framework-derived nickel-cobalt sulfide on ultrathin MXene nanosheets for electrocatalytic oxygen evolution. *ACS Appl. Mater. Interfaces* **2018**, *10*, 22311–22319.
- [295] Zhao, L.; Dong, B. L.; Li, S. Z.; Zhou, L. J.; Lai, L. F.; Wang, Z. W.; Zhao, S. L.; Han, M.; Gao, K.; Lu, M. et al. Interdiffusion reaction-assisted hybridization of two-dimensional metal-organic frameworks and Ti₃C₂T_x nanosheets for electrocatalytic oxygen evolution. *ACS Nano* **2017**, *11*, 5800–5807.
- [296] Du, C. F.; Sun, X. L.; Yu, H.; Fang, W.; Jing, Y.; Wang, Y. H.; Li, S. Q.; Liu, X. H.; Yan, Q. Y. V₄C₃T_x MXene: A promising active substrate for reactive surface modification and the enhanced electrocatalytic oxygen evolution activity. *InfoMat* **2020**, *2*, 950–959.
- [297] Hunt, S. T.; Milina, M.; Alba-Rubio, A. C.; Hendon, C. H.; Dumesic, J. A.; Román-Leshkov, Y. Self-assembly of noble metal monolayers on transition metal carbide nanoparticle catalysts. *Science* **2016**, *352*, 974–978.

- [298] Ran, J. R.; Gao, G. P.; Li, F. T.; Ma, T. Y.; Du, A. J.; Qiao, S. Z. Ti_3C_2 MXene co-catalyst on metal sulfide photo-absorbers for enhanced visible-light photocatalytic hydrogen production. *Nat. Commun.* **2017**, *8*, 13907.
- [299] Shinde, P. V.; Mane, P.; Chakraborty, B.; Rout, C. S. Spinel NiFe_2O_4 nanoparticles decorated 2D Ti_3C_2 MXene sheets for efficient water splitting: Experiments and theories. *J. Colloid Interface Sci.* **2021**, *602*, 232–241.
- [300] Zubair, M.; Ul Hassan, M. M.; Mehran, M. T.; Baig, M. M.; Hussain, S.; Shahzad, F. 2D MXenes and their heterostructures for HER, OER and overall water splitting: A review. *Int. J. Hydrogen Energy* **2022**, *47*, 2794–2818.
- [301] Lu, Y.; Fan, D. Q.; Chen, Z. P.; Xiao, W. P.; Cao, C. C.; Yang, X. F. Anchoring Co_3O_4 nanoparticles on MXene for efficient electrocatalytic oxygen evolution. *Sci. Bull.* **2020**, *65*, 460–466.
- [302] Xie, Y. Y.; Yu, H. Z.; Deng, L. M.; Amin, R. S.; Yu, D. S.; Fetohi, A. E.; Maximov, M. Y.; Li, L. L.; El-Khatib, K. M.; Peng, S. J. Anchoring stable FeS_2 nanoparticles on MXene nanosheets via interface engineering for efficient water splitting. *Inorg. Chem. Front.* **2022**, *9*, 662–669.
- [303] Bai, K. K.; Fan, J. C.; Shi, P. H.; Min, Y. L.; Xu, Q. J. Directly ball milling red phosphorus and expanded graphite for oxygen evolution reaction. *J. Power Sources* **2020**, *456*, 228003.
- [304] Yuan, Z. K.; Li, J.; Yang, M. J.; Fang, Z. S.; Jian, J. H.; Yu, D. S.; Chen, X. D.; Dai, L. M. Ultrathin black phosphorus-on-nitrogen doped graphene for efficient overall water splitting: Dual modulation roles of directional interfacial charge transfer. *J. Am. Chem. Soc.* **2019**, *141*, 4972–4979.